MEDULLOBLASTOMA TUMOUR SUPPRESSOR FACTOR REN^{KCTD11}: STRUCTURE AND FUNCTION BASED DESIGN AND DEVELOPMENT OF NEW COMPOUNDS OF THERAPEUTICAL INTEREST

Luciano Pirone

Dottorato in Scienze Biotecnologiche XXII ciclo
Indirizzo Biotecnologie Molecolari
Università di Napoli Federico II

Dottorato in Scienze Biotecnologiche XXII ciclo
Indirizzo Biotecnologie Molecolari
Università di Napoli Federico II

MEDULLOBLASTOMA TUMOUR SUPPRESSOR FACTOR REN^{KCTD11}: STRUCTURE AND FUNCTION BASED DESIGN AND DEVELOPMENT OF NEW COMPOUNDS OF THERAPEUTICAL INTEREST

Luciano Pirone

Dottorando: Luciano Pirone

Relatore: Prof. Ettore Benedetti

Correlatore: Dott.ssa Emilia Maria Pedone

Coordinatore: Prof. Ettore Benedetti

A tutti coloro che hanno creduto in me!

Index

Abbreviations

APS	ammonium persulfate
AR	retinoic acid
BSA	albumin from bovine serum
BTB	bric-à-brac, tramtrack and broad
CD	circular dichroism
CNS	central nervous system
CTD	C-terminal domain
Cul	cullin
dam	DNA adenine methylase
Dhh	Desert Hedgehog
DMEM	Dulbecco's Modified Eagle Medium
dNTP	deoxy nucleotide tri-phosphate
DTT	dithiothreitol
ECL	enhanced chemi-luminescence
EDTA	ethylene-diamino-tetraacetic acid
ESI	electron spry ionization source
FBS	foetal bovine serum
FPLC	Fast protein liquid chromatography
GCP	Granule cell progenitors
GST	Glutathione S-Transferase
GTE	Glucose-Tris-EDTA
Hh	Hedgehog
HPLC	high performance liquid chromatography
HSQC	heteronuclear single quantum coherence
Kd	dissociation constant
IGL	internal germinal layer
Ihh	Indian Hedgehog
IPTG	isopropyl-beta-D-thiogalactopyranoside
KCTD	Potassium Channel Tetramerization Domain
LB	Luria-Bertani Broth
LC-MS	liquid chromatography mass spectrometry
MB	medulloblastoma
MBP	Maltose Binding Protein
MCS	multi cloning site
ms	millisecond
MWCO	molecular weight cut off
Ni-NTA	nickel-nitrilotriacetic acid
NMR	Nuclear Magnetic Resonance
NOESY	Nuclear Overhauser Effect Spectroscopy
NTD	N-terminal domain
orf	open reading frame
PBS	phosphate buffer saline
PCR	polymerase chain reaction
POZ	poxvirus zinc finger
PVDF	polyvinylidene fluoride
REN	retinoic acid, epithelial growth factor, nerve growth factor

SCF	Skp1–Cullin–F-box protein
SDS-PAGE	sodium dodecyl sulfate polyacrylamide gel electrophoresis
Shh	Sonic Hedgehog
STD	saturation transfer difference
TAE	Tris acetate EDTA
TE	Tris/HCl-EDTA
TEMED	N,N,N',N'-tetramethyl ethylene diamine
TEV	tobacco etch virus
Tris	Tris (hidroxy methyl) amino methane
TrxA	thioredoxin A
Ub	ubiquitin

Summary

Hedgehog (Hh) signaling is suggested to be a major oncogenic pathway in medulloblastoma, which arises from aberrant development of cerebellar granule progenitors. Hh signaling is regulated by ubiquitin ligases E3, that process the downstream transcription factors Gli via dual Cullin-based ubiquitin-dependent pathways. Interestingly, Cullin3 has been shown to require proteins containing BTB (Broad Complex, Tramtrack and Bric a Brac) domain to target substrates. Recently a human BTB protein has been identified, REN^{KCTD11}, which displays allelic deletion as well as significantly, reduced expression in medulloblastoma. Data *in vitro* have suggested that REN^{KCTD11} binds Cullin3 and indirectly promotes the degradation of Gli1 thus inhibiting the transactivation of the Hedgehog target genes. Although the available literature data clearly show the role of REN^{KCTD11} as tumour suppressor, its biochemical properties remain to be defined. In this context we have undertaken a structural and functional study on REN^{KCTD11} protein. Human genomic region coding for REN^{KCTD11} has been amplified by PCR, cloned and over-expressed in *Escherichia coli* in soluble form, as a fusion product with Maltose Binding Protein (MBP). The protein has been purified to homogeneity by only one purification step utilizing the presence of His-tag. Size exclusion chromatography allowed to structurally characterize REN^{KCTD11} as an homotetramer in agreement with *in silico* analysis. The TEV-digested protein sample was extremely unstable. The alignment of REN^{KCTD11} sequence with sequence databases shows that a region of almost one hundred residues presents a significant degree of similarity with the POZ/BTB domain of potassium (kv4) channel. Bioinformatic analyses have allowed to identify the exact extension of POZ/BTB domain of REN^{KCTD11}. It has been cloned, expressed as a fusion product with Thioredoxin-A (TrxA), purified in soluble form as a tetramer and characterized by mass spectroscopy, circular dichroism and light scattering. The homogeneous protein has been used for crystallization tests. Site-directed mutagenesis has been used to validate the ionic interactions responsible of the POZ/BTB domain tetrameric form. The mutant D69A/R74A/N78A/R81A resulted strongly unstable. These data confirmed the key role of these residues in the stabilization of the tetrameric form of the protein. The experimental evidence that POZ/BTB of REN^{KCTD11} forms a stable tetramer in solution prompted us to check the possibility to generate by homology modelling a REN^{KCTD11} POZ/BTB-Cul3 complex with a 4:4 stoichiometry. A peptide corresponding to residues 49-68 (NH_2-NSGLSFEELYRNAYTMVLHK-COOH) of Cul3 has been individuated as responsible of interaction with the domain POZ/BTB of REN^{KCTD11}. The peptide binds POZ/BTB of REN^{KCTD11} with an apparent affinity constant of 0.8 μM. Then, we tried to investigate whether the same region of Cul3 was responsible for interaction with POZ/BTB domains of other KCTD proteins. It was chosen as the starting point KCTD5, a cytosolic protein whose crystal structure has been recently deposited. The POZ/BTB domain of KCTD5 with five aminoacids added at N-terminus (region 40-151) was expressed in *E. coli* and obtained in large amount. The results obtained by ELISA show that this POZ/BTB domain binds the helix 49-68 of Cul3 with an affinity similar to that of the BTB/POZ of REN^{KCTD11}. Finally we present a mechanism of function of REN^{KCTD11} applicable to other members of KCTD family that, interacting with the ubiquitin-ligase-E3, regulate some of the most important cellular metabolic pathways by their POZ/BTB domains.

Riassunto

Questa tesi di dottorato si inserisce in un più ampio progetto volto alla definizione delle basi molecolari del ruolo biologico dell'oncosoppressore del medulloblastoma REN^{KCTD11}, una proteina presente nel *pathway* Sonic-Hedgehog (Shh). Le Hedgehog sono glicoproteine coinvolte in processi metabolici che regolano lo sviluppo e il differenziamento cellulare. Sonic Hedgehog in particolare regola lo sviluppo del sistema nervoso centrale e il differenziamento delle cellule progenitrici del cervelletto [Ruiz i Altaba, *et al*. 2002], [Palma V., *et al.* 2005]. La deregolazione di tale *pathway* determina la formazione di molti tumori del cervello. Tra questi vi è il medulloblastoma, che è causato da diverse alterazioni genetiche ed epigenetiche che influenzano lo sviluppo delle cellule progenitrici dei granuli del cervelletto (GPC) la cui proliferazione è regolata dalla proteina Sonic Hedgehog, secreta dalle cellule del Purkinjie. In seguito all'interruzione del segnale Shh le GPCs smettono di proliferare ed iniziano a differenziarsi. La mancata interruzione del segnale Shh si ritiene essere la principale causa dell'insorgenza del tumore [Argenti B., *et al.* 2005], [Carlotti C.G., *et al.* 2008]. Questi dati sono confermati da modelli murini che riproducono la malattia, in cui sono stati identificate mutazioni a carico di geni codificanti proteine appartenenti alla cascata del segnale Shh. In particolare, nel 39% dei casi di medulloblastoma è stata riscontrata una delezione allelica sul cromosoma 17, regione in cui è presente il locus genico codificante REN^{KCTD11} [Gallo R., *et al.* 2002], la proteina sulla quale abbiamo focalizzato la nostra attenzione. Analisi di sequenza mostrano che REN^{KCTD11} presenta all'N-terminale un dominio POZ/BTB: attraverso tale dominio interagirebbe con Cul3, promovendo la degradazione di un substrato non ancora identificato, che a sua volta regola l'attività del fattore trascrizionale Gli1, regolatore della trascrizione dei geni coinvolti nei processi di sviluppo. L'oncosoppressore REN^{KCTD11} potrebbe essere, pertanto, un importante target per la progettazione di piccole molecole mimetiche impiegabili a scopo terapeutico nel trattamento del medulloblastoma. REN^{KCTD11} è stata originariamente identificata come una proteina di 232 amminoacidi. Allineamenti di sequenza tra REN^{KCTD11} e proteine con struttura tridimensionale nota hanno mostrato che la regione N-terminale (residui 20-80) presentava una significativa identità di sequenza (circa 40%) con il dominio di tetramerizzazione del canale del potassio Kv4. Questo risultato ha suggerito che la forma attiva di REN^{KCTD11} in vivo potesse essere tetramerica. Nessun'altra identità di sequenza è stata rilevata considerando le altre regioni della proteina. I numerosi tentativi effettuati per esprimere eterologamente REN^{KCTD11} e suoi mutanti REN^{KCTD11} in sistemi sia eucariotici che procariotici, hanno dato esiti negativi. Successive indagini bioinformatiche hanno evidenziato un aspetto peculiare della sequenza N-terminale di REN^{KCTD11}. Allineamenti di sequenza con proteine contenenti domini POZ/BTB a struttura nota hanno rivelato, infatti, che il dominio POZ/BTB di REN^{KCTD11} fosse tronco. Considerando la sequenza di REN^{KCTD11} depositata in banca dati, nella proteina è presente solo una porzione del *core* conservato. Allineamenti di sequenza mostrano che manca la parte del dominio corrispondente ai foglietti beta B1 e B2 e l'alfa elica A1 secondo il modello proposto da Privè [Stogios P.J., *et al.* 2005]. Questo dato ci ha indotto a valutare la possibilità di un alternativo sito d'inizio della traduzione di REN^{KCTD11}. E' stata da noi evidenziata, quindi, una nuova sequenza (forma "lunga") per REN^{KCTD11} caratterizzata da un punto d'inizio della traduzione posto 39 amminoacidi a monte di quella precedentemente individuata. L'esistenza della forma "lunga" di REN^{KCTD11} è

stata confermata dagli esperimenti condotti dal gruppo del prof. Alberto Gulino (Università "La Sapienza", Roma). È stata intrapresa, quindi, la caratterizzazione biochimica e strutturale della forma "lunga" di REN^{KCTD11} (271 amminoacidi), rivelatasi più stabile rispetto alla forma "corta" originariamente identificata (232 amminoacidi). REN^{KCTD11} è stata espressa con diversi partners di fusione e, come proteina di fusione con la Maltose Binding Protein (MBP), è stata ottenuta in fase solubile; purificata e sottoposta a cromatografia ad esclusione molecolare, rivelando che MBP/REN^{KCTD11} non aggrega e presenta un peso molecolare riconducibile a quello di un tetramero, come previsto dai dati raccolti *in silico*. In seguito a digestione proteolitica e successivo allontanamento della MBP, REN^{KCTD11} tende a precipitare, mostrandosi ancora una volta instabile e quindi difficilmente caratterizzabile dal punto di vista strutturale. Sono stati quindi intrapresi studi biochimici e strutturali del dominio POZ/BTB di REN^{KCTD11}. La ricostruzione del dominio relazionato alla forma "lunga" di REN^{KCTD11} ha richiesto 24 residui amminoacidici a monte del punto d'inizio della traduzione della "forma corta". Tali studi hanno mostrato uno stato di organizzazione tetramerico, in accordo con il modello proposto da Privé. Studi di *light scattering* sul POZ/BTB hanno evidenziato un peso molecolare che conferma lo stato tetramerico, e un raggio idrodinamico di 4,5 nm, suggerendo una forma globulare. Inoltre, studi di dicroismo circolare hanno evidenziato la presenza di α-eliche e foglietti β e un'elevata stabilità del dominio (Tm pari a 54 °C), influenzata dalla presenza di sali (400 mM NaCl determina un aumento della temperatura di melting di 5°C). Questo dato è stato utilizzato per mettere a punto prove di cristallizzazione dalle quali si sono ottenuti cristalli che diffrangono ad una risoluzione di 4,5 Å, troppo bassa per consentire la risoluzione della struttura. Si è cercato, inoltre, di chiarire il preciso ruolo funzionale del dominio POZ/BTB nell'ambito dell'intera proteina. Com'è noto, il processo di tetramerizzazione nelle proteine con domini POZ/BTB è solitamente favorito dalla presenza di ioni zinco e da interazioni elettrostatiche tra le subunità. Studi di allineamento di sequenze hanno rivelato l'assenza nella proteina REN^{KCTD11} degli amminoacidi normalmente responsabili della coordinazione con lo zinco; al contrario i residui coinvolti nei ponti salini e nelle interazioni idrofiliche sono conservati. Questi dati, unitamente a studi di modelling molecolare, indicano che residui amminoacidici specifici possono essere importanti per il processo di oligomerizzazione di REN^{KCTD11}. Sulla base di tali informazioni, esperimenti di mutagenesi sito-diretta sono stati condotti sul costrutto producendo un tetramutante (D69A/R74A/N78A/R81A) che è stato anch'esso clonato ed espresso eterologamente in *E. coli*, per essere poi caratterizzato biochimicamente. In seguito a cromatografia ad esclusione molecolare il mutante si è rilevato instabile, suggerendo che i residui in esso sostituiti potessero svolgere uno specifico e cruciale ruolo nella tetramerizzazione del dominio. Considerando anche il dato precedentemente raccolto sullo stato oligomerico della proteina di fusione MBP/REN^{KCTD11}, si è potuto affermare che il dominio POZ/BTB è necessario per la strutturazione dell'intera proteina REN^{KCTD11} sotto forma di tetramero. Diversi costrutti di POZ/BTB sono stati progettati sulla base di allineamenti di sequenza e predizioni di struttura secondaria, nell'intento di inserire ulteriori motivi strutturali e così agevolare il corretto *folding* del dominio ma tali modifiche non hanno apportato i miglioramenti attesi: i prodotti ricombinanti ottenuti si sono dimostrati in parte meno stabili in parte hanno dato cristalli di morfologia diversa rispetto a quelli formati precedentemente, ma comunque non in grado di fornire alcun pattern di diffrazione. In seguito ad un'attenta analisi degli allineamenti di sequenza, la nostra attenzione si è focalizzata su una nuova "*open reading frame*", *kctd21*, che presenta il 40% d'identità con *kctd11*. Il

gene *kctd21* è localizzato sul cromosoma 11, che in alcuni rari casi di medulloblastoma mostra eventi di delezione allelica e codifica una putativa proteina di 260 amminoacidi. Poiché anche in essa è presente un ipotetico dominio POZ/BTB, si è pensato di clonare *kctd21* e in seguito di esprimere la proteina in *E. coli*, per ricavarne informazioni strutturali che potessero essere estese a REN^{KCTD11}. Pur avendo espresso KCTD21 con diversi partners di fusione, la proteina si è mostrata sempre instabile in soluzione e quindi anch'essa non caratterizzabile. Per quanto riguarda il dominio POZ/BTB di KCTD21, una volta espresso e purificato, si è visto che si organizza anch'esso in una struttura tetramerica, ma contrariamente al POZ/BTB di REN^{KCTD11} presenta un'elevata instabilità, che non ha permesso successive indagini cristallografiche. I dati fin qui riportati sono stati integrati con quelli ottenuti attraverso il *modelling* molecolare: secondo il modello basato sulla struttura già nota del complesso Skp1/Cul1 (omologhe rispettivamente a REN^{KCTD11} e Cul3), ciascuna delle subunità del tetramero di POZ/BTB interagirebbe con una molecola di Cul3, formando un complesso di enormi dimensioni a cui si aggiungerebbero altri partner d'interazione. Tale modello ha consentito di individuare la regione d'interazione tra Cul3 e POZ/BTB: un peptide corrispondente ai residui 49-68 di Cul3 è stato sintetizzato in fase solida mediante chimica Fmoc ed è stato utilizzato per allestire un saggio ELISA con il dominio POZ/BTB di REN^{KCTD11}. Il peptide lega POZ/BTB con una costante di affinità apparente di 0,8 μM. Studi NMR effettuati tra la proteina marcata con N^{15} ed il peptide di Cul3 hanno confermato tale interazione. Una volta individuata nell'elica 49-68 di Cul3 la regione d'interazione con il dominio POZ/BTB da noi studiato, si è cercato di investigare se la stessa regione di Cul3 fosse responsabile dell'interazione con i domini POZ/BTB di altri membri della famiglia di proteine KCTD. Si è scelto come membro di tale famiglia KCTD5 la cui struttura cristallografica è stata recentemente depositata [Dementieva I. S., *et al*. 2009]. Tramite un saggio ELISA si è verificato che anche il dominio POZ/BTB di KCTD5 è in grado di legare l'elica 49-68 di Cul3 con un'affinità apparente paragonabile a quella del dominio POZ/BTB di REN^{KCTD11}. Attualmente, sono state allestite prove di co-cristallizzazione con l'elica Cul3, allo scopo sia di identificare la regione del dominio POZ/BTB di KCTD5 coinvolta nell'interazione, che di ottenere informazioni utili alla caratterizzazione dell'interazione del dominio POZ/BTB di REN^{KCTD11} con Cul3. Grazie alla consistente mole di dati fin qui raccolti, è stato possibile far luce sui complessi meccanismi molecolari che sono alla base dell'attività biologica di REN^{KCTD11} nell'ambito del *signaling* Hedgehog e di identificare nell'elica di Cul3 un potenziale "*scaffold*" di interesse terapeutico.

1 Introduction

1.1 POZ/BTB Domain

The BTB domain (also known as the POZ domain) was originally identified as a conserved motif present in the *Drosophila melanogaster* bric-à-brac, tramtrack and broad (BTB) complex transcription regulators and in many poxvirus zinc finger (POZ) proteins. BTB/POZ domain is typically found in a single copy per protein, but in some proteins it is combined with a variety of additional protein-protein interaction domains, such as the kelch repeats, MATH domains, ankyrin repeats, the b-zip DNA binding domain and FYVE fingers [Bardwell V. J., *et al.* 1994], [Zollman S., *et al.* 1994]. Additionally, all the mammal potassium channels contain POZ (T1) domains in their N-terminus. BTB/POZ combining with a number of other domains forms a variety of distinct domain architectures (figure 1.1). Among the most common ones is the combination of the BTB/POZ domain with C-terminal zinc fingers. This domain architecture is abundantly represented in *Drosophila* and in vertebrates, and the respective proteins are typically involved in transcriptional regulation and chromatin remodelling. Given the extremely wide representation and functional significance of BTB/POZ domains, the structural basis of these interactions is of major interest. The biological properties of BTB/POZ-containing proteins seem to be contingent on the protein-protein interaction properties of this domain. Several lines of research have uncovered distinct roles for these proteins in diverse cellular locations. In particular, BTB/POZ domains appear to participate in a variety of processes ranging from transcriptional repression/activation to cytoskeletal organization. In several proteins, BTB/POZ domains have been shown to mediate homodimerization or multimerization [Aravind L., *et al*. 1999]. Several BTB/POZ structures have been determined by X-ray crystallography, establishing the structural similarity between different examples of the fold [Ahmad K. F., *et al.* 1998], [Kreusch A., *et al.* 1998]. A comparison of the solved structures of BTB domains from the Protein Data Bank (PDB), which included examples from BTB-ZF proteins, Skp1, ElonginC and T1 domains showed a common region of approximately 95 aminoacids consisting of a cluster of 5 α-helices made up in part of two α-helical hairpins (A1/A2 and A4/A5), and capped at one end by a short solvent-exposed three stranded β-sheet (B1/B2/B3), (figure 1.2 a). An additional hairpin-like motif consisting of A3 and an extended region links the B1/B2/A1/A2/B3 and A4/A5 segments of the fold. Because of the presence or absence of secondary structural elements in certain examples of the fold, they used the designation A1–A5 for the five conserved α-helixes, and B1–B3 for the three common β-strands. We refer to this structure as the core BTB fold. When present, other secondary structure elements are named according to the labels assigned to the original structures. Thus, the BTB-ZF family members, the promyelocytic leukemia zinc finger (PLZF) and B-cell lymphoma 6 (BCL6) contain additional amino-terminal elements, which are referred to as β1 and α1, Skp1 protein contains two additional carboxy-terminal helixes labelled α7 and α8, ElonginC is missing the A5 terminal helix, and the T1 structures from Kv proteins are formed entirely of the core BTB fold (figure 1.2 b). Thus, the BTB domain in BTB-zinc finger (ZF), Skp1, ElonginC and voltage-gated potassium channel T1 (T1-Kv) proteins all contain the BTB fold, even though some of these differ in their peripheral secondary structure elements and are involved in different types of protein-protein associations. For example, BTB domains from the BTB-ZF family contain an amino-terminal extension and form homodimers, whereas

the Skp1 proteins contain a family-specific carboxy-terminal extension and occur as single copies in heterotrimeric SCF complexes. The ElonginC proteins are also involved in protein degradation pathways, although these proteins consist only of the core BTB fold and are typically less than 20% identical to the Skp1 proteins. Finally, T1 domains in T1-Kv proteins consist only of the core fold and associate into homotetramers. Thus, while the structures of BTB/POZ domains show good conservation in overall tertiary structure, there is little sequence similarity between members of different families. As a result, the BTB/POZ fold is a versatile scaffold that participates in a variety of types of family-specific protein-protein interactions [Stogios P. J., *et al.* 2005]. More recently, some BTB proteins have been characterized as substrate-specific adaptors for cullin(CUL)3-based E3 ligases. The BTB/POZ domain of these substrate-specific adaptors, in particular, binds to Cul3. In mammalian cells, a few other BTB/POZ proteins, e.g. SPOP, a BTB-MATH protein, and KEAP1, a BTB-KELCH protein, have been described as adaptors of Cul3-based E3 ligases [Kwon J.E., *et al.* 2006], [Zhuang M., *et al.* 2009].

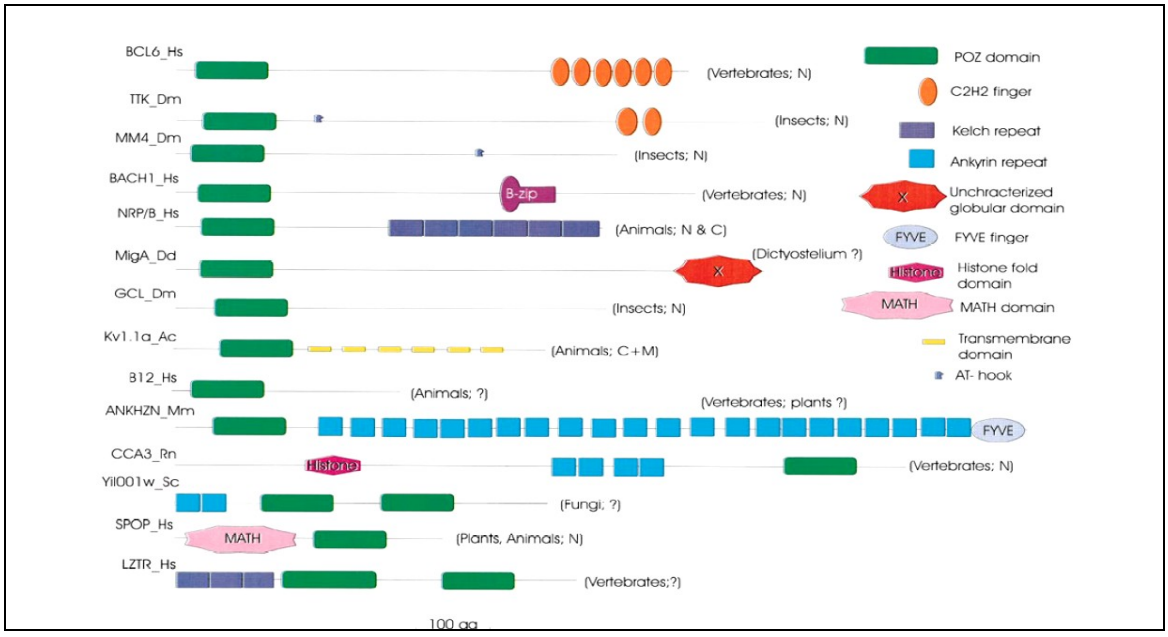

Figure 1.1. Domain architectures of the POZ/BTB-containing proteins [Aravind L., *et al.* 1999].

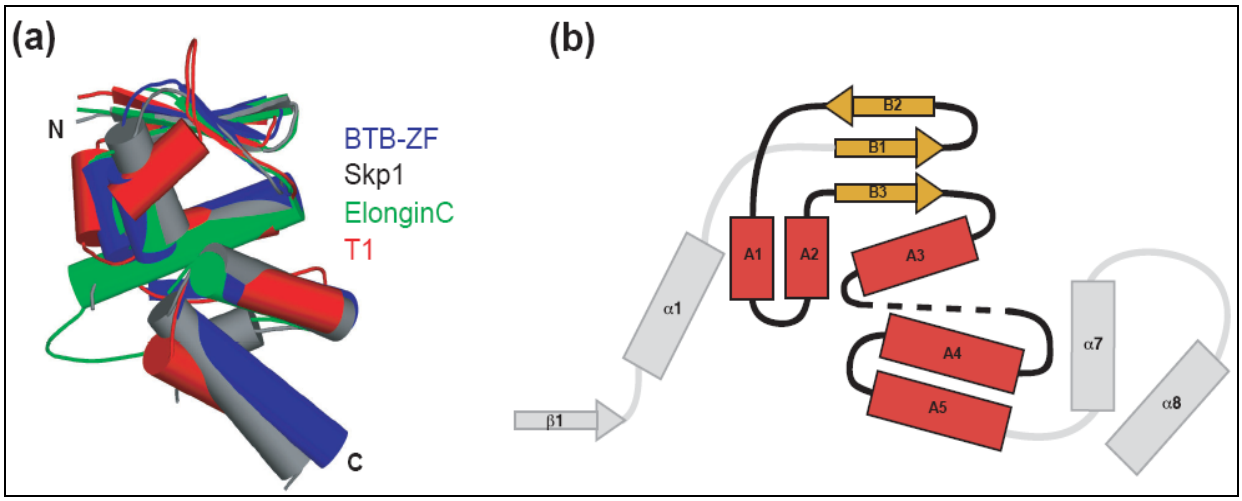

Figure 1.2. Comparison of structures containing the BTB/POZ fold: **(a)** superposition of the BTB/POZ core fold from currently known BTB/POZ structures. The BTB/POZ core fold is retained across four sequence families. The BTB-ZF, Skp1, ElonginC and T1 families are represented by the domains from Protein Data Bank (PDB) structures; **(b):** schematic of the BTB/POZ fold topology. The core elements of the BTB/POZ fold are labelled B1 to B3 for the three conserved β-strands, and A1 to A5 for the five α-helixes. Many families of BTB/POZ proteins are of the 'long form', with an amino-terminal extension of α1 and β1. Skp1 proteins have two additional α-helices at the carboxyl terminus, labelled α7 and α8. The dashed line represents a segment of variable length that is often observed as strand β5 in the long form of the domain, and as an α-helix in Skp1 [Stogios P.J., *et al.* 2005].

1.2 Potassium Channel Tetramerization Domain (KCTD) Proteins

The human genome has 21 *kctd* genes that encode potassium channel tetramerization domain containing (KCTD) proteins. *kctd* genes are so named because the N-terminus of KCTD proteins and some voltage-gated K^+ (Kv) channels are homologous. KCTD proteins are soluble with N-terminal BTB/POZ domains and variable C-terminal. The 21-*kctd* genes predict proteins that can be sorted into seven groups based on the alignment of their N-terminal sequences. Some *kctd* genes are single-exon loci (4, 11, 12, and 14), while others appear to be subject to splice variation that would increase diversity. Group I contains KCTD 2, 3, 5, 9, and 17. KCTD5 is most closely related to KCTD2 and KCTD17, while KCTD3 and KCTD9 display ~ 60% similarity to the KCTD5 N-module and have dissimilar C-terminal. The N-module of KCTD5 displays 20% identity to the T1 domains of Kv1, Kv2, Kv3, and Kv4 channels (figure 1.3). The biological function of KCTD proteins remains unclear. High expression of transcripts in foetal tissues and low levels in adults suggest that they play a role during development. Thus, KCTD12 is implicated in the maturation of inner ear neurons by linkage to a progressive dominant auditory neuropathy; KCTD11 is proposed to suppress Hedgehog signalling and to promote tumour growth in medulloblastoma. A point mutation in KCTD7 has been associated with neurodegeneration and progressive myoclonic epilepsy, and KCTD5 has been reported to interact with human Golgi reassembly stacking protein 55 (GRASP55) [Dementieva I. S., *et al*. 2009].

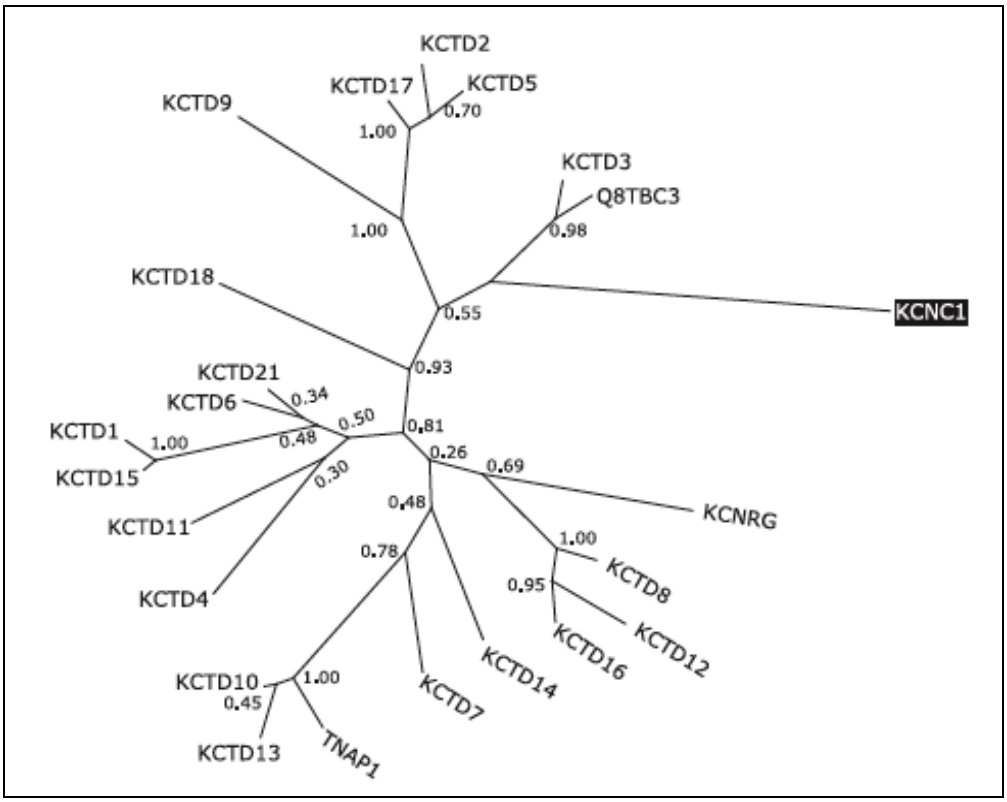

Figure 1.3. Phylogenetic tree built from human paralogs of KCTD5 [Bayon Y., *et al*. 2008].

1.3 KCTD5

KCTD5 has been reported to interact with human GRASP55. GRASP proteins contribute to the stacked organization of Golgi cisternae and are thought to participate in protein trafficking [Shorter J. *et al.* 1999]. KCTD5 has been the first member of the family KCTD to be characterized so far. The structure reveals a pentameric assembly with N- and C-modules and a central complex-spanning cavity. The high sequence identity of N-terminus (70%) of KCTD5 with the N-terminus of KCTD2 and KCTD17 suggests that the latter will also form pentameric assemblies. One KCTD5 pentamer is assembled with one GRASP55 monomer with an apparent equilibrium affinity of ~1 μM. KCTD5 binds to both full-length GRASP55 and the GRASP55 N-terminal domain (residues 1–263) with micromolar affinity. An intact KCTD5 C-module is required to bind GRASP55, while the pentameric KCTD5 N-module (residues 40–145) binds neither full-length nor truncated GRASP55. KCTD5 interacts specifically with Cul3, and forms oligomers through its BTB domain. Analysis of the interaction with Cul3 showed that, the C-terminal region of KCTD5 was dispensable for this interaction, while the BTB/POZ domain interacted with additional five aminoacids (40-45) on the N-terminus. Studies with other BTB/POZ proteins, e.g. SPOP [Zhuang M., *et al.* 2009], have also shown that other parts of their sequence, in addition to the BTB/POZ domain, are involved in the association with Cul3. On the other hand, the Cul3 region involved in this interaction was the N-terminus, as described for other BTB/POZ proteins. Taking into account that KCTD5 could be an adaptor of Cul3 E3 ligases, it was hypothesized that the region C-terminal could participate in substrate recognition, and that this could be a new protein interaction domain conserved through evolution. The fact that KCTD5 can

form oligomer through its BTB/POZ domain and the recent description of heterodimerization of Cul3 would indicate that complexes of higher order could be formed between Cul3 and BTB substrate adaptors, implying the recruitment of a great number of substrates by these E3 ligases. The same BTB surfaces, recently demonstrated, mediate pentamer and tetramer formation in KCTD5 and Kv channels, respectively, while BTB motifs had previously been demonstrated to mediate aggregation of two and four subunits via separate portions of the domain. These findings suggest that KCTD5 is a substrate-specific adaptor for Cul3-based E3 ligases [Bayon Y., *et al*. 2008], [Dementieva I. S., *et al*. 2009].

1.4 E3 ubiquitin-protein ligases

Ubiquitin-dependent proteolysis regulates protein abundance and serves a central regulatory function in many biological processes. Ubiquitination is involved in a wide range of cellular functions, such as cell proliferation, differentiation, and apoptosis, mainly by targeting proteins for degradation by the 26S proteasome, but it is also involved in protein transport and signalling through additional mechanisms. The ubiquitination of a target protein is mediated by the ubiquitin–protein ligases, which represent a diverse super-family of proteins and protein complexes. The SCF (Skp1–Cullin–F-box protein) and SCF-like complexes are the largest family of ubiquitin–protein ligases and ubiquitinate a broad range of proteins involved in cell cycle progression, signal transduction and transcription [Zhou P., *et al.* 1998]. Deregulation of SCF-dependent proteolysis can contribute to neoplastic transformation. Ubiquitin-protein ligases (also known as E3s) act at the last step of a three-enzyme cascade involving the ubiquitin-activating (E1) and ubiquitin-conjugating (E2) enzymes. The E3 mediates the transfer of ubiquitin from the E2 to the substrate protein by promoting the formation of an isopeptide bond between the ubiquitin (Ub) carboxy-terminus and specific lysine side chains on the substrate. E3s bind both the protein target and a cognate E2 and have a central role in conferring specificity to the ubiquitination pathway. Two functionally distinct types of E3s have been identified: HECT-type E3s catalyse ubiquitination by first forming an E3–ubiquitin thioester intermediate, RING-type E3s do not appear to form such an intermediate. The mechanism by which they promote ubiquitination has not been well understood. The crystal structure, recently solved, highlights an elongated structure with Rbx1 and the Skp1–Fbox-Skp2 complex segregated to opposite ends (figure 1.4). This arrangement is organized by Cul1, which interacts with all three subunits and serves as a scaffold. Cul1 consists of a 415 aminoacids with a N-terminal helical region, N-terminal domain (NTD), that adopts a long stalk-like structure and binds the Skp1–Fbox-Skp2 complex, and a 360 aminoacids C-terminal globular domain (CTD) that binds Rbx1. The Cul1 NTD stalk consists of three repeats of a novel five-helix structural motif (the cullin repeat). The three cullin repeats are arranged in a regularly repeating fashion resulting in an arc-shaped structure spanning, 110 A° (figure 1.4). The N-terminal tip of the first repeat binds the Skp1–Fbox-Skp2 complex. At the opposite end the C-terminal two helixes of the third repeat pack with a four-helix bundle from the Cul1 CTD. The CTD structure consists of a four-helix bundle (4HB), an a/b domain with an intermolecular five-stranded b-sheet, which contains as its second strand an N-terminal segment of Rbx1, and two copies of the winged-helix motif (WH-A and WH-B); the Cul1 CTD contains several structural units that assemble around the Rbx1 protein to form a single globular unit. Part of the Cul1

CTD forms a five-stranded intermolecular b-sheet that contains as its second b-strand an N-terminal sequence of Rbx1. The rest of the Cul1 CTD forms a 30 A° wide groove wherein the Rbx1 RING domain is embedded. The RING domain of Rbx1 is a variant of the canonical RING motif, with a 20 aminoacids insertion that forms a third zinc coordination site. Cul1 is modified through the covalent attachment of the ubiquitin like small molecule Nedd8. Cul1 is neddylated at Lys 720, which is on the WH-B domain and is positioned at the rim of a cleft formed by conserved residues from the WH-B, 4HB and Rbx1 RING domain The N-terminal tip of the first repeat binds the Skp1–Fbox-Skp2 complex. The proximity of Lys 720 to the Rbx1 RING domain supports the model that Nedd8 might modulate the binding and positioning of the E2 or the E2–ubiquitin conjugate [Zheng N., *et al*. 2002]. The large number of F-box proteins in eukaryotic genomes is thought to allow for the specific ubiquitination of a large number of functionally and structurally diverse substrates [Schulman B. A., *et al.* 2000], [Cardozo T., *et al.* 2004]. In the canonical example of Cul1, substrate receptors are recruited by the adaptor protein Skp1. Skp1 is divided into two domains: an N-terminal segment that binds Cul1 and a C-terminal region that binds the F-Box motif of substrate receptors (figure 1.5 a). The N-terminal segment of Cul1 that contacts Skp1 is highly conserved among Cul1 orthologues from different species, but not among other cullins, which reveals a structural basis for how each cullin specifically recruits a different set of substrates. Skp1 interacts selectively with Cul1 and Cul7. However, the adaptor proteins that are used by other cullins show considerable structural homology to Skp1. The cullin-binding region of elongin C, which binds Cul2 and Cul5 (figure 1.5 b), shares with Skp1 a fold that was first observed for the BTB/POZ domain. This indicated that BTB-domain proteins might be adaptors for a RING-type E3s, and this has now been shown to be the case for several BTB-domain proteins, which bind specifically to Cul3 (figure 1.5 c). The most poorly understood adaptor protein, DNA damage-binding protein-1 (DDB1), is not related to Skp1, elongin C or BTB domains, so it is unclear how it links substrate receptors to Cul4A [Kamura T., *et al.* 1998], [Furukava M., *et al.* 2003].

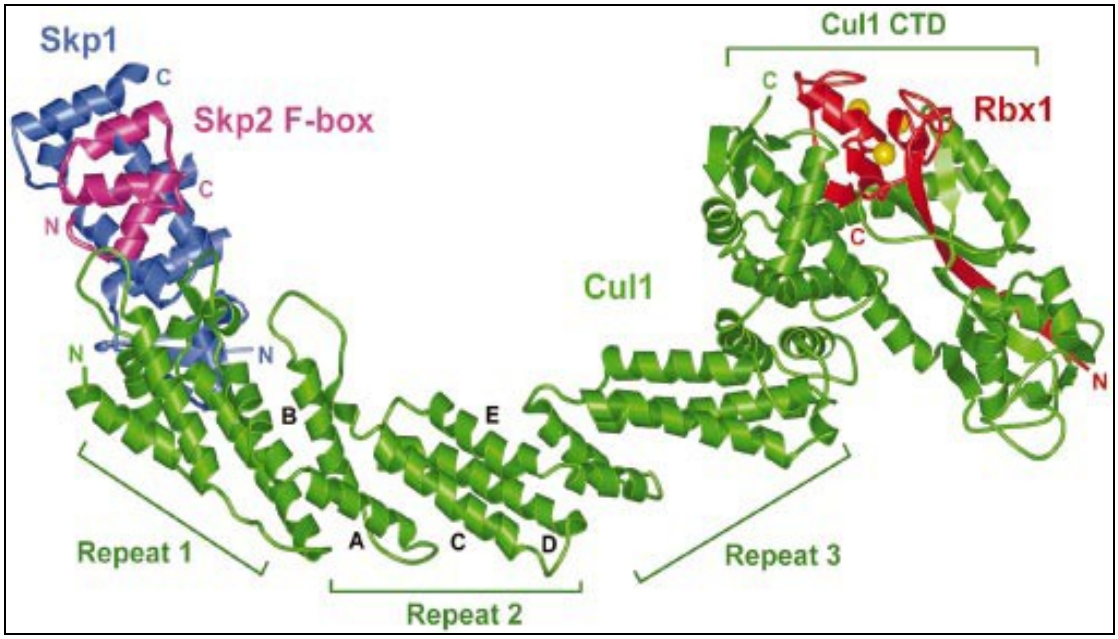

Figure 1.4. Overall structure of the Cul1–Rbx1–Skp1–F boxSkp2 quaternary complex. Cul1, Rbx1, Skp1 and the F-box of Skp2 are coloured in green, red, blue and magenta, respectively. The five helices that make up the cullin-repeat motif are labelled for the second repeat [Zheng N., *et al.* 2002].

As DDB1 is a much larger protein than Skp1 and elongin C, it might somehow compensate for the shorter length of the N-terminal stalk region of Cul4A (Figure 1.5 d). Cullin can assemble with numerous substrate receptors to form ubiquitin ligases that share a common catalytic core yet recruit different substrates. These receptors typically contain an N-terminal domain that binds an adaptor and a C-terminal region that binds substrate. Two distinct adaptor-binding domains are known: F-boxes binds Skp1, which, in turn, binds Cul1 and Cul7; whereas suppressor of cytokine signalling/elongin-BC (SOCS/BC) boxes binds elongin BC, which, in turn, binds Cul2 and Cul5 (figure 1.5 a, b). For Cul3-based ligases, the adaptor and substrate receptor functions are merged into a single polypeptide that binds Cul3 directly through an N-terminal BTB domain and the substrate through a C-terminal domain (figure 1.5 c). Substrate receptors that are recruited to DDB1–Cul4A do not share an obvious motif (figure 1.5 d). Cul3 is capable of interacting with a variety of BTB proteins, analogous to Cul1, which interacts with various F-box proteins. The fact that multiple BTB-domain proteins interact with Cul3 and that many BTB-domain proteins also contain additional protein interaction domains points to the possibility that BTB proteins function directly as adaptors that recruit substrates to Cul3, thereby forming an SCF-like E3. It is possible to identify a family of BTB-domain proteins as substrate-specific receptor modules for Cul3-based E3 ligases. BTB proteins contain a variety of putative protein interaction domains, including MATH domains, WD40 repeats, Zn finger repeats and kelch repeats. It was found that human BTB proteins containing MATH and kelch domains, as well as BTB-only proteins, interact with human Cul3. Although most BTB-domain proteins contain additional known protein interaction domains, approximately 30% lack recognizable domains and may have specialized protein interaction domains to recruit substrates or be substrates themselves, like some F-box proteins. Given the number of F-box, BC-box and BTB proteins in eukaryotes, SCF-like complexes seem to have the potential to control an extremely large number of signalling events through the ubiquitin–proteasome pathway. Although initially used to designate Skp1–Cul1–F-box protein complexes, the term SCF can be used conceptually in the description of a larger collection of cullin-based E3 ligases. Each SCF-like complex contains, in addition to the common catalytic core, a modular substrate-specific receptor that possesses structural homology with Skp1 and functional homology with C-terminal substrate interaction domains of F-box proteins. In addition, some SCF complexes contain further components, for example, elongin B in the case of Cul2 and Cul5 complexes [Xu L., *et al.* 2003], [Kwon J. E., *et al.* 2006], [Bayon I., *et al.* 2008].

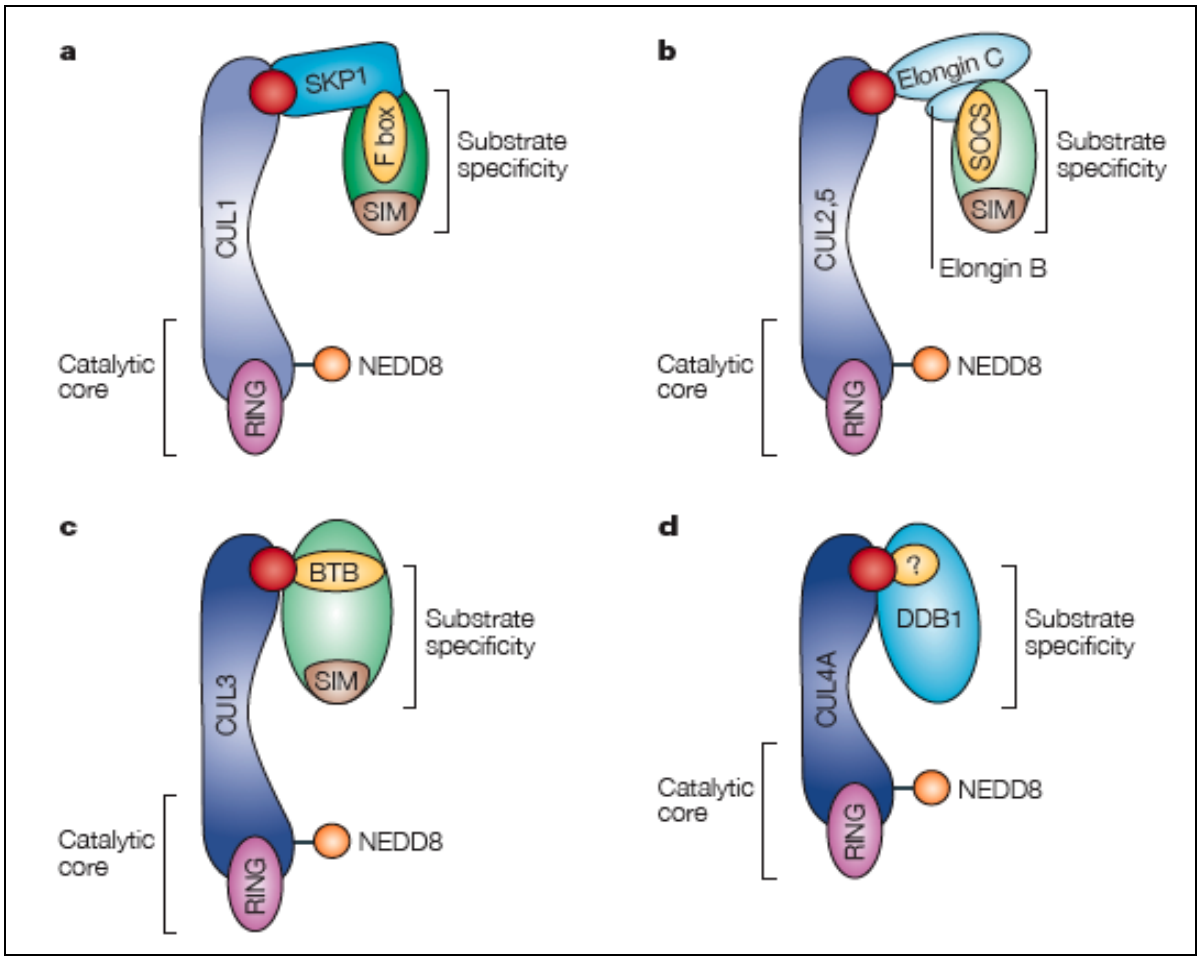

Figure 1.5. The modularity of cullin–RING ligases. Although the N-terminal region is thought to be similar in structure between family members, a segment of it is variable in sequence (red), and cullins use this region to interact with their own specific adaptor proteins. The motifs that link substrate receptors to their cognate adaptors are shown in yellow. In addition to an adaptor-binding motif, substrate receptors contain a second protein–protein interaction motif that binds to the targeted substrate (substrate interaction motif (SIM), which is shown in brown); a: Cul1 CRLs, which are known commonly as Skp1, Cul1, F-box (SCF) proteins, recruit substrates through the adaptor protein Skp1 and an F-box-protein substrate receptor. b: Cul2 and Cul5 CRLs recruit substrates through an elongin-BC adaptor and a suppressor of cytokine signalling/elongin BC-box-protein substrate receptor (labelled SOCS in the figure). c: Cul3 CRLs recruit substrates through BTB-domain-containing substrate-receptor proteins. d: Cul4A CRLs might recruit substrates through the adaptor protein DNA damage-binding protein-1 (DDB1), which interacts with Cul4A using an unknown motif [Petroski M.D., *et al.* 2005].

1.5 Sonic Hedgehog pathway

Hedgehog (Hh) proteins are secreted glycoproteins that activate a membrane-receptor complex that, in turn, activates Gli zinc-finger transcription factors. Hh proteins are synthesized as 45-kDa precursors, consisting of an N-terminal signalling domain and a C-terminal catalytic domain. An important feature of these proteins is their post-translational processing involving lipid modification of their two terminals, increasing the hydrophobicity and influencing the movement of Hh proteins between cells. In mammals, the Hh family consists of three members: Sonic hedgehog (Shh), Indian hedgehog (Ihh), and Desert hedgehog (Dhh). Dhh is required for

spermatogenesis and also is secreted by Schwann cells where it is important for the formation of the perineurial sheath and maintenance of trophic signals in peripheral nerves. Shh and Ihh share same overlapping roles in regulating left–right asymmetry, neural tube development, and the formation of a variety of organs including the bony skeleton, but they also have different properties. Ihh is critical in mediating the communication between the uterine epithelium and stroma required for embryo implantation. Shh plays an active role in the formation of the central nervous system (CNS), especially the cerebellum, and is responsible for midline facial development and the induction of neural tissue by mesodermal notochord [Palma V., *et al.* 2004], [Palma V., *et al.* 2005]. The Shh-Gli pathway has been the focus of much recent attention, and the positive action of the pathway is tightly regulated at different levels by many inhibitors. For example, Shh signalling activates a receptor complex that is formed by Patched (Ptc) and Smoothened (Smo) [Huangfu D., *et al.* 2006]. Hh inhibits Ptc, which, in turn, normally inhibits Smo. Inhibition of Ptc by Hh activates the Hh pathway and results in Gli activity. The function of Ptc, and other inhibitors, is to silence the pathway in the absence of active Hh ligands. This implies that the Hh–Gli pathway must be off most of the time, and only active at the precise points and locations at which the Hh signals act. Gli proteins are large multifunctional transcription factors, and their activities are intricately regulated. They reside in both the nucleus and the cytoplasm, where they are components of a multimolecular complex that is tethered to the cytoskeleton. The state of Shh signalling directly affects the fate of Gli proteins. In the absence of Shh, Gli proteins are cleaved by the proteasome, and carboxy-terminally truncated forms translocate to the nucleus, where they act as dominant transcriptional repressors. Following Shh signalling, Gli repressor formation is inhibited and full-length labile activators of transcription are made instead (figure 1.6). The three Gli proteins behave differently. In addition to being transcriptionally regulated in different ways, Gli1 does not seem to yield a strong repressor, whereas Gli2 and Gli3 do. Shh inhibits repressor formation by Gli3, but not by Gli2, and the formation of potent activators of Gli2, and perhaps of other Gli proteins, depends on Hh signalling. Gli proteins have partially redundant and partially distinct functions and induce distinct targets indicating that they act in a combinatorial manner that is context dependent and, possibly, species-specific. The generation of transcription repressor forms and degradation of activator forms represent an important control of Hh signaling output and occur via multiple proteolytic processing mechanisms involving a dual Cullin based and a HECT-based ubiquitin-dependent pathways. In the absence of Hh signal, phosphorylation at multiple sites of Gli2 and Gli3 by PKA, GSK3 and CKI, enables the recruitment of the E3 ubiquitin ligase belonging to the SCF complex including the F-box protein bTrCP, Skp1, Cul1 and Rbx1 proteins. The subsequent proteolytic processing generates truncated Gli2 and Gli3 provided of transcription repressor function. Additional molecules influence in a positive and negative way the signalling pathway. Some of the negative regulators have been described to be relevant in Hh pathway-dependent diseases such as brain tumours. For instance, suppressor of fused (SUFU) binds Gli proteins thereby inhibiting nuclear accumulation and interfering with their transcriptional activity [Taylor M. D., *et al.* 2002]. The Shh–Gli pathway seems to regulate many processes in cells. For instance, it can regulate survival in both differentiated and undifferentiated cell types, induce floor-plate differentiation and induce proliferation of neuron precursors in the developing cerebellum. Shh controls the growth of the cerebellum, and it orchestrates the positioning and differentiation of several cell types. Among other functions, Shh promotes proliferation of granule-

neuron precursors in the external germinal layer (EGL) of the cerebellum. Medulloblastomas are predicted to arise when granule-neuron precursors inappropriately maintain an active Shh–Gli pathway and express Gli1. Normally, this signalling and patterning information is tightly regulated and when it persists inappropriately, precursor cells might be instructed to proliferate abnormally, thereby initiating a tumour. The regulation of proliferation in the EGL has two conflicting tasks: to fulfil the need for the cerebellum to grow to the appropriate size for a given species, while preventing tumorigenesis. Endogenous secreted factors that might regulate the time at which outer EGL cells stop cycling could be useful as anticancer agents. A clear molecular understanding of how the Shh–Gli pathway operates in the cerebellar cortex is likely to not only reveal how this CNS organ is formed, but also provide clues for possible rational therapies [Ruiz i Altaba, *et al*. 2002], [Rubin L. L., *et al.* 2006], [Gulino A., *et al*. 2007].

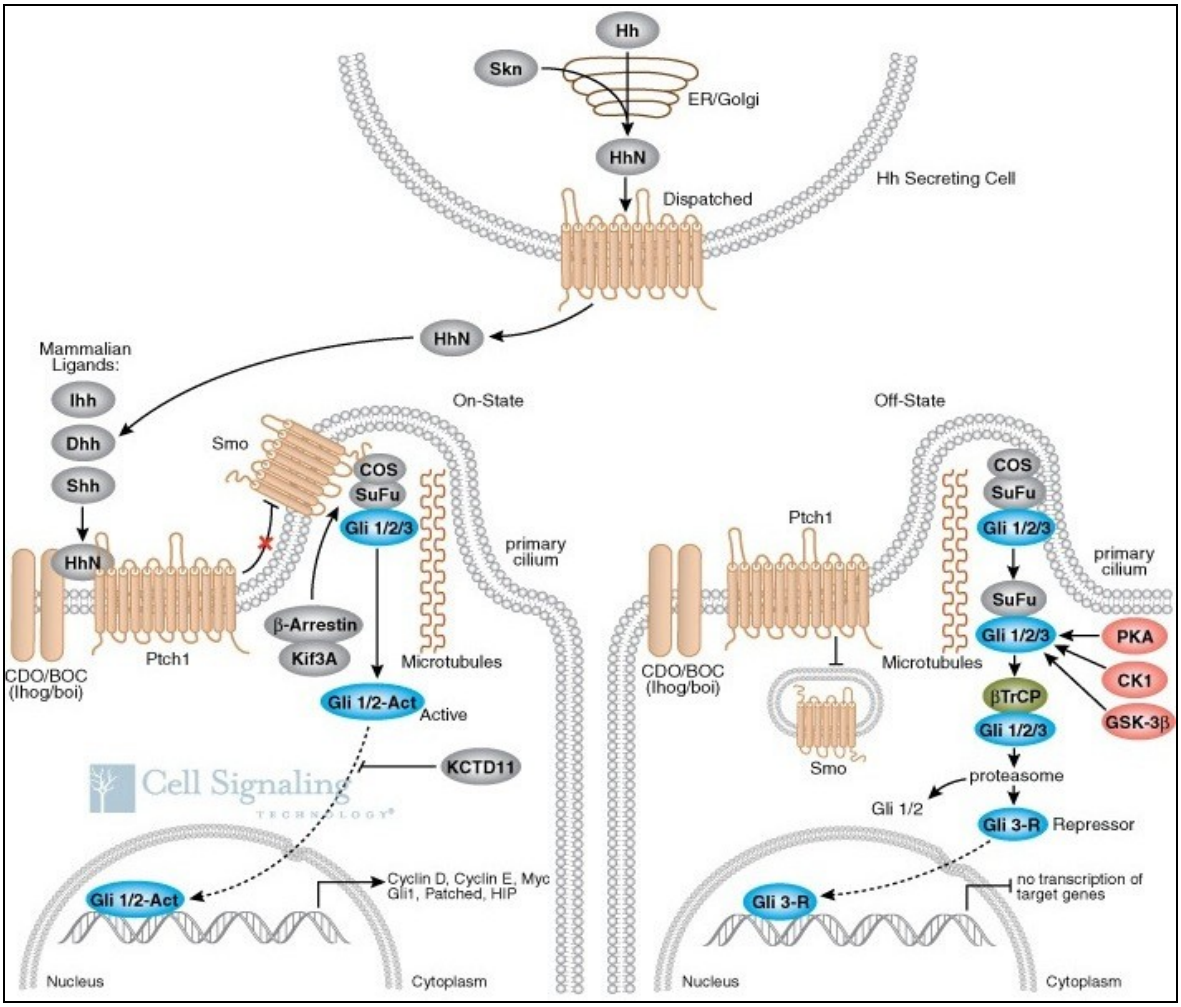

Figure 1.6. Mechanisms of activation of Hegehog signalling. In the absence of hedgehog ligand in the receiving cell (Off-state), the receptor for hedgehog-family ligands, patched, represses the activity of another transmembrane protein called smoothened. In the On-state, hedgehog binding to Patched leads to activation and translocation of Smoothened to the primary cilium. Consequently, the conserved action of hedgehog ligands is to switch the Gli-factors from being transcriptional repressors to activators [Cell signalling technology©].

1.6 Medulloblastoma (MB)

Survival rates of pediatric brain tumour patients have significantly improved over the years due to developments in diagnostic techniques, neurosurgery, chemotherapy, radiotherapy, and supportive care. However, the causes of pediatric brain tumours are largely unknown. Environmental factors, such as smoking, diet, and other exposures, do not predispose the brain to develop tumours. Only a very small proportion of brain tumours are caused by hereditary gene defects, irradiation, or immune suppression. Medulloblastomas are the most common cerebellar tumours of central nervous system in childhood. They are neuroepithelial tumours arising from the cerebellum and account for ~20% of all intracranial tumours in children, and for 40% of all childhood posterior fossa tumours [Crawford J. R., *et at.* 2007]. Although medulloblastoma peaks at 8 years of age, ~ 30% of medulloblastomas occur in adults. Historically, medulloblastomas and other central nervous system embryonal tumours are classified on the basis of their location and of their histological features [Ellison D. 2002], [Rossi A., *et al*. 2008]. Although most medulloblastomas occur sporadically, some may arise within patients with known familial cancer syndromes. As a group, the familial cancer syndromes provide us with clues regarding embryonic alterations in key signalling or growth factor activation pathways that must be involved in the pathogenesis of medulloblastoma. As a rule, these growth factor families, including Hh, Wnt, and Notch pathways, control embryonic patterning and cell fate determination in species ranging from *Drosophila* to humans (figure 1.7) [Dahmane N., *et al.* 1999], [De Bont J. M., *et al*. 2008] [Wechsler Reya R., *et al*. 2001]. They also regulate the development of the cerebellum including the proliferation of the granule cells in the external granular layer, the site of origin of at least a subset of medulloblastomas. In addition, there is now strong evidence that suggests that normal embryogenesis and tumourigenesis share many properties involving alterations in cell proliferation, differentiation, motility, angiogenesis, apoptosis, and stem cell control. It is commonly believed now, and in fact has been shown, that certain genes that are involved in normal neuro-embryogenesis, if deregulated, will contribute to medulloblastoma formation [Carlotti Jr C.G., *et al*. 2008]. Several observations suggest that alterations of molecular events regulating the development of cerebellum are responsible for uncontrolled cell growth, eventually leading to medulloblastoma formation. The cerebellum is composed of different cell layers, including granule cells and Purkinije cells. During development, cerebellar granule cell progenitors GCPs migrate from the rhombic lip over the outer layer of the cerebellar surface (external granule layer); after an initial burst of cell proliferation, they start a differentiation program by exiting the cell cycle and moving into the inner EGL. They migrate farther inward into the internal granule layer (IGL), where differentiated granule neurons reside. There is considerable evidence that factors secreted by Purkinije cells regulate the proliferation of GCPs in the EGL. In particular, Purkinije cells secrete Sonic Hedgehog (Shh) that is involved in the initial EGL cell population expansion and is the most potent mitogen for GCPs, whereas what causes GCPs to stop dividing in the inner EGL is not well understood. Importantly, failure to contain the proliferation of developing GCPs is involved in tumorigenesis, because constitutive activation of the Hedgehog pathway is responsible for medulloblastoma development (figure 1.8) [Wechsler Reya R.J., *et al*. 1999], [Ruiz et Altaba A., *et al*. 2002], [Lai K., *et al.* 2003], [Argenti B., *et al.* 2005], [Thompson M. C., *et al.* 2006], [Carlotti C. G., *et al.* 2008]. Among the different alterations observed in medulloblastoma, the most frequent one is represented by

allelic deletion on the short arm of chromosome 17, occurring in up to 50% of tumours and frequently restricted to a common region at 17p13.2-13.3. However, the identification of candidate tumour suppressors located in this region has been so far elusive. *p53*, one of the most important tumour suppressor genes, was initially suggested to be of importance in medulloblastoma, because it is localized on chromosome region 17p13. However, it is shown that the incidence of *p53* mutations in sporadic medulloblastoma is low. Besides *p53*, several other candidate tumour suppressor genes on 17p have been suggested. Interestingly, 17p carries several genes suggested to be involved in the regulation of SHH signalling. ren^{KCTD11}, a putative tumour suppressor gene located on chromosome 17p13.2, is deleted in 39% of medulloblastomas. REN^{KCTD11} is haplo-insufficient in several human MB, as a consequence of allelic deletion, in association with down-regulated expression [Di Marcotullio L., *et al*. 2004], [De Smaele E., *et al*. 2004], [Ferretti E., *et al.* 2005]. Additional knowledge about the biological characteristics of pediatric brain tumours may provide new information about pathogenesis, facilitate diagnosis, contribute to better risk-group stratification for therapy, or be used to develop new therapeutic targets. A major hope for the future is that the incorporation of biological agents targeting specific signalling pathways will not only make treatment more effective, but also allow a reduction in neurotoxic therapy [Gilbertson R. J., 2004], [Marino S., *et al.* 2005], [Grill J., *et al.* 2007].

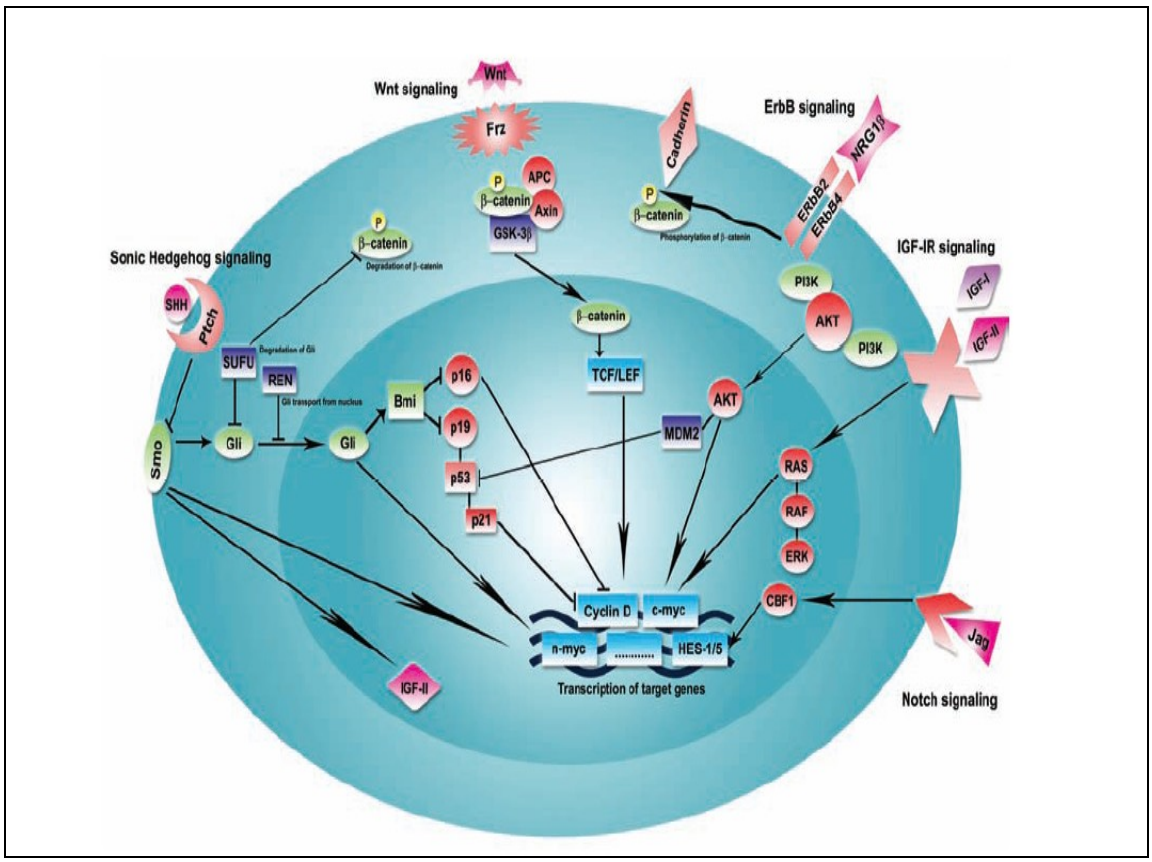

Figure 1.7. Signalling pathways involved in the development of the brain and pathogenesis of medulloblastoma. Interactions among these pathways are multiple and complex. Deregulation of these pathways is important in the pathogenesis of medulloblastoma [De Bont J.M., *et al.* 2008].

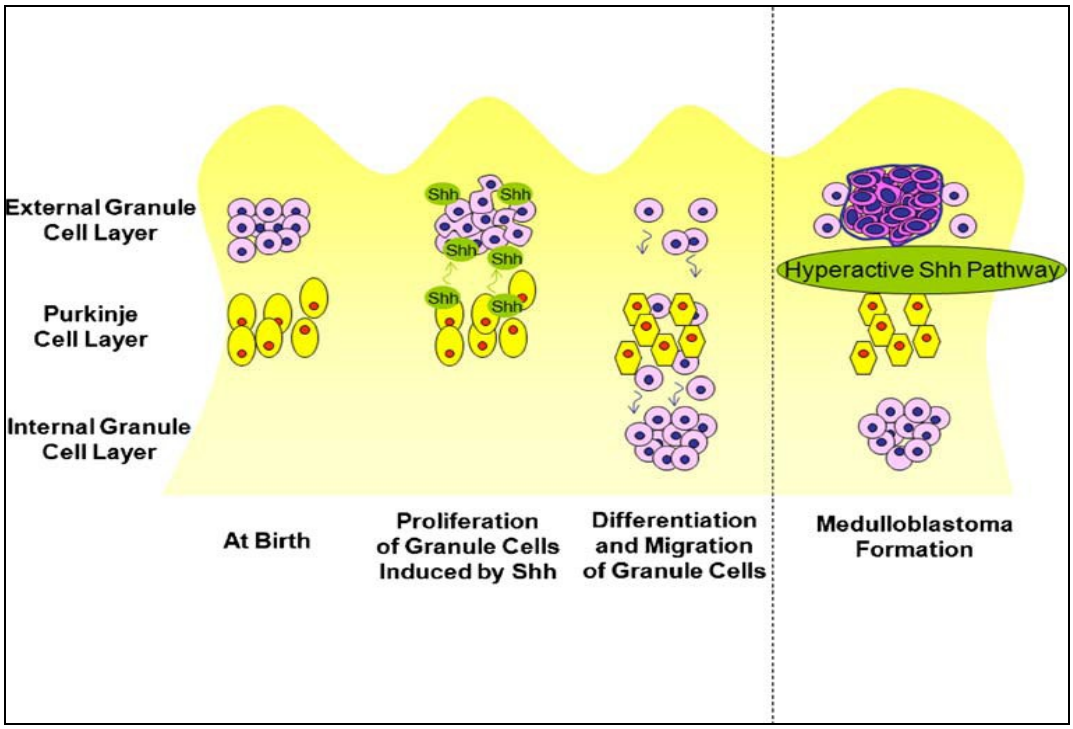

Figure 1.8. In neuro-embryogenesis the cerebellum is comprised of external granule cell and Purkinje cell layers. What ensues at birth is a proliferation of external granule cells as induced by Shh as secreted by the Purkinje cells. Then, there is differentiation and migration of the external granule cells as they move past the Purkinje cells to help form the internal granule cell layer. In the context of overactive Shh signalling, there is uncontrolled proliferation of the external granule cells with medulloblastoma formation [Carlotti C.G., *et al.* 2008].

1.7 REN^{KCTD11}

REN^{KCTD11} (retinoic acid (RA), epithelial growth factor (EGF) and nerve growth factor (NGF) responsive gene) represents a novel component of the neurogenic signalling cascade and is both a marker and a regulator of neuronal differentiation. The sequence exhibits no significant homology with previously described murine or human genes nor carries putative functional domains observed in other classes of proteins, with the exception of a BTB/POZ motif located at the N-terminus between amino acid residues 21 and 77 (figure 1.9 and 1.10). REN^{KCTD11} regulation is at the cross-roads of several neurogenic signals characterized by diverging outputs. REN^{KCTD11} expression is specifically enhanced by EGF receptor/ErbB1-generated signals that are reported to regulate cerebellar development, being involved in all phases of neurogenesis, including enhanced proliferation of EGL granule progenitors and their migration and differentiation phases. REN^{KCTD11} is up regulated by RA and NGF also that, conversely, promote growth arrest and neuronal differentiation [Gallo R., *et al*. 2002]. Consistent with these observations, REN^{KCTD11} expression is mainly restricted to embryonal life and is developmentally regulated. An active role in neurogenesis is suggested by the ability of REN^{KCTD11} to promote neural cell growth arrest and to antagonize EGF-induced mitogenesis and neuronal differentiation of neural progenitors. A dysfunctional REN^{KCTD11} is expected to be associated with

medulloblastoma. REN^{KCTD11} is a candidate for playing such a role in EGL development, as suggested by the following evidence. First, REN^{KCTD11} expression inversely correlates with granule cell proliferation along the transition from outer to inner EGL GCPs and in IGL cells of the developing cerebellum. Such a cell maturation process *in vivo* is paralleled by the up regulation of REN^{KCTD11} expression also occurring along GCP differentiation in culture. Second, REN^{KCTD11} is able to inhibit Shh-dependent events, thus antagonizing both Shh induced growth and block of differentiation of cultured GCPs. Finally, an active role for REN^{KCTD11} is also suggested by the requirement of REN^{KCTD11} expression to restrain Hedgehog signalling and cell growth and to promote the differentiation of cultured GCPs. These observations strongly support the notion that REN^{KCTD11} may be involved in the control of the expansion of GCPs during the transition from outer to inner EGL (Argenti B., *et al.* 2005). The loss of function of REN^{KCTD11}, as a consequence of cancer associated genetic–epigenetic events, might relieve a restraint of Hedgehog signalling at the transition from outer to inner EGL GCP and withdraw a limiting signal for immature cell expansion, thus favouring tumourigenic events. Indeed, has been recently reported that human REN^{KCTD11} is haplo-insufficient (as a consequence of hemizygosity and significantly reduced expression with respect to normal cerebellar tissue) in all medulloblastomas bearing the 17p loss, while downregulated expression is observed also in bi-allelic tumours. Treatment with the demethylating agent 5'-azacytidine restores higher levels of gene expression, suggesting that the low REN^{KCTD11} expression is also due to active gene silencing in medulloblastoma. Interestingly, the inappropriate activation of HH signalling detected in medulloblastoma cells is specifically targeted by REN^{KCTD11} which inhibits cell growth by antagonizing Gli1-mediated transactivation of HH target genes via impairment of Gli1 nuclear transfer. Therefore, REN^{KCTD11} is a novel suppressor of HH signalling and its inactivation, due to 17p loss, might lead to a deregulation of the tumour promoting HH pathway. REN^{KCTD11} inhibits medulloblastoma cell proliferation by antagonizing the activation of SHH target genes. Deletion of this gene might thus result in enhanced SHH signalling and increased proliferation of granule cell precursors (figure 1.11) [Di Marcotullio L., *et al*. 2004] [De Smaele E., *et al*. 2004].

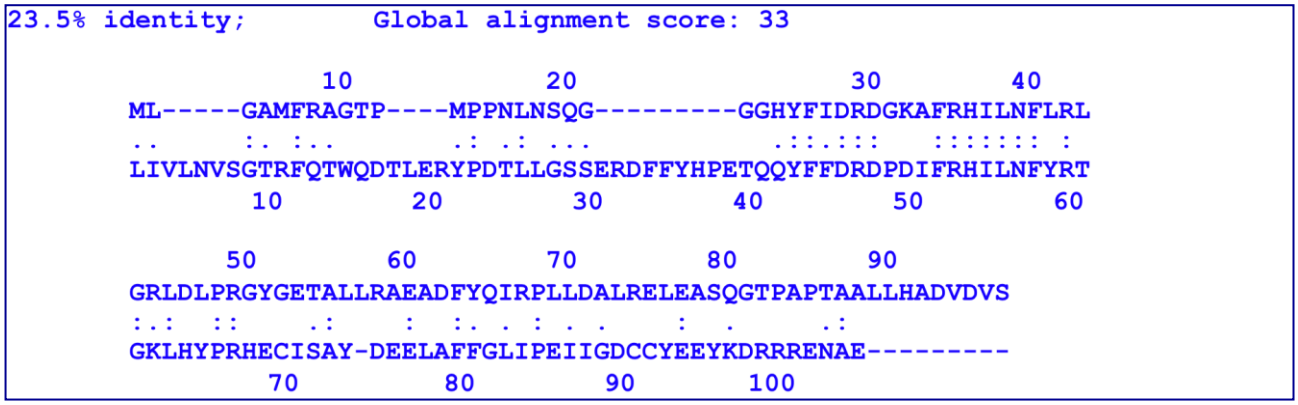

Figure 1.9. Sequence alignment of REN^{KCTD11} and Kv4 tetramerization domain.

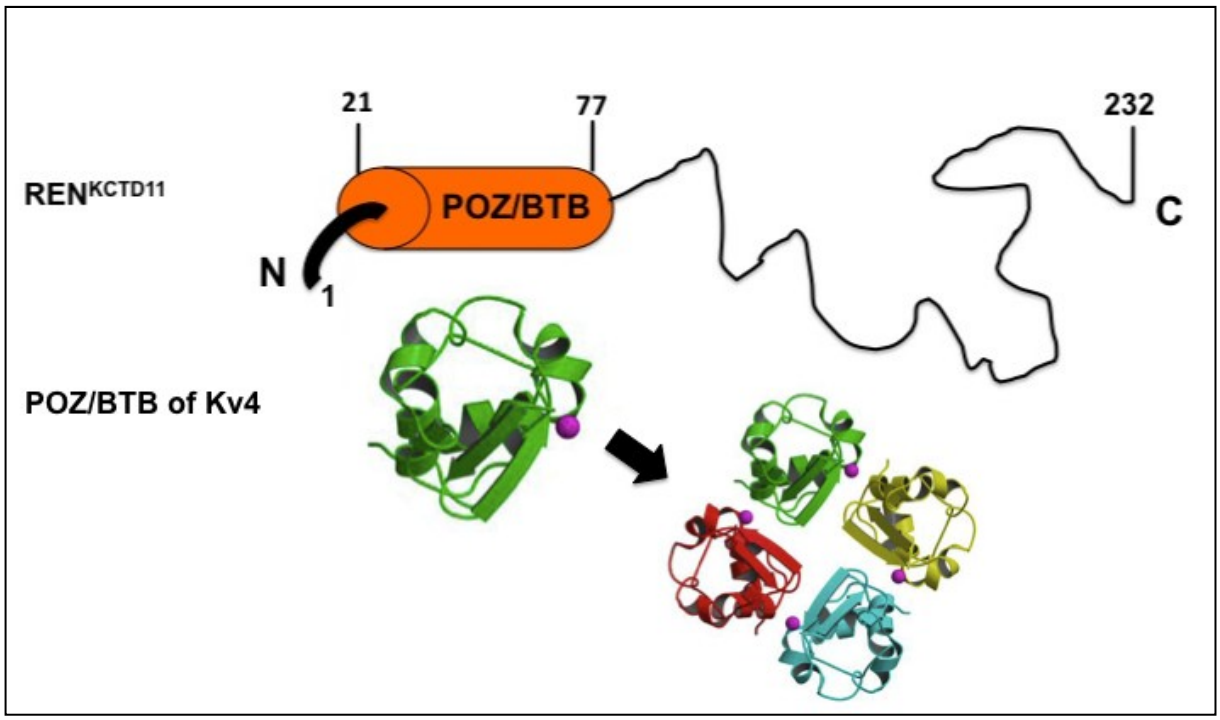

Figure 1.10. Fragments of REN^{KCTD11} that show significant sequence similarity with proteins with known 3D structure.

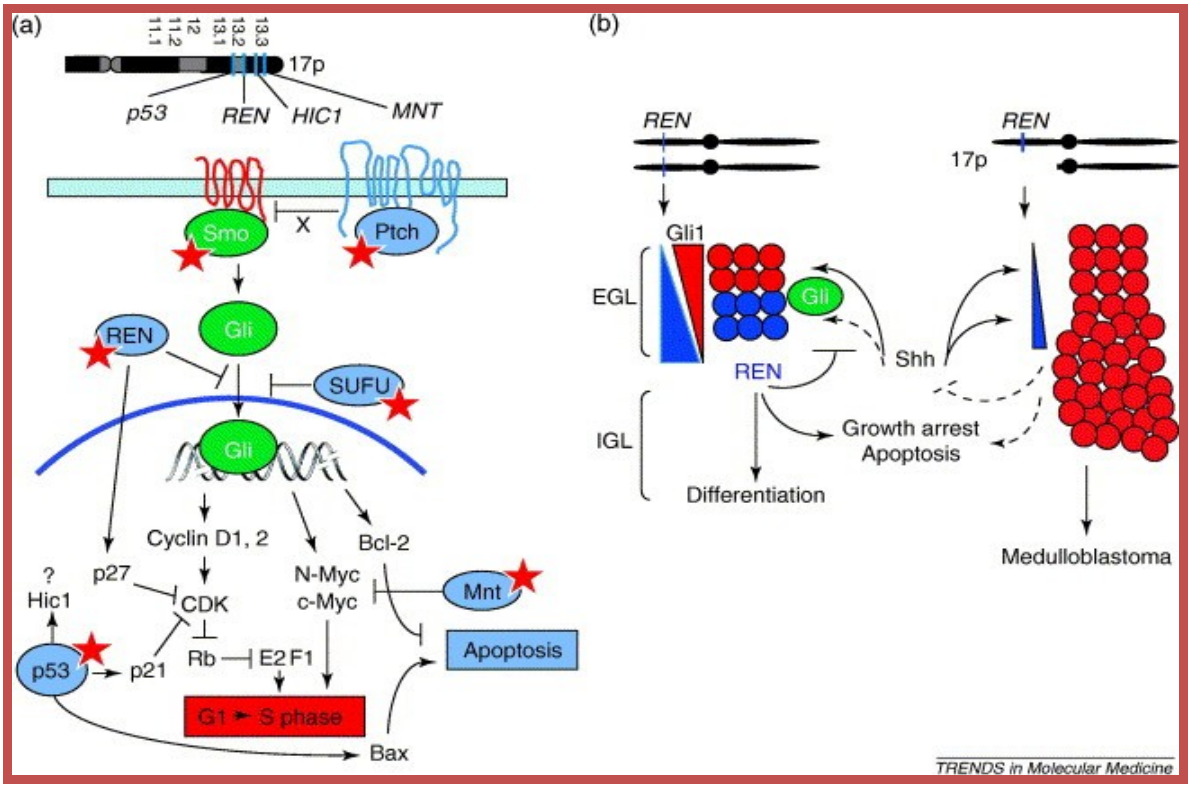

Figure 1.11. Hedgehog antagonists encoding genes mapping to chromosome 17p13.2.13.3. 17p-associated Hedgehog antagonist gene products suppress Gli nuclear transfer (REN^{KCTD11}) or the function of Hedgehog target genes [Ferretti E., *et al.* 2005].

1.8 The aim of the work

REN^{KCTD11} represents a restraint of Shh signalling and its loss of function might favour tumorigenesis. Since no information is available in the literature on the structure of REN^{KCTD11}, the aim of this PhD thesis has been the biochemical characterization of this protein. Subsequently, on the basis of sequence identity found between the N-terminal REN^{KCTD11} domain (POZ/BTB) and the tetramerization domain of the potassium channel KV4, a three-dimensional model was designed for the N-terminal region of the protein, to identify aminoacid residues of REN^{KCTD11} crucial for the oligomerization status, stability and interaction with its partner Cul3. REN^{KCTD11} function carries on through a network of protein-protein interactions finely regulated. So, a further aim of this project has been to provide the structural basis for the design of small molecules that mimic the biological activity of REN^{KCTD11} and to test them by immunological assays and NMR studies. Moreover, other POZ/BTB proteins, like KCTD5, have been object of this thesis in order to evaluate the biotechnological application of the identified molecules as agonist or antagonist of KCTD proteins involved in de-regulated pathways.

2 MATERIALS AND METHODS

2.1 Strains, enzymes, reagents and instruments

Reagents used for preparation of buffers and growth media of *Escherichia coli* and the reagents for polyacrylamide gels electrophoresis (Acrylamide, APS, TEMED, SDS, Tris, Glycine) were supplied by Sigma Aldrich, Euroclone, Applichem and ICN Biomedicals. The molecular weight markers for proteins were from Sigma Aldrich. The restriction enzymes and the modification enzymes (calf intestine phosphatase and T4 DNA ligase) were supplied by New England Biolabs (NEB) and the molecular weight markers for nucleic acids were from NEB and Roche. The *Pfu Turbo* polymerase (2.5 U/µL) was supplied by Stratagene, while *Taq* DNA polymerase (5 U/µL) was from NEB. The synthesis of the oligonucleotides was committed at Sigma-Genosys; pETM11, pETM20, pETM30 and pETM41 *E. coli* expression plasmids were supplied by Novagen; gene constructs cloned in pRSETb were kindly provided by prof. Alberto Gulino (Department of Experimental Medicine and Pathology, University La Sapienza of Rome), while pET28a/*kctd5N-module* vector was supplied by prof. Steve A. N. Goldstein (Department of Pediatrics and Institute of Molecular Pediatric Sciences, University of Chicago). *E. coli* TOPF'10 strain, used for cloning, was supplied by Invitrogen; *E. coli* BL21*CodonPlus*(DE3)RIL cells, used for overexpression, were supplied by Stratagene. BL21(DE3), BL21(DE3)STAR and JM101 strains were supplied by Invitrogen, while Rosetta-GAMI(DE3) were from Novagen. Complete Protease Inhibitor Cocktail Tablets were supplied by Roche and used as a mixture of protease inhibitors, according to manufacturer's instruction. Ethanol, methanol, isopropilic alcohol and acetic acid were supplied by J.T. Baker. TFA was from Fluka. Identity of protein samples and of tryptic digestion products were assessed by liquid chromatography mass spectrometry (LC-MS) performed on Phenomenex Jupiter C4 and C18 columns, connected to a Thermo Electron Corporation mass spectrometer, equipped with an ESI source. Light scattering studies were performed on a miniDAWN™ TREOS triple-angle light scattering detector, and a Shodex RI-101 refractive index detector, supplied by Wyatt Technology Corporation. All size exclusion and affinity chromatography columns were connected to AKTA Purifier and FPLC systems (GE-Healthcare).

2.2 Antibiotics

Ampicillin (supplied by Sigma Aldrich as ampicillin sodium salt) and kanamycin (supplied by Sigma Aldrich as kanamycin sulphate) were solubilized in deionized water at a concentration of 1000X, filter sterilized and stored at –20 °C until use. Ampicillin was used at a concentration of 100 µg/mL and kanamycin was used at a concentration of 50 µg/mL in both solid and liquid media. Chloramphenicol and tetracycline were solubilized in ethanol 96% and used at a concentration of 33 µg/mL and 12.5 µg/mL, respectively.

2.3 *E. coli* cells transformation techniques

2.3.1 Preparation of *E. coli* TOPF'10 cells and transformation by electroporation

2.5 mL of an overnight culture of *E. coli* TOPF'10 cells were inoculated into 250 mL of LB medium. The cells were grown up to mid-log phase (0.6 OD_{600nm}) at 37 °C, stored on ice for 30 min and then harvested by centrifugation (6000 rpm, 10 min, 4 °C). The pellet was washed in 250 mL of sterile water. After the second centrifugation the cells were washed in 125 mL of sterile water. The third washing was performed in 5 mL 10% glycerol; the cells were then harvested by centrifugation and the pellet was resuspended in 750 µL of 10% glycerol. Aliquots of 10^{10} cells/mL (40 µL) were mixed with 1 µL of the DNA ligase reaction, incubated for 1 min on ice and transferred into chilled plastic cuvettes with an electrode gap of 0.2 cm (M-Medical). High voltage electroporation (25 µF) was performed with a Bio-Rad Gene Pulser Xcell^{TM} at a field strength of 2.5 kV/cm and 200 Ohm. A shock pulse was applied to competent cells producing pulse length of ~5.0-5.5 ms. Immediately after electroporation cell mixtures were diluted to 1 mL with LB medium and incubated for ~1 h at 37 °C under shaking. The cells were then plated onto selective solid medium supplemented with 100 µg/mL ampicillin, 33 µg/mL chloramphenicol or 50 µg/mL kanamycin to isolate the recombinant clones. Single clones were inoculated in 5 mL LB medium with the same antibiotics and grown over night at 37 °C under shaking. Finally, were harvested by centrifugation (13000 rpm, 2 min, 4 °C) and processed to extract plasmidic DNA by using the *QIAprep Spin Miniprep Kit* or the *QIAGEN plasmid Maxi Kit* (both supplied by Qiagen).

2.3.2 Preparation of *E. coli* competent cells and transformation by heat shock

Single clones of *E. coli* strains, grown at 37 °C in LB agar, were inoculated into 2.5 mL of LB medium and incubated overnight at 37 °C on a shaker. The cells were inoculated into 250 mL of LB medium and the culture was grown up to mid-log phase (0.6 OD_{600nm}) at 37 °C, stored on ice for 30 min and then harvested by centrifugation (6000 rpm, 10 min, 4 °C). The pellet was washed in 125 mL of cold 50 mM $CaCl_2$ and stored on ice for 30 min. Successively, the cells were harvested by centrifugation and the pellet resuspended in 16 mL of cold 50 mM $CaCl_2$. Aliquots of 200 µL of competent cells were mixed with 50 ng of plasmidic DNA and stored on ice for 30 min. The cells mixtures were transferred at 42 °C for 90 sec, on ice for 2 min (heat shock) and then diluted to 1 mL with LB medium. An incubation of 1 h at 37 °C under shaking was performed before plating the cells onto selective solid medium supplemented with the opportune antibiotics, depending on the strain.

2.4 Expression in *E. coli* of *poz/btb*^{kctd11}, *ren*^{kctd11} ("long form"), *poz/btb*^{kctd21} and *kctd21*

2.4.1 Cloning of different constructs

Genes were amplified by PCR from genomic DNA. The amplification was performed by using the following couples of primers (the residue numeration is referred to the new translation start point):

poz/btb ^{kctd11} (+15 - +116):
Forward: 5'-CATGCCATGGGCCCCGTGACCCTGAA-3'
Reverse: 5'-CCGCTCGAGTTACCTCCAGTTCCCGCAG-3'

poz/btb ^{kctd11} (+15 – +125):
Forward: 5'-CATGCCATGGGCCCCGTGACCCTGAA-3'
Reverse: 5'-CCGCTCGAGTTATGTGGGTGCAGGGG-3'

poz/btb ^{kctd11} (+15 - +134):
Forward: 5'-CATGCCATGGGCCCCGTGACCCTGAA-3'
Reverse: 5'-CCGCTCGAGTTAATCTACATCTGCGTGGAGC-3'

poz ^{kctd11} (+15 - +146):
Forward: 5'-CATGCCATGGGCCCCGTGACCCTGAA-3'
Reverse: 5'-CCGCTCGAGTTAAGAGAAGTGCACCAGGC-3'

poz ^{kctd11} (+1 - +125):
Forward: 5'-CATGCCATGGCCAAAATTTCTCCTCCTCC-3'
Reverse: 5'-CCGCTCGAGTTACCTCCAGTTCCCGCAG-3'

ren^{kctd11} (+1 - +271):
Forward: 5'-CATGCCATGGCCAAAATTTCTCCTCCTCC-3'
Reverse: 5'-CCGCTCGAGTCAGTGCCGGAC-3'

poz^{kctd21}
Forward: 5'-CATGCCATGGCATCCGACCCCATCACGCTG-3'
Reverse: 5'-CCGCTCGAGTTAACGCTGGTTCAGTGTGATG-3'

kctd21
Forward: 5'-CATGCCATGGCATCCGACCCCATCACGCTG-3'
Reverse: 5'-CCGCTCGAGTTACCTGTACCGTATTAATCG-3'

The forward primers indicated above contained the *Nco* I restriction site, while the reverse primers were designed with the *Xho* I restriction site (underlined in the sequences) and a codon stop at the end of the construct (highlighted in the sequences).
All amplification reactions were performed in a final volume of 50 µL, using 50 ng of template DNA. The reaction mixture contained the specific primers (0.25 µM each), dNTPs (0.25 mM each) and the *Pfu turbo* polymerase (5U) with its buffer 1x.
PCR was performed using an *Eppendorf Mastercycler personal* apparatus, following the procedure indicated below:

- ✓ Initial denaturation (step 1) 3 min at 95 °C
- ✓ Denaturation (step 2) 1 min at 95 °C
- ✓ Annealing (step 3) 1 min at the convenient temperature for each gene amplified
- ✓ Elongation (step 4) 1 min at 72 °C
  for 30 cycles, from step 2.
- ✓ Elongation (step 5) 10 min at 72 °C

All amplification products were analyzed by 1% agarose (Euroclone) gel electrophoresis performed in TAE buffer (18.6 g/L EDTA, 242 g/L Tris base. Add Acetic acid until pH 7.8). PCR products were purified by using the *QIAquick PCR Purification Kit* (Qiagen), and digested with *Nco* I (20 U/µL) and *Xho* I (20 U/µL) restriction enzymes. Each amplified fragment (1µg) was digested with 4 U of restriction enzymes for 3 h at 37 ºC in a buffer containing 50 mM NaCl, 10 mM Tris-HCl, 10 mM $MgCl_2$, 1 mM DTT pH 7.9 supplemented with BSA 100 µg/mL. Following the digestion, each fragment was cloned into the corresponding sites of the pETM11 expression vector, downstream to the His-tag sequence. To this purpose, the expression vector was previously digested with the same restriction enzymes (4 U/µg), and treated with calf intestine phosphatase (CIP, 10 U) (NEB) for 30 min at 37 ºC. CIP enzyme (10 U/µL) was then inactivated at 75 °C for 10 min. After digestion, PCR amplifications were purified by *QIAquick PCR Purification Kit*, while the *Nco*I/*Xho*I pETM11 was purified by *QIAquick Gel Extraction Kit* (Qiagen). For ligation reactions was used a 1:3 molar ratio (vector/insert DNA). The reactions were performed using 20 U/µg DNA of the T4 DNA Ligase (400 U/µL), in a final volume of 10 µL, for 3 h at RT. *E. coli* TOPF'10 strain was used for cloning. The identity of the inserts in the resulting recombinant plasmids was confirmed by DNA sequencing (MWG-Biotech). Positive gene constructs were transferred into pETM20 expression vector by subcloning. *ren*^{kctd11} ("long form") and *kctd21* genes were also subcloned in pETM30 and pETM41 expression vectors.

2.4.2 *poz/btb* ^{kctd11} gene mutagenesis

Asp69, Arg74, Asn78 and Arg81 residues of POZ/BTB^{kctd11} domain were mutated in alanine by using the QuikChange Site Directed Mutagenesis Kit (Stratagene). The primers employed for mutagenesis PCR reaction are reported below:

Forward:
5'-ACCGGGCTGGCAAGGCCTTCGCGCACATCCTCGCTTTCCTGGCGGG-3'
Reverse:
5'-CCCAGCGCCAGGAAAGCGAGGATGTGCGCGAAGGCCTTGCCAGCCCGGT-3'

Codons corresponding to the mutated aminoacids are underlined in primers sequences. The recombinant construct pETM20/*ren*^{kctd11} was used as template. The PCR reaction was performed, according to the Kit instructions, following the procedure indicated below:

- ✓ Initial denaturation step (step 1) 1 min at 95 °C
- ✓ Denaturation (step 2) 50 sec at 95 °C
- ✓ Annealing (step 3) 50 sec at 58 °C
- ✓ Elongation (step 4) 1 min at 68 °C
  for 16 cycles from step 2.

XL1-Blue supercompetent cells (supplied by the mutagenesis Kit) were used for the transformation of the circular nicked dsDNA, obtained by digesting the methylated, non-mutated, parental DNA from PCR with the restriction enzyme *Dpn*I (10 U/µL), for 2 h at 37 °C. The right insertion of desired mutations was confirmed by DNA sequencing.

2.4.3 Expression vector properties

pET plasmids were chosen as they represent a powerful host-vector system for cloning and expression of recombinant proteins in *E. coli*. All of them contain a strong promoter from T7 bacteriophage, for chemical induction and overexpression of recombinant proteins, a multiple cloning site (MCS) and a TEV protease recognition site for cleaving the fusion protein. In particular, pETM11 contains only a 6xHistidine-tag while to improve the solubility of the gene products pETM20 contains a 6xHistidine-TrxA fusion tag, pETM30 a 6xHistidine-GST fusion tag, and pETM41 a 6xHistidine-MBP fusion tag (figure 2.1, 2.2, 2.3 and 2.4).

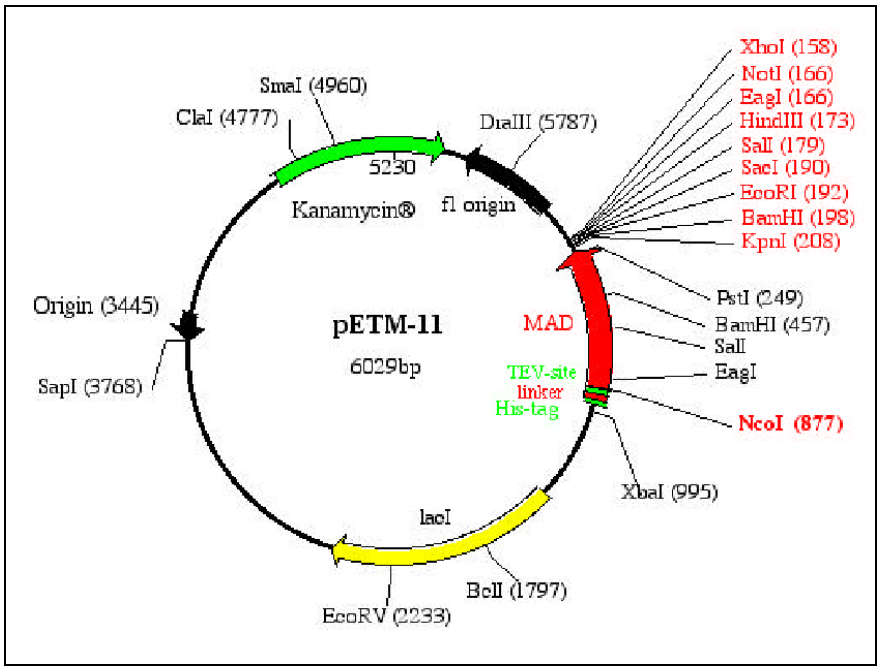

Figure 2.1. Map of expression vector pETM11.

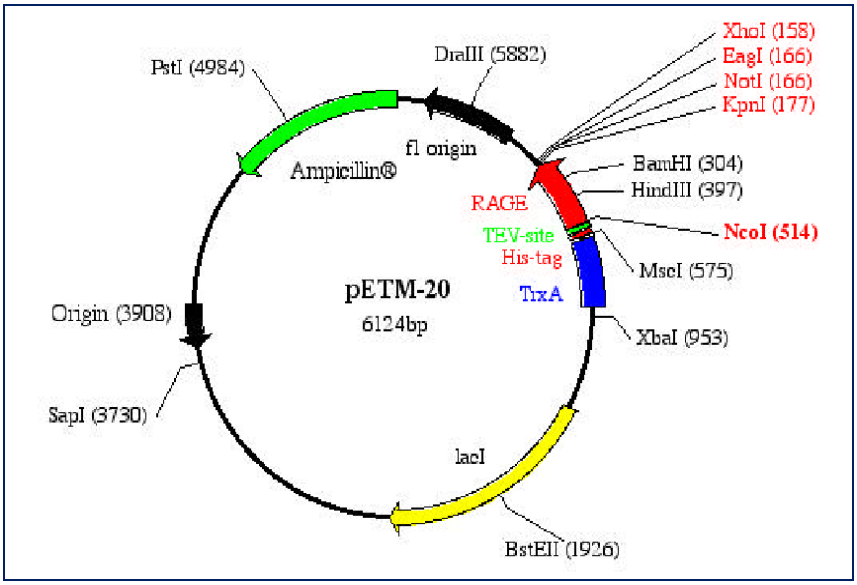

Figure 2.2. Map of expression vector pETM20.

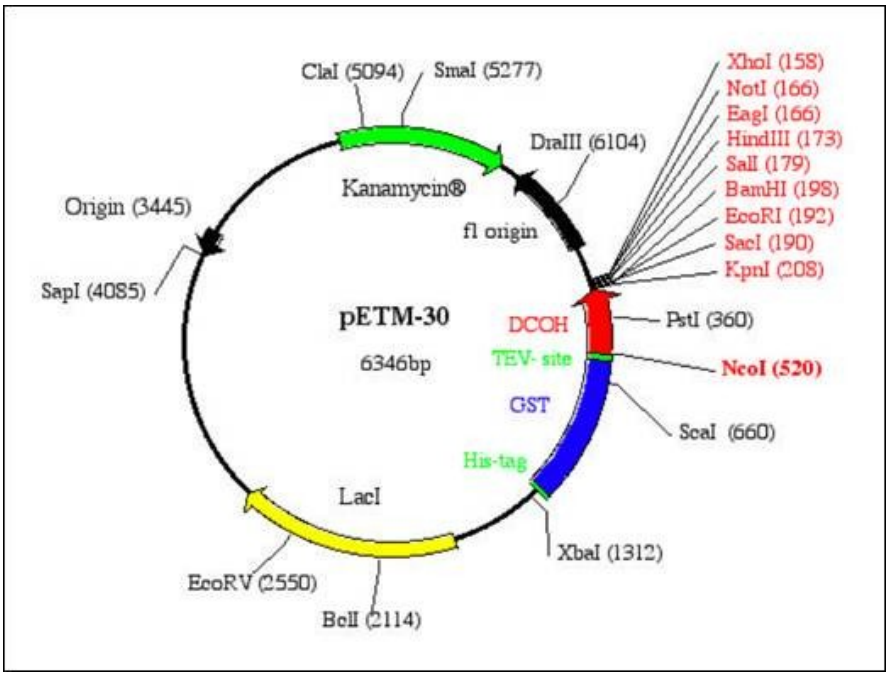

Figure 2.3. Map of expression vector pETM30.

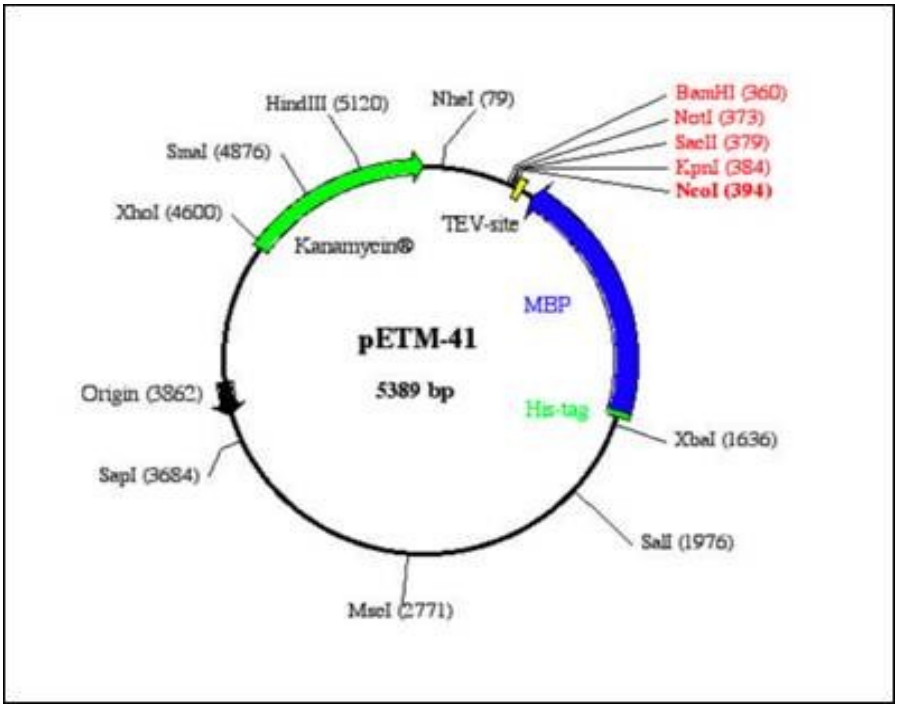

Figure 2.4. Map of expression vector pETM41.

2.4.4 Large-scale expression

After a first screening of small-scale expression cultures, performed using different strains, temperatures, IPTG concentration and induction length, recombinant constructs were transferred into *E. coli* strain that assured the best expression level in soluble phase. Single clones of *E. coli* strain, previously transformed with each recombinant expression vector and grown at 37 ºC on LB agar containing the appropriate antibiotic, were inoculated into 10 mL of LB medium, containing the same antibiotic. The overnight cultures were inoculated into 1L of pre-warmed LB medium. Cultures were grown at 37 °C under shaking until they reached the mid-log phase (0.7/0.8 OD_{600nm}); then, they were induced with the optimal IPTG concentration and growth was proceeded at 22° or 37 °C as appropriate. After 3 or 16 h the cells were harvested by centrifugation (6000 rpm, 15 min, 4 °C). Cell pellets were resuspended in a lysis buffer containing 50 mM Tris/HCl pH 8.0, 150 mM NaCl and protease inhibitors. The suspension was sonicated for 10 min, by using a Misonix Sonicator 3000 apparatus with a micro tip probe and an impulse output of 1.5/2 (=9/12 Watt). Bacterial lysates were then centrifuged (16000 rpm, 30 min, 4 °C) and the surnatant (soluble fraction) was collected and analyzed by SDS-PAGE to assess the presence of recombinant products of interest.

2.4.5 Purification of 6xHis-TrxA/MBP/GST tagged proteins

Lysates containing tagged recombinant proteins were purified by affinity chromatography onto HisTrap columns connected to an AKTA-FPLC system. Before loading the lysate, the resin was extensively washed with water and then equilibrated in buffer A (50 mM Tris/HCl pH 8.0, 300 mM NaCl). The lysate was loaded in presence of 10 mM imidazole to avoid non-specific binding of *E. coli* contaminants. Flow-through containing all unbound proteins was collected and the resin was washed with buffer A; finally His-tagged proteins were eluted with high concentrations of imidazole (300 mM). All collected pools (flow-through, washes and elutions) were analyzed on SDS–PAGE gels and stained with Coomassie Brilliant Blue R-250. Pools of interest were dialyzed to remove imidazole by using Spectra/Por membranes with the appropriate MWCO.

2.4.6 TEV digestion of tagged proteins

After purification by affinity chromatography, all partner-tagged proteins were dialyzed overnight against TEV buffer (50 mM Tris/HCl, pH 7.0/8.0) at 4 °C. TEV protease was added to protein substrates, using a molar ratio (protease : substrate) of 1 : 50; the cleavage was allowed to proceed 3 h at 30 °C. Cleavage products were analyzed by polyacrylamide gel electrophoresis; then, mixture was loaded onto an HisTrap column and purification was performed in the same conditions described above: protein product of interest was eluted in flow-through, while the fusion partner and un-cut complexes were bound to resin and removed with imidazole.

2.4.7 Size Exclusion Chromatography

Size exclusion chromatography was performed to purify all recombinant proteins by removing aggregates and contaminants. Runs were carried-out at a flow of 1 ml/min onto a Superdex-200 and Superdex-75 16/60, Superdex-200 and Superdex-75 10/300 columns connected to an AKTA Purifier system, in 50 mM Tris/HCl pH 8.0 and 150 mM NaCl. Molecular weight standards from GE-Healthcare were used to calibrate column. Pools of interest were concentrated on Amicon-Ultra membranes (Millipore).

2.5 PROTEINS ANALYSES

2.5.1 Determination of the protein concentration

The concentration of the proteins in solution was determined according to the Bradford's method (Bradford, 1976). The Coomassie Brilliant (Bio-Rad) reagent was added to the samples and the absorbance at 595_{nm} was monitored. A solution of bovine serum albumin (BSA) was used as standard. Protein concentration was also measured by UV spectroscopy, reading the tryptophan absorbance at 280_{nm}, using a Jasco V-550 UV-VIS spectrophotometer, in a 1 cm quartz cell.

2.5.2 Electrophoretic analysis of proteins (SDS-PAGE)

The electrophoresis on 12%, 15% or 18% polyacrylamide gel in denaturing conditions was performed according to Laemmli's protocol (Laemmli, 1970). The samples were denatured at 100°C for 10 min in 1% SDS (Applichem), 5% β-mercaptoethanol (Sigma), 0.001% bromophenol blue (ICN Biomedicals) and 10% glycerol (Applichem). The samples were then loaded on a polyacrylamide gel and the electrophoresis was performed in 0.025 M Tris/HCl, 0.2 M glycine pH 8.3 and 0.1% SDS, at 30 mA for ~1 h. The proteins were then revealed by Coomassie Brilliant-Blue (Applichem) staining; the gel was submerged in the staining solution (0.1% Coomassie Brilliant-Blue R250, 25% isopropilic alcohol and 10% acetic acid) for 30 min with gentle agitation. The gel was washed in a solution containing 30% ethanol and 10% acetic acid to remove the excess of Coomassie and then stored in 10% acetic acid. For silver staining, the gel was extensively washed in deionised water, submerged in the sensibilization solution A (25% ethanol, 0.5 M potassium acetate, 0.5% glutaraldehyde, 0.3% potassium tetrathionate) and washed again in deionised water for 2 times for 10 min each. Then, the gel was equilibrated in solution B (0.2% silver nitrate, 0.009% formaldehyde) and stained in solution C (3% potassium carbonate, 0.001% sodium thiosulfate, 0.015% formaldehyde), in a dark box, till desired contrast was obtained; solution B and C were freshly prepared. Finally, the staining reaction was stopped with 10% acetic acid and the gel stored in water. All reagents used for silver staining were supplied from Sigma, Del Chimica and Fluka. Alternatively, the proteins were transferred by electroblotting from gel to a polyvinylidene fluoride (PVDF) membrane as described in the paragraph "Western blot analysis". For native PAGE the samples were loaded on a 10% polyacrylamide gel in 0.001% bromophenol blue and 10% glycerol and run in Tris-glycine buffer

without SDS. The electrophoresis was performed at 15 mA for 2 h, after a gel pre-run of 30 min. Then, the proteins were revealed by Coomassie Brilliant-Blue staining as described above.

2.5.3 Western Blot analysis

After gel electrophoresis, proteins were transferred to a polyvinylidene fluoride (PVDF) membrane (Immobilon-P, Millipore) in Blotting Buffer (25 mM Tris/HCl pH 8.0, 190 mM Glycine and 10% methilic alcohol) at 4 °C overnight, using a 25 V electric field. The PVDF membrane was submerged in methilic alcohol for 2 min before using, to eliminate the hydrophobic properties, washed in H_2O for 2 min and equilibrated in Blotting Buffer for 5 min. After overnight electro-blotting, membrane was stained with Ponceau Red to verify proteins transferring and incubated in the blocking solution (5% BSA in PBS buffer, containing 0.05% Tween 20) at room temperature for 1 h. It was washed with PBS buffer (137 mM NaCl, 2.7 mM KCl, 10 mM Na_2HPO_4, 2 mM KH_2PO_4 pH 7.4), containing 0.05% Tween 20, and incubated in a mouse anti-His monoclonal antibody (Sigma Aldrich) 1:1000 dilution, at room temperature for 1 h. Successively, membrane was washed with PBS buffer and incubated on a shaker, for 1 h at room temperature, in a 1:1000 dilution of horseradish peroxidase-conjugated anti-mouse antibody (Pierce), as the secondary antibody. Membrane was finally washed with PBS buffer. The detection of immunopositive species by enzyme-linked chemi-luminescence (enhanced chemi-luminescence: ECL) was performed according to the manufacturer's instructions (Super Signal®West Pico Chemiluminescent Substrate, Pierce), using a ChemiDoc XRS apparatus (Bio-Rad).

2.6 Mass spectroscopy and trypsin digestion

LC-MS, using a Phenomenex Jupiter C_{18} column (4.6 x 250 mm, 5 µm, 300Å), was performed to confirm the mass of POZ/BTB. The method developed at 1 mL/min with a linear gradient of 0.05% TFA in H_2O (buffer A) in 0.05% TFA in CH_3CN, from 5% to 70% for 30 min.
At the aim to estimate the globular state of POZ/BTB domain, a trypsin digestion was performed in 50 mM Tris-HCl pH 7.5 and 20 mM $CaCl_2$, choosing a molar ratio trypsin:POZ/BTB of 1:100. The reaction was allowed to proceed at 37 °C and was analyzed at different times (30, 45, 60, 90 min) by LC-MS, using a Phenomenex Jupiter C_4 column (250x2.00 mm, 5 µm, 300 Å) and a method developed at 0.2 mL/min with a linear gradient of 0.1% aqueous TFA in CH_3CN, from 5% to 70% for 30 min.

2.7 CD analyses

Far-UV circular dichroism spectra of POZ/BTB were obtained by using a Jasco J-715 spectropolarimeter, equipped with a PTC-423S/15 Peltier temperature controller, in a 0.1 mm quartz cell. Spectra were acquired according the following parameters: far UV range of 190-260_{nm}, band width of 1_{nm}, response of 8 sec, data pitch of 0.2_{nm} and scanning speed of 10 nm/min. Spectra were performed at 20 °C, at a protein concentration of 15 μM, in 20 mM phosphate buffer pH 7.0, with and without salts in different amounts (NaCl, $MgCl_2$, $MgSO_4$, $CoCl_2$, $ZnCl_2$ and Sodium Citrate, see "Results" for details). CD data were expressed as mean residue ellipticity (θ). Spectra processing was obtained by using the Spectra Manager software, while the analysis of the secondary structure content of the proteins was performed with neural network program: CDNN (Bohm, G. *et al*., 1992).
POZ/BTB thermal unfolding was performed at 20 μM protein concentration in 20 mM phosphate buffer pH 8.0, by using the same Jasco apparatus and the temperature/wavelength scan measurement program of the Spectra Manager software. The temperature was increased from 20 °C to 100 °C at a rate of 60 °C/h. The CD signals were acquired at 1 °C intervals at the indicated wavelength (223_{nm}).
The conformational behaviour of peptide 49-68 of Cul3 (see results for details) was investigated by CD spectroscopy in 10 mM phosphate buffer at pH 7.0 and room temperature. CD spectrum was collected on a Jasco J-715 spectropolarimeter from 185 to 260_{nm} by using a 1 mm quartz cuvette, a scan speed of 10 nm/min, a bandwidth of 1.0 nm and a time constant of 8 s. Peptide concentration (5.8×10^{-5} M) was determined by monitoring Tyr absorbance at 278_{nm} and using the molar extinction coefficient of 2290 M^{-1} cm^{-1}. CD intensitiy is expressed as mean residue ellipticity (deg $\times cm^2 \times dmol^{-1}$ of amino acid) calculated referring to the total amino acid concentration.

2.8 Light scattering (LS)

We used a SEC-LS system consisting of a semi-preparative size exclusion chromatography column (Superdex-200 10/30, GEHealthcare) coupled to a light scattering detector (miniDAWN TREOS) and a differential refractive index detector (Shodex RI-101).
The Astra (5.3.4 version, Wyatt Technology Corporation) software allowed us to the collect, record, and process the scattering data.

2.9 ELISA Assays

For ELISA assays, 5 µg/ml streptavidin in phosphate/citrate buffer pH 5.0 was incubated over night at 37 °C for coating. First binding was executed with 0.8 µM biotinylate peptide 49-68 of Cul3 in PBS 1X for 1 h at room temperature. Second binding was performed with different concentrations of His-TrxA/POZ/BTB^{KCTD11} or His/KCTD5 N-module (0.8 µM, 1.5 µM, 3.8 µM, 7.6 µM, 15.6 µM) in PBS 1X. His-TrxA was employed as negative control in the same concentrations. As blocking solution 1% BSA, 0.05% Tween-20 in PBS 1X was used for 1 h at room temperature. In order to reveal the occurred interaction mouse anti-His monoclonal antibody was incubated in 1:1000 dilution at room temperature for 2 h; then, horseradish peroxidase-conjugated anti-mouse antibody (Pierce) was diluted 1:10000 in PBS 1X and incubated at room temperature for 1 h. The colorimetric reaction has been performed with SIGMA-*FAST* OPD reagent (Sigma Aldrich), according to the manufacturer's instructions. Finally, a Model 680 Microplate Reader (Bio-Rad) has been used for readings at 490_{nm}; data were processed by a Microplate Manager 5.2 program.

2.10 Synthesis of Cul3 peptide

Cul3 peptide encompasses the protein sequence 49-68 (Ac-NSGLSFEELYRNAYTMVLHK-NH_2) of the Cul3 protein. The peptide was acetylated and amidated to avoid the electrostatic repulsion between peptide terminal charges and putative helix dipole. The peptide was synthesized on solid phase by using Fmoc–MBHA rink amide resin to afford a C-terminal amide sequence and standard Fmoc (N-9-Fluorenylmethyloxycarbonyl) strategy. The coupling reactions were carried out with a ten-fold excess of amino acid using 2-(1H-benzotriazole-1-yl)-1,1,3,3-tetramethyluronium hexafluorophosphate (HBTU) as coupling reagent and *N*,*N*-diisopropylethylamine (DIEA) in DMF (*N*,*N*-dimethylformamide). The deprotection step from Fmoc group was performed with 30% piperidine in DMF. Before the cleavage from the resin the peptide was acetylated at N-terminus by a solution of acetic anhydride/DIEA/ DMF (2.6:4.8:92.6 v/v/v). The crude product was cleaved from the resin by treatment with trifluoroacetic acid (TFA)/H_2O/1,2-ethanedithiol (EDT)/triisopropylsilane (TIS) (94:2.5:2.5:1 v/v/v/v) at room temperature for 3 h. The resin was then filtered off and Cul3wt peptide was precipitated using diethyl ether.

2.11 Synthesis of Biotin-Cul3 peptide

The synthesis of Biotin-Cul3 peptide (Biotin-NSGLSFEELYRNAYTMVLHK-NH_2) was performed as reported above. Before the reaction with TFA the peptidyl-resin was treated with a solution of biotin/HATU/DIEA (5:2:2 eq/eq/eq) in DMF to functionalize the peptide for the following in vitro studies. The crude product was cleaved from the resin as reported for Cul3wt peptide.

2.12 Peptide purification and identification

Both peptides were purified by preparative RP-HPLC on a Shimadzu system equipped with a Diode Array SPD10AVP using a Phenomenex C12 column (Jupiter 10 µm; Proteo 90 Å) and a linear gradient of H_2O (0.1% TFA)/CH_3CN (0.1% TFA) from 20 to 70% of CH_3CN (0.1% TFA) in 20 min at flow rate of 20 mL/min. Purity and identity of the peptides were assesed by analytical RP-HPLC and LC-MS (liquid chromatography mass spectometry system). The final yields were 45% and 40 % for Cul3 peptide and Biotin-Cul3 peptide, respectively.

2.13 Database sequence/structure surveys

Sequence analyses were conducted by using the tools of the server ExPASy (http://www.expasy.org/). These analyses were also performed by using data available at the POZ/BTB database (http://btb.uhnres.utoronto.ca/index.html) developed by Privé and co-workers. The sequence of REN^{KTCD11} c-DNA was retrieved from the site http://www.ensembl.org/ (gene=ENSG00000184542). Compute pI/Mw was used for the computation of the theoretical pI and Mw of sequences of interest.

2.14 Molecular modelling

A three-dimensional model for POZ/BTB domain of REN^{KTCD11} was generated by using standard molecular modelling techniques. The structure of the Kv4.3 BTB/POZ domain determined at 2.1 Å was used as template (PDB code 1NN7). The model, generated by using the program Insight II, was energy minimized to remove bad contacts and minor stereochemical problems. The overall architecture of the complex between POZ/BTB^{KTCD11} and Cul3 was generated by taking into account the crystal structure of the complex between Skp1 and Cul1 (PDB code 1LDK). The model of Cul3 was generated from the structure of the closely related Cul4. The larger complex formed by POZ/BTB^{KTCD11} tetramer with Cul3, Rbx1, and E2 was generated by considering the crystal structure of the complex Skp1-Cul1–Rbx1 by docking of E2 on Rbx1 taking into account the architecture of the related complex E2-cCbl.

2.15 Crystallization tests

Protein samples of POZ/BTB were concentrated to 10 mg/mL, in 20 mM Tris/HCl pH 8.0, using Microcon centrifugal filter units with a YM-3 membrane of molecular-weight cut-off 3 kDa (Millipore, Bedford, Massachusetts). Protein concentration was estimated by the method of Bradford, using BSA as standard (Bradford, 1976). Crystallization experiments were carried out at 20 °C using the hanging-drop vapour-diffusion technique. Initial crystallization conditions were found using commercially available crystallization-screening kits (Crystal Screen I and II, Hampton Research, Riverside, CA). Drops containing equal volumes (1 µL) of protein and reservoir solution were equilibrated against 1 mL of reservoir solution. Several crystal forms were obtained, but the best diffracting crystals were grown using a reservoir solution containing 1.0 M Li_2SO_4, 0.4-0.6 M $(NH_4)_2SO_4$, 0.1 M ADA (pH = 6.0-6.6). Only low-

resolution data were obtained from these crystals (about 4 Å). They belonged to the space group $P6_322$ (unit cell parameters: a = b = 198 Å, c = 139 Å; □ = □ = 90° and □ = 120°). Several parameters such as crystallization technique, buffer composition, pH, protein concentration and ionic strength were varied in order to improve the quality of the crystals. New crystallization conditions were achieved at 20 °C adding 300 mM NaCl to the protein buffer and using a reservoir solution consisting of 1.0 M Li_2SO_4, 0.5 M $(NH_4)_2SO_4$, 0.1 M tri-sodium citrate (pH = 5.6). This last crystallization experiment was carried out using the sitting-drop vapour-diffusion method, by equilibrating 0.2 µL drops against 100 µL of reservoir solution.

2.16 Expression of ^{15}N-labelled recombinant POZ/BTB^{KCTD11} for NMR studies

A single clone of JM101 strain was cultured for 3 h at 37 °C in 5 ml of LB medium without antibiotics. The cells were then inoculated in M9 medium (see composition in tables 1 and 2), containing $^{15}NH_4Cl$ (1 g/l) as the sole nitrogen source, and grown overnight at 37 °C. The harvested cells were lysed with 37% HCl at 95 °C for 8 h, to obtain a mixture of single ^{15}N labeled amino acids; this mixture was used to enrich M9 medium for the expression of POZ/BTB^{KCTD11} in *E. coli* BL21*CodonPlus*(DE3)RIL strain previously transformed with pETM20/*poz/btb*^{kctd11} recombinant expression vector. The expression and protein purification were performed as described for the unlabeled protein.

M9 salt solution 10X	100 ml
1 M $MgSO_4$	1 ml
10 mM $CaCl_2$	10 ml
1 % thiamine	1 ml
20% glucose	10 ml
ddH_2O	878 ml
Total volume	1 liter

Table 1: M9 medium composition.

Na_2HPO_4	6 g
KH_2PO_4	3 g
NaCl	0.5 g
$^{15}NH_4Cl$	1 g
ddH_2O to	100 ml
Total volume	100 ml

Table 2: M9 salt solution 10X composition.

2.16.1 NMR Spectroscopy - Peptide-protein interactions

NMR measurements were performed on a Varian Unity Inova 600 MHz spectrometer equipped with a cold-probe, using either unlabeled (500 μM) or uniformly ^{15}N labeled (400 μM) POZ/BTB in 50 mM Tris/HCl and 150 mM NaCl, pH 8.0. Peptide-protein interactions were performed using the peptide 49-68 Cul3 and were monitored by identifying perturbations in 2D [^{1}H, ^{15}N] HSQC spectra. ^{15}N-POZ/BTB^{KCTD11} was titrated increasing peptide concentrations. 2D [^{1}H, ^{15}N] HSQC spectra were acquired with 32 transients per t_1 value. Pre-saturation of water was employed during a recycle delay of 1.5 s. 1K complex points were acquired in t_2, with an acquisition time of 102.5 ms, while 128 complex points were acquired in t_1 with an acquisition time of 64 ms. To determine the *per residue* chemical shift perturbation upon binding and account for differences in spectral widths between ^{15}N and ^{1}H resonances, weighted average chemical shift differences, Δav(HN), were calculated for the amide ^{15}N and ^{1}H resonances, using equation:

$$\Delta av(HN) = [\Delta H^2 + (\Delta N/2)_2]^{½}$$

ΔH and ΔN represent the differences between free and bound chemical shifts.
Spectra of the unlabeled POZ/BTB/peptide complex were recorded with 2048 scans and selective saturation of the protein resonances at 12 ppm and 3 ppm. Time dependence of the saturation transfer was investigated using an optimized saturation times ranging from 0.2 to 4.0 s. STD NMR spectra were acquired using a series of equally spaced 50 ms Gaussian-shaped pulses for selective saturation, with 1 ms delay between the pulses. Subtraction of the protein FID resonance was performed by phase cycling.

2.17 Expression in yeast of REN^{KCTD11} ("short form")

ren^{KCTD11} gene was first cloned into pGEM-T Easy vector (Promega) and then recovered from it by digesting with *Nsi* I and *Pst* I restriction enzymes; finally the insert was subcloned in the expression vector YEp352 (Yeast Expression plasmid) (figure 2.5), previously digested with the restriction enzymes *Pst* I and *Nar* I. *ren*^{KCTD11} was cloned in frame with a strong non-regulated promoter (PGK promoter), that allows a continuous gene expression. Moreover, a signal sequence that vehicles the expressed protein in the extracellular medium is placed upstream the insert. The recombinant vector YEp/*ren*^{KCTD11} was used to transform a strain of *Saccharomyces cerevisiae* (gently provided by prof. Giovanni Sannia, Department of Biological Sciences, University Federico II of Naples). 1 ml of 0.1 M lithium acetate has been added to the cells of *S. cerevisiae* for 5 min at 30 °C. The sample was centrifuged, the supernatant removed and the pellet resuspended in 0.35 ml of PLATE (40% PEG 4000, 0.1 M lithium acetate, 0.1 M Tris/HCl pH 7.5, 1 mM EDTA), 100 µg of DNA of salmon sperm and 5 µg of plasmid YEp/*ren*^{KCTD11}. The sample was incubated for 20 min at 42 °C and then centrifuged. The supernatant was discarded and the pellet resuspended in 0.2 ml of sterile H_2O. The transformed cells were plated on selective medium (6.7 g/l base nitrogenous, 5 g/l casein, 2% glucose, 30 mg/l adenine, 40 mg/l tryptophan, 50 mM succinate buffer pH 5.3). The plates were incubated at 30 °C for 4 days. A colony of *S. cerevisiae* transformed with the vector YEp/*ren*^{KCTD11} was grown in 10 ml of selective medium, with a shaking of 150 rpm, at 30 °C for three days. The culture was diluted in 50 ml of selective medium, and grown until an optical density of 0.5 (600_{nm}). 2 ml of culture were collected every 24 h for 7 days and cells were separated from the extracellular medium. The extracellular media was concentrated; REN^{KCTD11} protein expression was verified through SDS-PAGE analysis followed by silver staining and also by Western Blot, using the α-REN^{KCTD11} antibody.

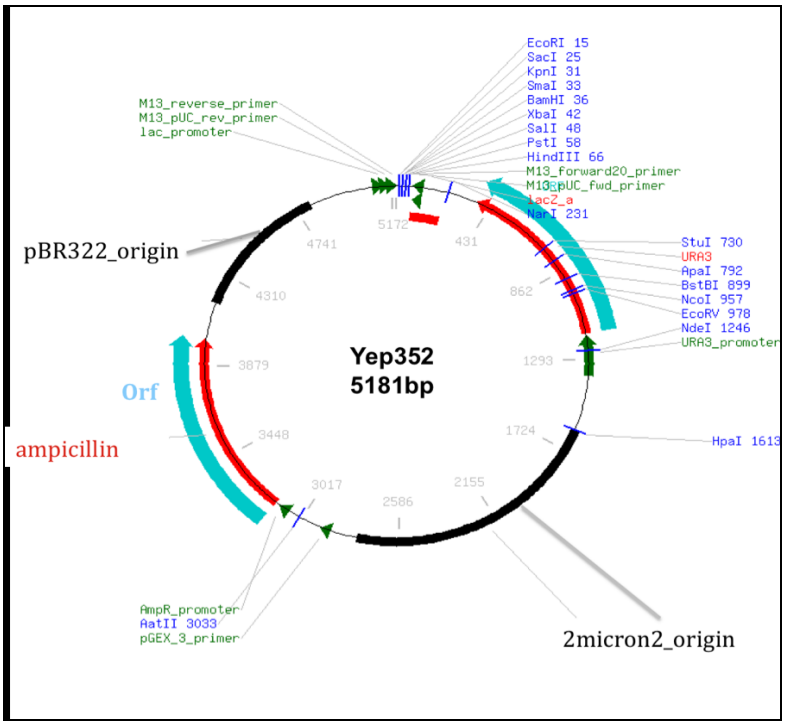

Figure 2.5. Map of expression vector Yep352.

2.18 Expression in mammalian cells

2.18.1 Cloning of *ren*^{KCTD11} in pBOS

Cloning of *ren*^{KCTD11} ("short" and "long form") in pBOS eukaryotic vector was based on a three steps PCR strategy. As a first step, a "leader sequence" was amplified from the pBOS/*apo-AI* recombinant vector, already available in our lab, by using the following couples of primers:

Short form
Forward1: 5'-CCGGAATTCATGAAAGCTGGTGTG-3'
Reverse1: 5'-CATGGCCCCCAGCATAGCCTGGCTCCCCG-3'

Long form
Forward1: 5'-CCGGAATTCATGAAAGCTGCTGCGGTGCTG-3'
Reverse1: 5'-TCACGGGGCCAGCCTGGCTCCCCGTC-3'

In the second PCR, *ren*^{KCTD11} was amplified from pRSET/*ren*^{KCTD11} by using the following couples of primers:

Short form
Forward2: 5'-CGGGGAGCCAGGCTATGCTGGGGGCCATG-3'
Reverse2: 5'-CCGGAATTCTCAGTGGCGCACAAAGC-3'

Long form
Forward2: 5'-GAGCCAGGCTGGCCCCGTGACCCTGA-3'
Reverse2: 5'-CCGGAATTCTCAGTGCCGCACAAAGC-3'

Forward1 and *Reverse2* primers contained the *EcoR* I restriction site (underlined in the sequences), while *Reverse1* primer contained the 5'-terminal portion of *ren*^{KCTD11} (in red), and *Forward2* the 3'-terminal portion of "leader sequence" (in blue).
First and second PCR products (with overlapping ends) were used as templates in the third PCR performed with *Forward1* and *Reverse2* primers; in this way, the "leader sequence" was inserted upstream *ren*^{KCTD11} gene. After a digestion with *EcoR* I restriction enzyme, the final product has been purified and cloned into pBOS mammalian expression vector, previously digested with the same enzyme. This vector contains the strong *EF1α* promoter, in frame with the insertion site, and the SV40 replication origin. PCR, digestion and ligation reactions were performed in the same conditions described above (see paragraph "Cloning"). Identity of the insert was confirmed by DNA sequencing.

2.18.2 Cell culture and transfection

293T and CHO KI cells were cultured in DMEM supplemented with 50 units/ml penicillin, 50 µg/ml streptomycin, 4 mM L-glutamine (Euroclone), and 10% FBS (HyClone Perbio). They were splitted every 3-4 days with 1:10 to 1:20 dilution and cultured at 37 °C, in 5% CO_2. Transient transfection was performed at a confluence of 60-70% in OptiMEM medium (Invitrogen) with 3 µg of recombinant plasmidic DNA (pBOS/*ren*^{KCTD11}), by using Lipofectamine Reagent from Invitrogen, according to manufacturer's instructions. After 5 h of incubation, the medium was changed with DMEM supplemented with 0,5% FBS and 4 mM L-glutamine. After 24 h the proteasome inhibitor MG132 (30 µM, from Calbiochem) was added for 6 h. Then, medium was harvested and centrifuged, protease inhibitors were added to surnatant, and the sample analyzed by Western Blotting. For stable transfection, cells were co-transfected with 3 µg of pBOS/*ren*^{KCTD11} and 300 ng of pSV2*neo* (Clontech), containing the gene for neomycin resistance. After 5 h of incubation, the medium was changed with DMEM supplemented with 0,5 % FBS, 4 mM L-glutamine and 500 µg/ml G418 (Euroclone). Stably transfected clones were isolated, amplified, and then analyzed by Western Blotting, using for the detection a monoclonal anti-REN^{KCTD11} antibody, kindly provided by prof. A. Gulino's co-workers. As negative control, not transfected cells were used.

3 RESULTS

3.1 The protein REN^{KTCD11}

The protein REN^{KTCD11} is an important regulator of the Hedgehog pathway and is involved in the development of medulloblastoma. REN^{KTCD11} is a 232 aminoacids protein detected in several mammalian species. Although its role in the development of the disease has been clearly demonstrated, the biological action of the protein has not been fully characterized yet. The limited similarity of REN^{KTCD11} with proteins with known sequence/structure also prevents straightforward prediction of its function. Sequence similarity searches carried out for REN^{KTCD11} indicate that three distinct regions presumably compose the protein: N-terminal domain (POZ/BTB), residues 1-80, a putative central domain, residues 81-180 and a putative COOH domain, residues 181-232. In collaboration with the group of prof. Alberto Gulino the constructs for REN^{KCTD11} full length and the deleted forms ΔPOZ, ΔCter were cloned in the expression vector pRSET. Tests of expression have been conducted in several strains of *E. coli*, varying temperature, concentration of IPTG and time of induction. The recombinant proteins formed inclusion bodies under all the analyzed conditions. Various protocols of refolding have been used, then, to recover the recombinant proteins from the inclusion bodies, but despite the numerous efforts the final yield has been low. Our attention has been focused on the protein full length and on the possibility that post-translational modifications could have for the correct folding. REN^{KCTD11} has been expressed, therefore, in mammalian and yeast cells.

3.2 Expression of REN^{KCTD11} in yeast

In order to express REN^{KCTD11} in yeast, the corresponding gene, cut with the restriction enzymes *Nsi* I and *Pst* I, was sub-cloned in the expression vector YEp352 previously cutted with the restriction enzymes *Pst* I and *Nar* I. The recombinant vector, YEpREN^{KCTD11}, was used to transform a strain of *Saccharomyces cerevisiae*. *S. cerevisiae* was grown in selective medium and the recombinant protein, REN^{KCTD11}, was expressed in the extracellular medium. 2 ml of culture were collected every 24 h for 7 days and the cells were separated from the extracellular medium. The extracellular media were concentrated up to 0.1 ml. REN^{KCTD11} expression was verified by SDS-PAGE analysis followed by silver staining. The SDS-PAGE analysis highlights the presence of a protein band corresponding to a molecular weight of 25 kDa, expected for REN^{KCTD11} in the medium of *S. cerevisiae* cells transformed with the vector YEpREN^{KCTD11}. In order to improve the expression of REN^{KCTD11}, we have prepared a sample of 10 ml (figure 3.1). Finally Western Blot analysis confirmed the presence of a protein in the extracellular medium derived from transformed cells, which is absent in the medium of wild-type cells. The final yield, nevertheless, has been very low and unsuitable structural characterization (figure 3.2).

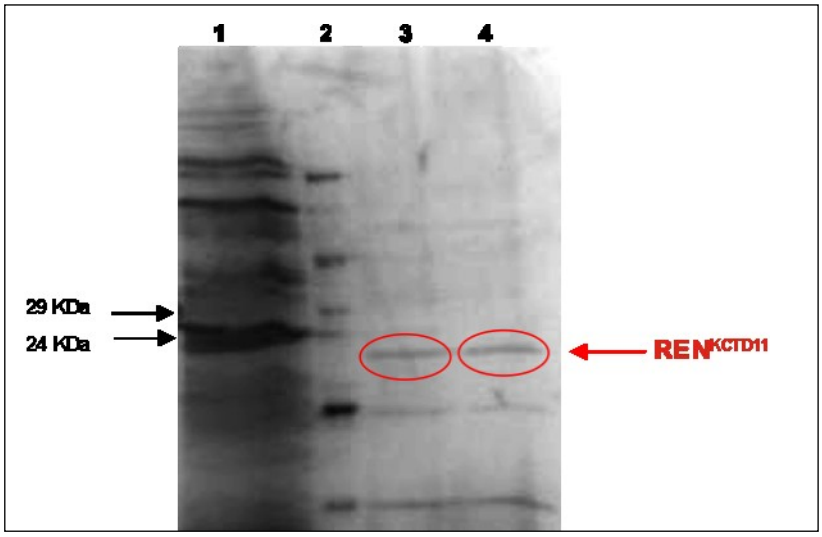

Figure 3.1. SDS-PAGE analysis of expression of REN^{KCTD11} in yeast. Lane 1 shows extracellular medium of *S. cerevisiae* wild-type after 96 h, in lane 2 low-range protein marker (Sigma) and lane 3 and 4 show extracellular medium of the recombinant *S. cerevisiae* after 72 and 96 h.

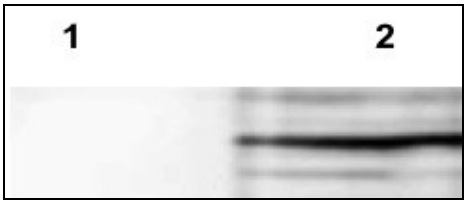

Figure 3.2. Western blot analysis of REN^{KCTD11} expression in yeast cells. In lane 1 extracellular medium of *S. cerevisiae* wild-type after 96 h; in lane 2 extracellular medium of recombinant *S. cerevisiae* after 96 h.

3.3 Expression of REN^{KCTD11} in mammalian cells

In order to express REN^{KCTD11} in mammalian cells the recombinant vector pBOS/*ren*^{kctd11} has been used thus to obtain the protein secreted into culture medium. CHO K1 cells were transfected with this vector and treated with and without the proteasome inhibitor MG132. The media were analyzed by western blot, using, for the detection, a monoclonal anti-REN^{KCTD11} antibody, kindly provided by A. Gulino's co-workers. Only in the samples treated with the proteasome inhibitor a chemiluminescent signal in correspondence of REN^{KCTD11} expected molecular weight (~27 KDa) has been detected (data not shown). This suggests that, soon after the expression, the recombinant protein was targeted to the degradation by host defence mechanisms, preventing its secretion outside the cell. Anyway, even in presence of MG132, REN^{KCTD11} expression level was not sufficient for subsequent purification.

3.4 REN^{KCTD11} "long form"

Since the early characterizations of the protein, it was shown that the sequence N-terminus of REN^{KTCD11} exhibits significant similarities with the POZ/BTB domains. Analyses of sequence databases did not reveal any significant similarity for the rest of the protein. POZ/BTB are widespread and well-characterized domains detected in several systems involved in a variety of biological processes. For several members of this family, three-dimensional structures are available. Recent comparative analyses have clearly indicated that the structures of these domains are characterized by variations on a conserved structural theme. Indeed in every structure a module formed by a three-stranded β-sheet and five α helixes is present. Alignments of POZ/BTB sequences of members with unknown structures suggest also that these elements are strictly conserved among the proteins of the family. Intriguingly, the POZ/BTB domain of REN^{KTCD11} is peculiar in this general framework. According to the available sequences of REN^{KTCD11} isolated from different sources, only a portion of the conserved core of the POZ/BTB domain is present in these proteins. Sequence alignments show that the part of the domain corresponding to the β-strands B1 and B2 and the to the α-helix A1 is absent (figure 3.3). This unusual scenario prompted us to check the possibility of an alternative initiation point of REN^{KTCD11} mRNA translation. The analysis of the REN^{KTCD11} cDNA sequence clearly indicates that the entire POZ/BTB conserved core could be generated simply using an alternative starting point for the traduction of the protein. Indeed, the DNA triplets preceding those corresponding to the putative first residue of the reported sequence (Met1) encode for residues that are very similar to those observed in the other POZ/BTB domains. The building of the entire POZ/BTB requires 24 extra aminoacids at the N-terminal side of the protein (figure 3.4 and 3.5). In this scenario, subsequent research activities followed two different directions aimed to characterize the two alternative forms of REN^{KTCD11} POZ/BTB domain and evaluate the possibility of an additional initiation point of translation by *in vitro* experiments. All these important findings have been confirmed by *in vitro* experiments performed by Alberto Gulino's group. They mutated each valine and isoleucine residue placed upstream the methionine +1, in order to identify the real start point of translation. The results of these experiments identified the isoleucine -39 as translation start point for the REN^{KCTD11} (figure 3.6); consequently the complete protein sequence of REN^{KTCD11}, 271 aminoacids, has been redefined. Further research activities were focused to characterize the new "long" form of REN^{KTCD11} and its POZ/BTB domain, individuated as aminoacid residues +15 - +116.

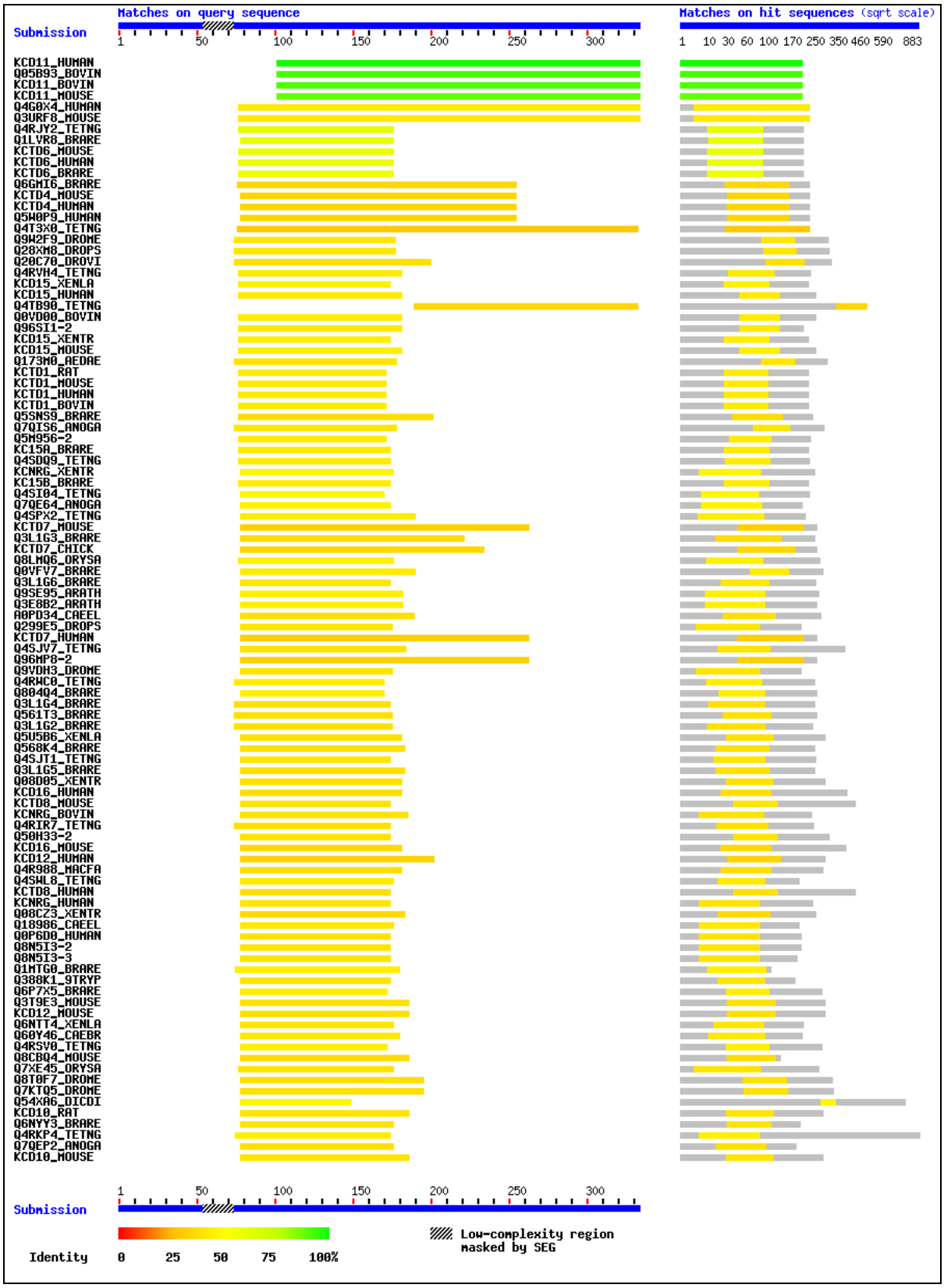

Figure 3.3. Alignments of BTB/POZ domains reported in sequences databases. The sequence of the translated REN^{KTCD11} c-DNA sequence was used in the query. The methionine that is the starting residue in the short REN^{KTCD11} form is the residue 101 in this sequence. With the exception of the human, mouse and bovine REN^{KTCD11} (shown in green) sequences, all others present an extra region at the N-terminal side, which likely corresponds to the structural elements B1, B2 and A1 of the domain core.

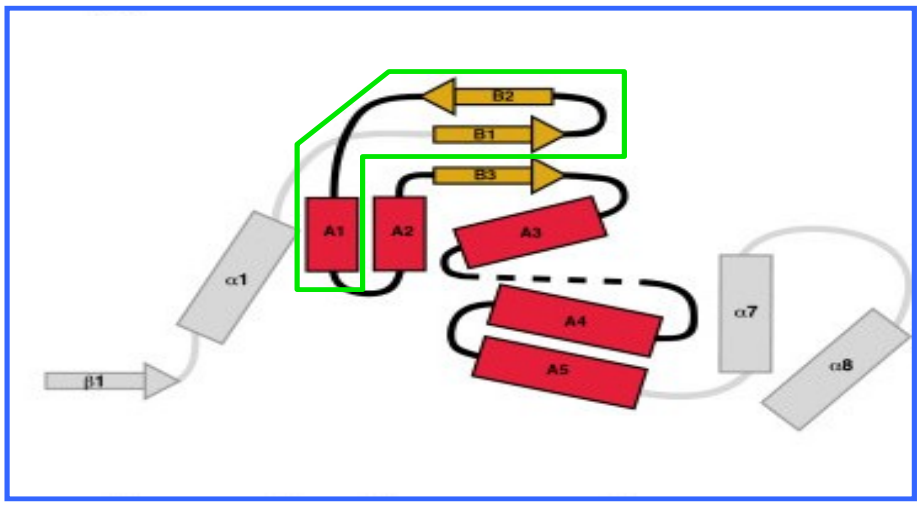

GFLCPDTTSPSTTKVAGVSPKPYWVCSTCASNPANLTASTQFCTHPGSSAFSFLSVSPVL
PKISPPPVPSSPPSFGGPVTLNVGGTLYSTTLETLTRFPDSMLGAMFFAGTPMPPNLNSQ
GGGHYFIDRDGKAFRHILNFLRLGRLDLPRGYGETALLRAEADFYQIRPLLDALRELEAS
QGTPAPTAALLHADVDVSPRLVHFSARRGPHHYELSSVQVDTFRANLFCTDSECLGALRA
RFGVASGDRAEGSPHFHLEWAPRPVELPEVEYGRLGLQPLWTGGPGERREVVGTPSFLEE
VLRVALEHGFRLDSVFPDPEDLLNSRSLRFVRH

Figure 3.4. Building of the entire POZ/BTB with addition of 24 extra aminoacids at the N-terminal side of the protein, corresponding to the β-strands B1 and B2 and to the α-helix A1.

Figure 3.5. Model of the "long" form of POZ/BTB, in red are represented the β-strands B1 and B2 and the α-helix A1 added.

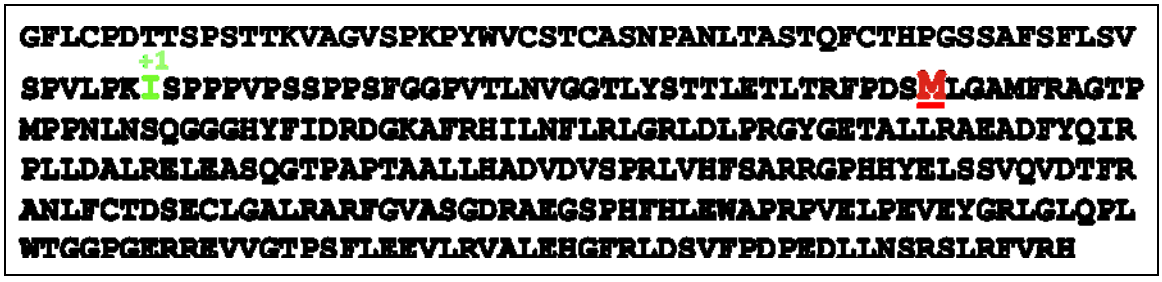

Figure 3.6. Isoleucine placed 39 aminoacids upstream of methionine +1 as new translation start point of REN^{KCTD11}.

3.5 Expression of REN^{KCTD11} "long form" in *E. coli*

The "long" form of REN^{KCTD11} with isoleucine as new translation start point was cloned in pETM41 and expressed in *E. coli* as a fusion protein with the Maltose Binding Protein (MBP). The strain BL21(DE3)STAR was chosen for the expression and the expression was conducted at 22 °C for 16 h. The soluble fusion protein MBP-REN^{KCTD11} was purified by affinity chromatography exploiting the presence of a tail of histidines situated at N-terminus of MPB. The consequent molecular exclusion chromatography (Superdex 200 10/30) combined with light scattering analysis allowed us to highlight a tetrameric organization of the recombinant protein and a hydrodynamic radius of 9.2 nm (figure 3.7). REN^{KCTD11} was separated from the fusion partner through proteolysis conducted at 30 °C for 3 h in the presence of TEV protease. The protein, without partner, aggregates in solution by forming complexes of high molecular weight that did not allow us to continue the structural analysis of the protein.

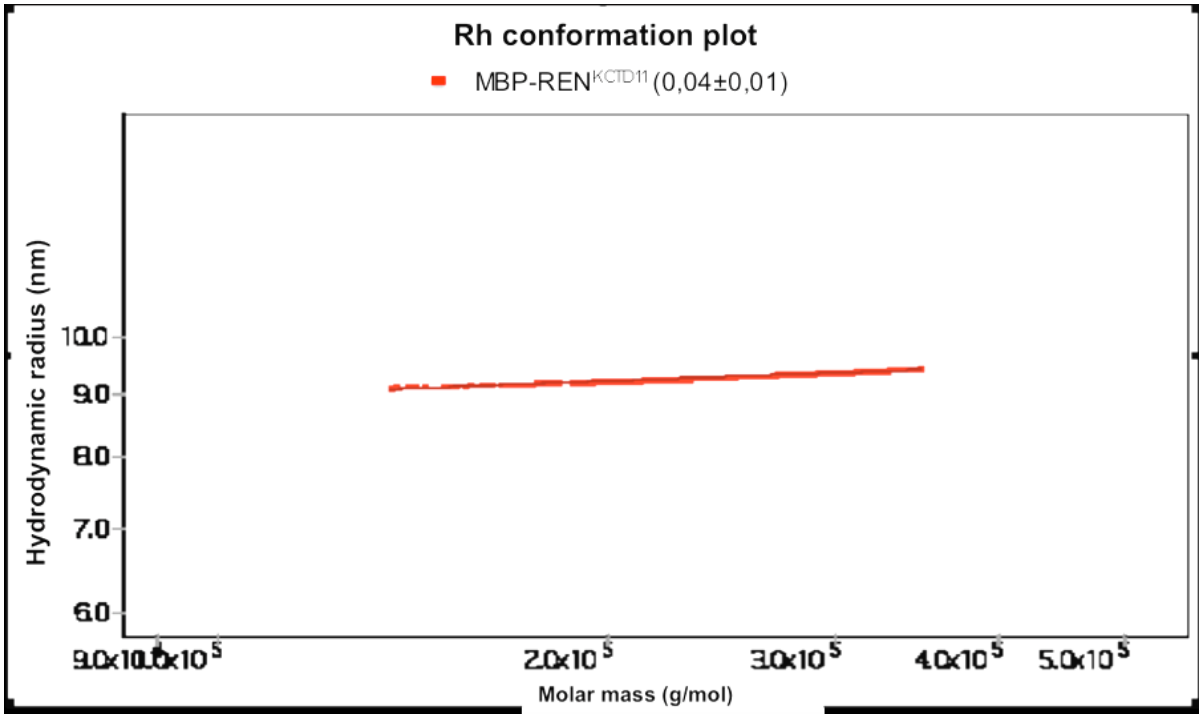

Figure 3.7. Rh conformation plot obtained by light scattering analysis of MBP-REN^{KCTD11}: hydrodynamic radius versus molecular mass plot.

3.6 Expression of REN^{KCTD11} "long form" in mammalian cells

REN^{KCTD11} without fusion partner is unstable, probably because the recombinant protein isolated from *E. coli* lacks of eventual post-translational modifications, which could be required for protein stability. Therefore, a new mammalian recombinant construct was designed, inserting the long sequence of REN^{KCTD11} into pBOS, in frame with the leader sequence for outside secretion. CHO KI cells have been stably transfected with it and the culture medium was collected after 24 and 48 h from transfection. Western blot analysis of a selected stable clone has shown a significant expression level of REN^{KCTD11} in the sample collected after 24 h (figure 3.8). This result has been obtained without proteosome inhibitor suggesting a higher stability of the protein expressed and it was encouraging for next characterization phases. At present, an expression large-scaling is in progress.

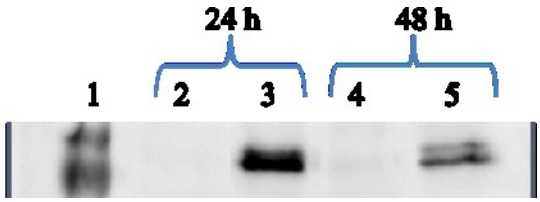

Figure 3.8. Western blot analysis of REN^{KCTD11} expression in CHO KI cells. Lane 1: prestained Mw markers. Lane 2 and 4: culture medium of untransfected cells, as negative control. Lane 3 and 5: culture medium of stable clone 6 at 24 and 48 h from transfection.

3.7 Expression of POZ/BTB^{KCTD11} domain in *E. coli*

The "long" form of POZ/BTB (residues +15 - +116) has been cloned in pETM20 and expressed in strain BL21(DE3)STAR of *E. coli*. The induction was performed with 0.5 mM IPTG, added to cells at an optical density of 0.8 OD_{600nm}, for 16 h at 22 °C. This strategy permits to obtain the domain as fusion protein with Thioredoxin-A (Trx-A). The POZ/BTB domain has been purified to homogeneity by three purification steps utilizing its nickel affinity and molecular weight properties. The extract was loaded on a his-trap column equilibrated with 50 mM Tris/HCl pH 8.0, 300 mM NaCl and 10 mM imidazole (buffer A). The fusion protein, then, was eluted with the same buffer A supplemented with 250 mM imidazole (figure 3.9). The active fractions were pooled and dialyzed against 20 mM Tris/HCl pH 8.0, 100 mM NaCl, 1 mM DTT. The Trx-A has been separated by the domain POZ/BTB through a proteolysis conducted for 3 h at 30 °C with the protease TEV. The optimal conditions for TEV digestion were achieved at a protease/protein molar ratio of 1:50. The next affinity chromatography enabled to remove the Trx-A and the protease TEV from interest protein. The concentrated sample was applied onto the HiLoad Superdex 75 column connected to an AKTA FPLC system and eluted with 50 mM Tris/HCl pH 8.0, 200 mM NaCl at a flow rate of 1 mL/min. After molecular exclusion chromatography, only one protein band was observed on SDS-PAGE analysis (figure 3.10). The protein yield from 1L of cultures was about 40 mg of the recombinant protein. The production of significant amounts of the domain in a pure and homogeneous form allowed a detailed characterization of its properties in solution. Analytical gel-filtration chromatography clearly indicates that the protein has a tetrameric organization with a molecular

weight of about 55 kDa. No significant peaks are found at the elution time expected for the monomeric form.

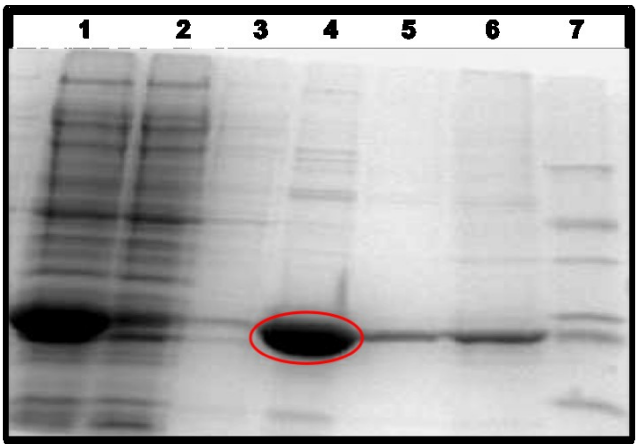

Figure 3.9. SDS-PAGE analysis: purification of Trx-A-POZ/BTB by nickel affinity chromatography. Lane 1 shows cytosolic extract, lane 2 flow throught, lane 3-4-5-6 elutions with increasing concentrations of imidazole, lane 7 low range protein marker (sigma).

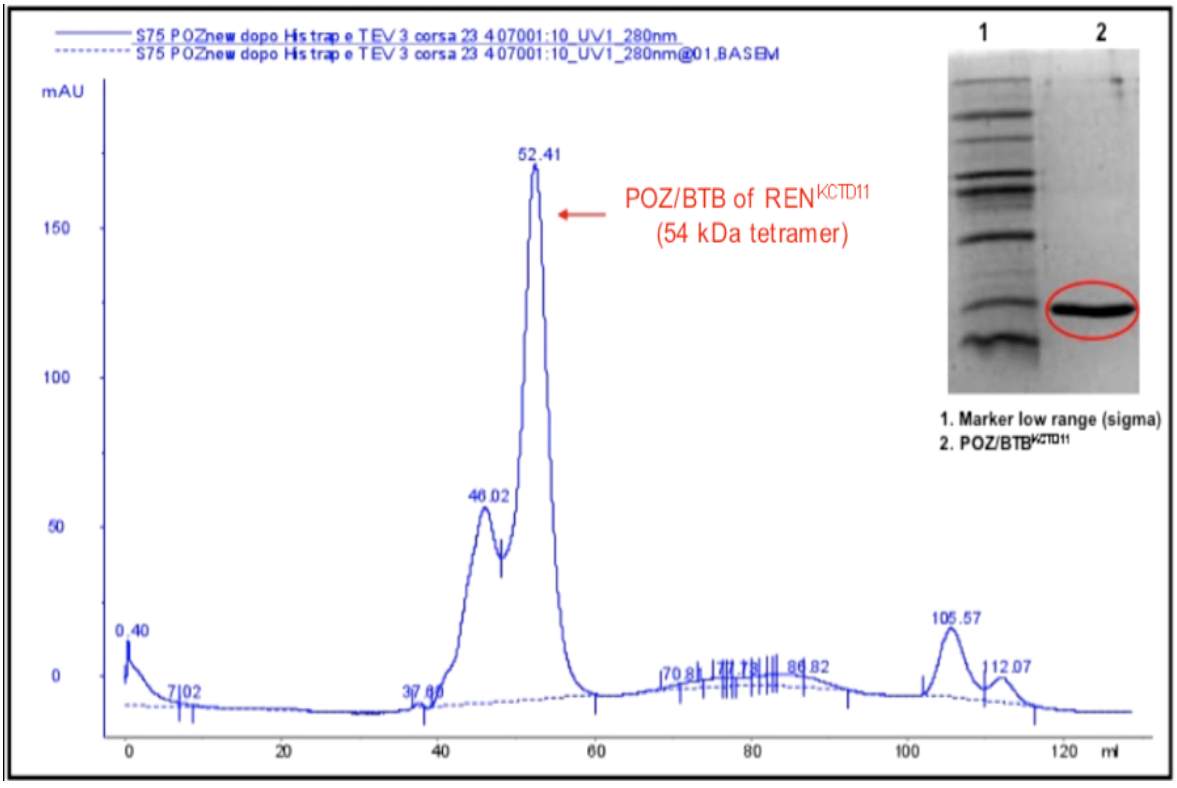

Figure 3.10. Chromatographic elution profile of POZ/BTB^{KCTD11} obtained by size exclusion chromatography with a S75 16/60 column.

3.8 Biochemical characterization of POZ/BTB^{KCTD11} domain

Accurate information about the quaternary structure of POZ/BTB domain was obtained combining molecular exclusion chromatography (Superdex 75 10/30) with light scattering analysis. The report provides a molecular weight of 56 KDa, comparable to that expected for a tetrameric organization of POZ/BTB, and a hydrodynamic radius of domain, 4.5 nm (figure 3.11). The value of radius indicates a globular form for POZ/BTB in agreement with data *in silico*.

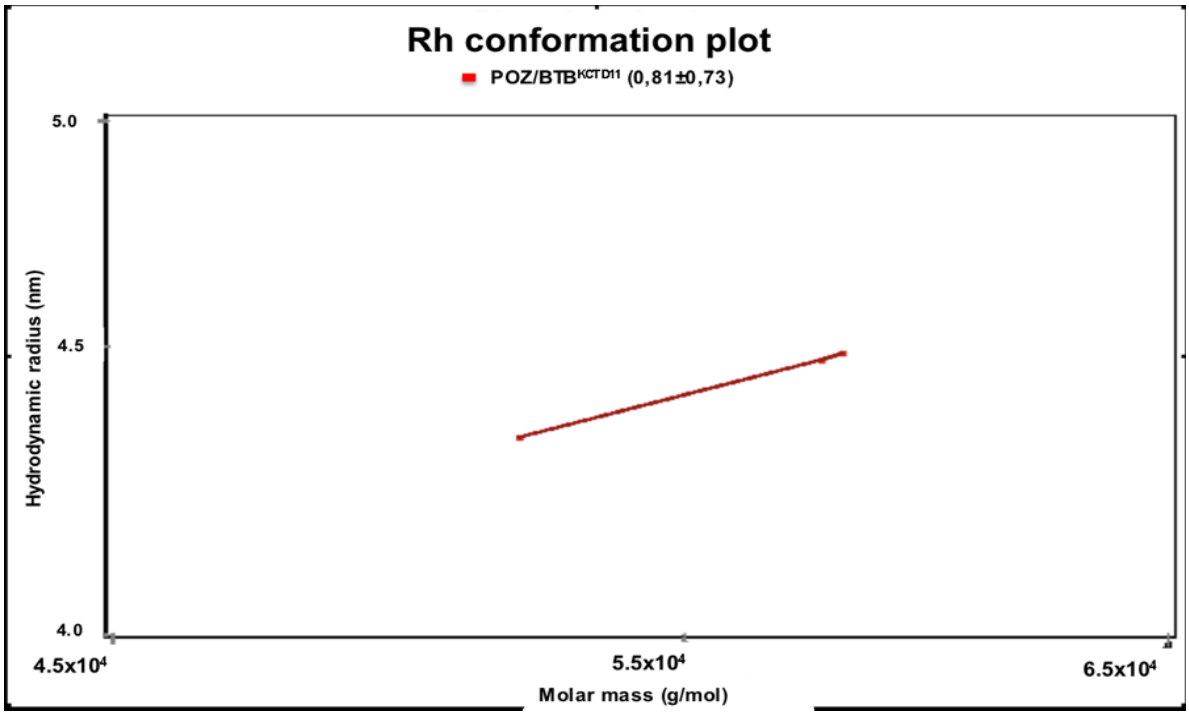

Figure 3.11. Rh conformation plot derived from light scattering analysis of POZ/BTB: hydrodynamic radius versus molecular mass plot.

The structural integrity of the POZ/BTB domain was valued by native PAGE. The sample presents a single protein band showing the homogeneity of the sample (figure 3.12).

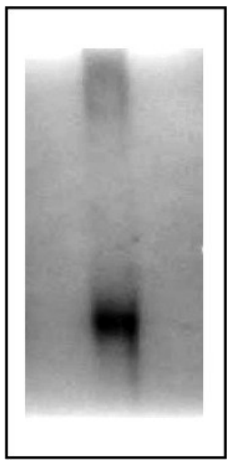

Figure 3.12. Native PAGE analysis of POZ/BTB^{KCTD11}.

The protein identity was assessed by liquid chromatography mass spectrometry. The molecular weight calculated from experimental data was in agreement with theoretical one (figure 3.13). BTB/POZ, then, was subjected to a trypsin digestion, in order to estimate the globular state of the protein. Trypsin was added to the mix in a molar ratio enzyme: BTB/POZ of 1:100. The reaction was analyzed by LC-MS at different times (30 min, 45 min, 1 h, 2 h) and showed a stable conformation of the protein that was not drastically digested by trypsin, as attended for a compact domain.
Further, POZ/BTB was analyzed by far-UV CD spectroscopy. CD spectra, recorded in the 190-260$_{nm}$ region, clearly demonstrated that the domain exhibits an ordered structure. The location of the maximum and the minima in the spectrum suggests that the protein contains both α and β structural elements (figure 3.14). The thermal stability of the protein was investigated by following the CD signal at 223$_{nm}$ in the temperature range 20-100 °C. As shown in figure 3.15 a transition is observed at 54 °C and its thermal denaturation is irreversible. POZ/BTB after the thermal denaturation is unstable because it precipitates. Finally, the sample was subjected to numerous tests of crystallization in collaboration with G. De Simone IBB CNR, but in all conditions carried out POZ/BTB produced small crystals (figure 3.16).

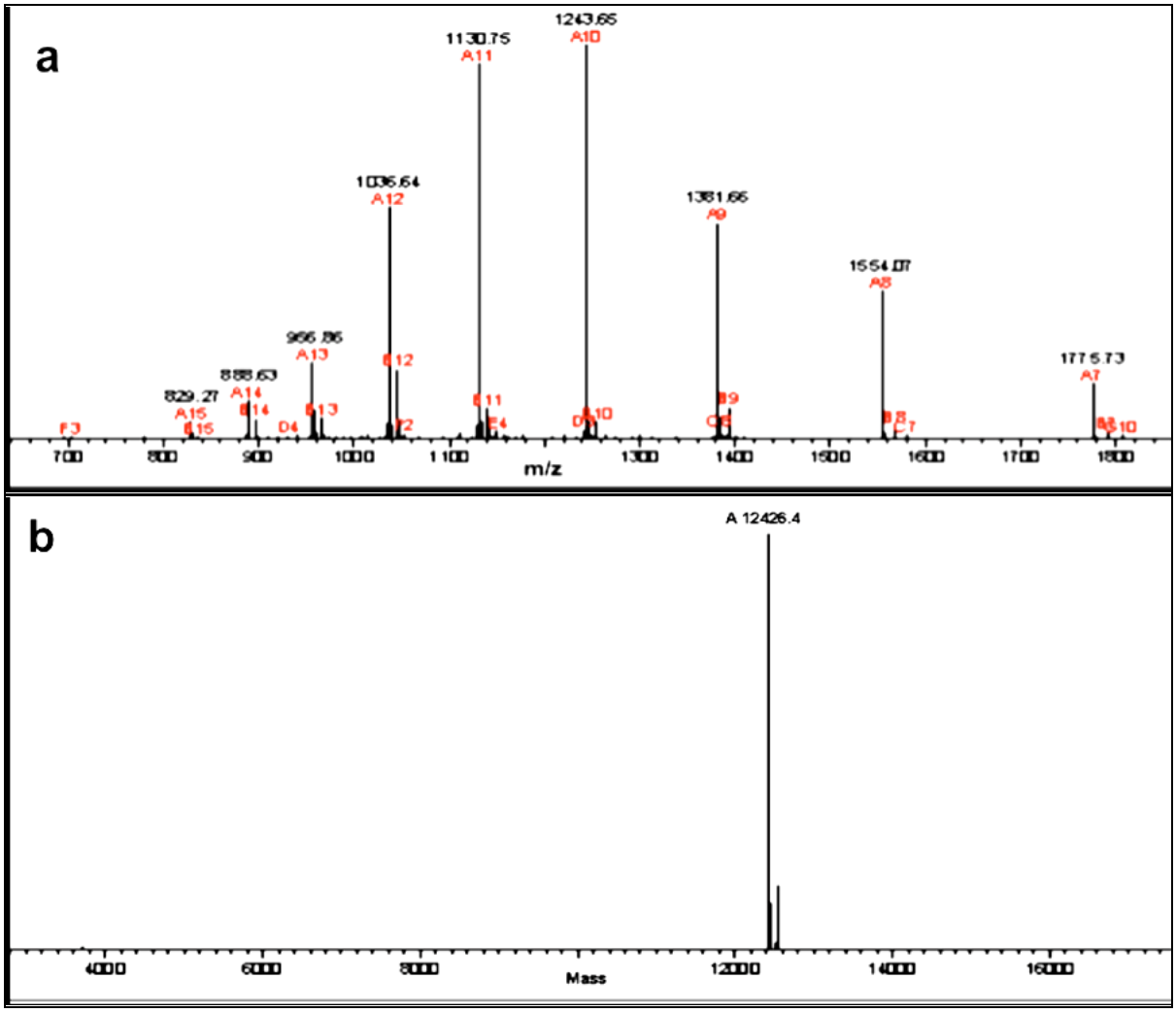

Figure 3.13. LC-MS analysis of the POZ/BTB^{KCTD11}; a: ESI spectrum; b: deconvolution analysis of POZ/BTB^{KCTD11} charged states corresponds to a mass of 12426.4 Da that is in agreement with the theoretical one.

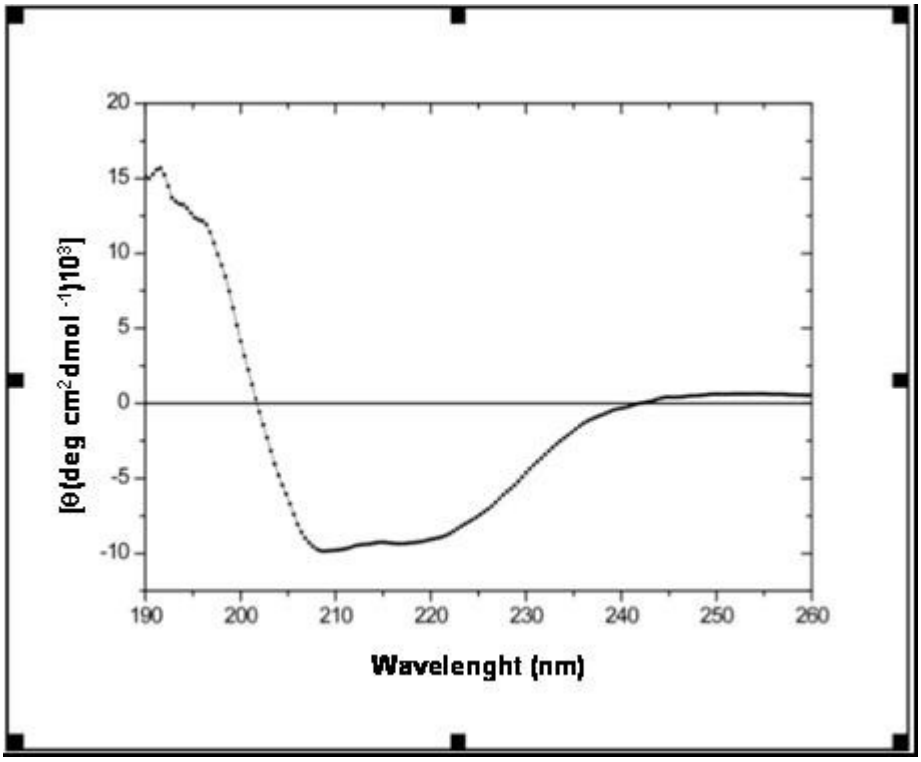

Figure 3.14. Far-UV spectrum POZ/BTB^{KCTD11} domain.

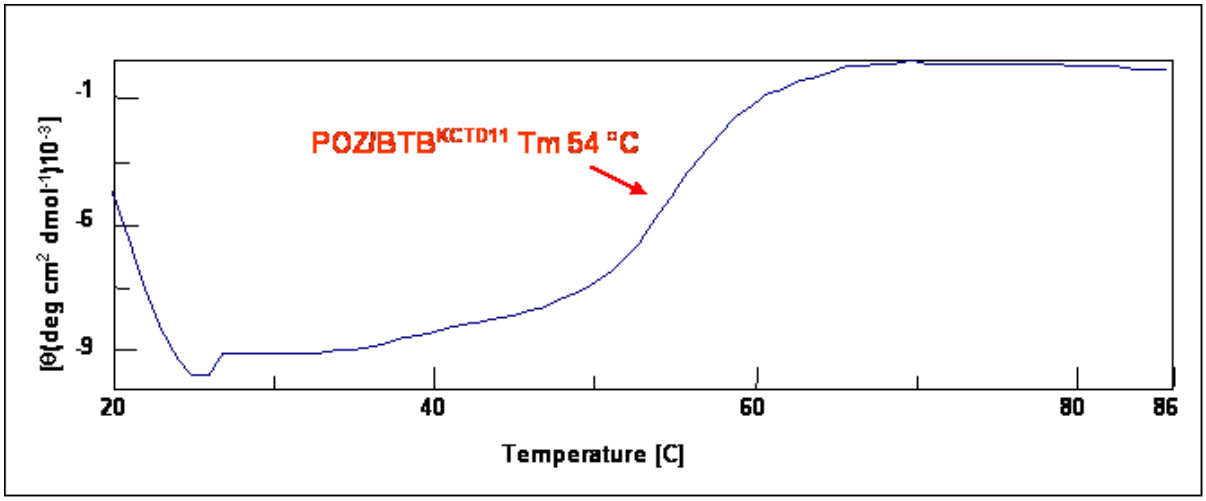

Figure 3.15. Thermal denaturation of POZ/BTB^{KCTD11}: CD signal was followed at 223_{nm} in the temperature range 20-100 °C.

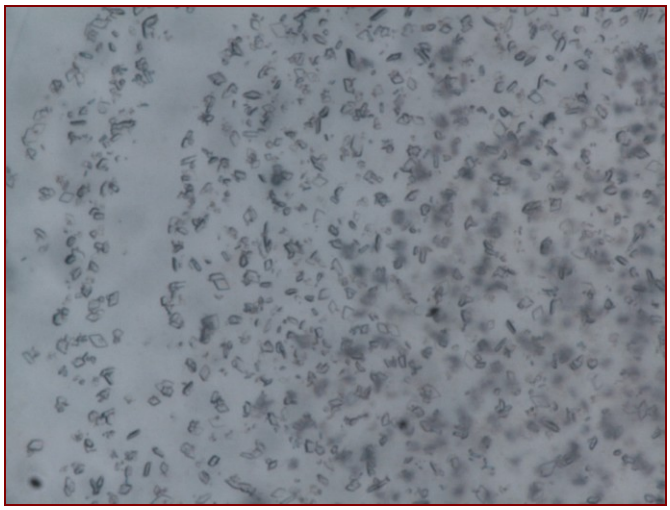

Figure 3.16. Micro-crystals of BTB/POZ obtained at 20 °C using the hanging-drop vapour-diffusion technique.

3.9 Design of construct POZ/BTB +15 – +125

In order to improve the size and the quality of POZ/BTB crystals, it was decided to reconsider the extension of the domain on the basis of structural predictions: the C-terminal domain was extended with 9 residues downstream of the last putative alpha helix. The new construct, POZ/BTB +15 - +125 (figure 3.17), was cloned and expressed in *E. coli* using the same conditions described above.

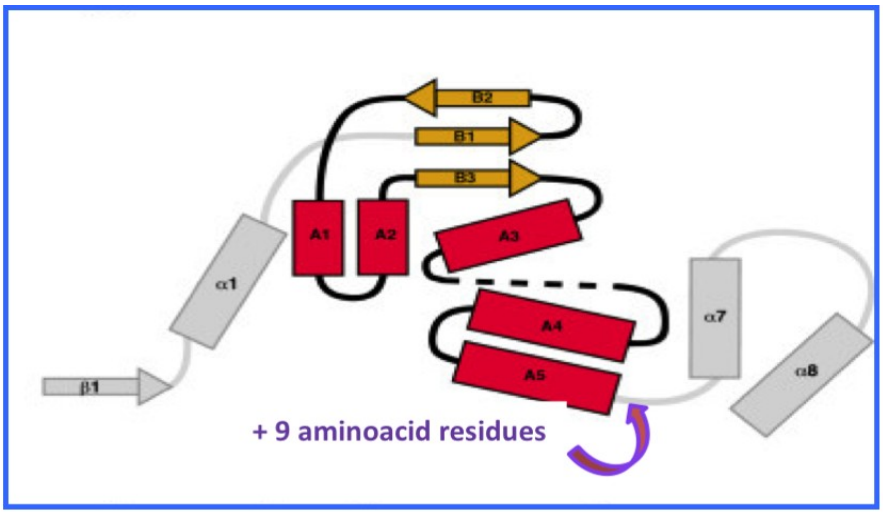

GFLCPDTTSPSTTKVAGVSPKPYWVCSTCASNPANLTASTQFCTHPGSSAFSFLSVSPVL
PKISPPPVPSSPPSFGGPVTLNVGGTLYSTTLETLTREPDSMLGAMERAGTPMPPNLNSQ
GGGHYFIDRDGKAERHILNELRLGRLDLPRGYGETALRAEADEYQIRPLLDALRELEAS
QGTPAPTAALLHADVDVSPRLVHFSARRGPHHYELSSVQVDTFRANLFCTDSECLGALRA
RFGVASGDRAEGSPHFHLEWAPRPVELPEVEYGRLGLQPLWTGGPGERREVVGTPSFLEE
VLRVALEHGFRLDSVFPDPEDLLNSRSLRFVRH

Figure 3.17. Construct of POZ/BTB +15 - +125; in purple is reported the sequence (9 aminoacids) added at C-terminal of domain.

In order to identify the optimal conditions for the stabilization of the tetrameric form, and hence its crystallization CD thermal denaturation in the presence of different salts, including sodium citrate, sodium chloride and magnesium chloride were carried out. All these salts were able to stabilize the domain, in particular increasing the concentration of sodium chloride until 400 mM an increase in melting temperature of 5 °C (54 °C to 59 °C) was observed (figure 3.18). This information has been used to develop new tests of crystallization from which were obtained crystals bigger than those previously analyzed. Unfortunately, these crystals diffracted a 4.0 Å of resolution, not enough to solve the structure (figure 3.19).

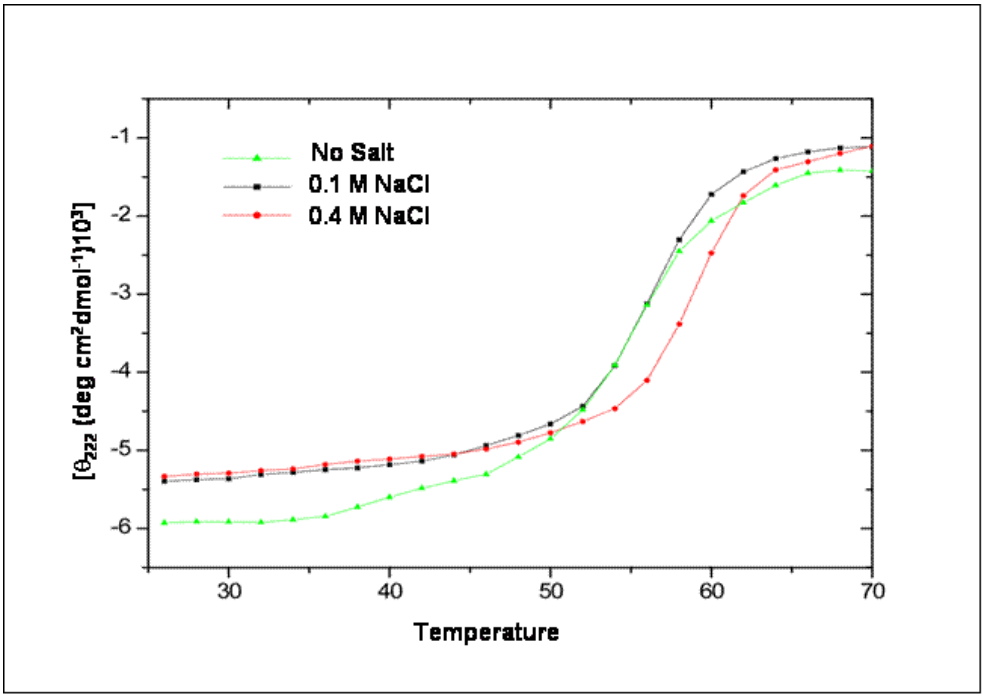

Figure 3.18. Far-UV CD spectra of BTB/POZ in the presence of increasing concentrations of NaCl.

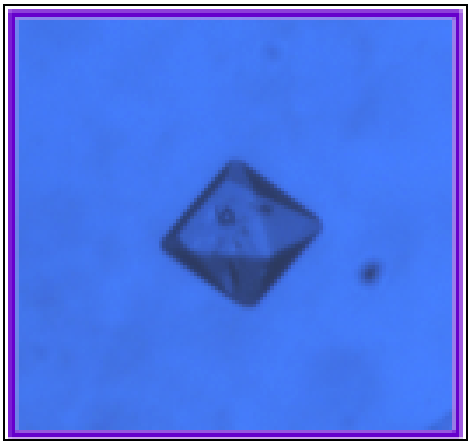

Figure 3.19. Crystals of BTB/POZ obtained at 20 °C using the hanging-drop vapour-diffusion technique.

3.10 New constructs of POZ/BTB^{KCTD11} domain

In order to add further structural motifs and to facilitate the correct folding of the domain, three new POZ/BTB constructs based on sequence alignments and secondary structure predictions were designed. In particular, two constructs were designed with further 9 and 21 residues at C-terminal in order to introduce two additional alpha helixes present in Privè' s model; while the third construct was prolonged at N-terminus until translation start residue (figure 3.20). The three constructs were cloned in pETM20 vector and expressed in *E. coli* under the same conditions used to express POZ/BTB (+15 - +125). These changes haven't obtained the expected improvements; in fact the new constructs were less stable. The construct with 9 additional residues at the C-terminus forms crystals of different morphology compared to those obtained by previous POZ/BTB domain, but these crystals do not provide a diffraction pattern with a better resolution (figure 3.21).

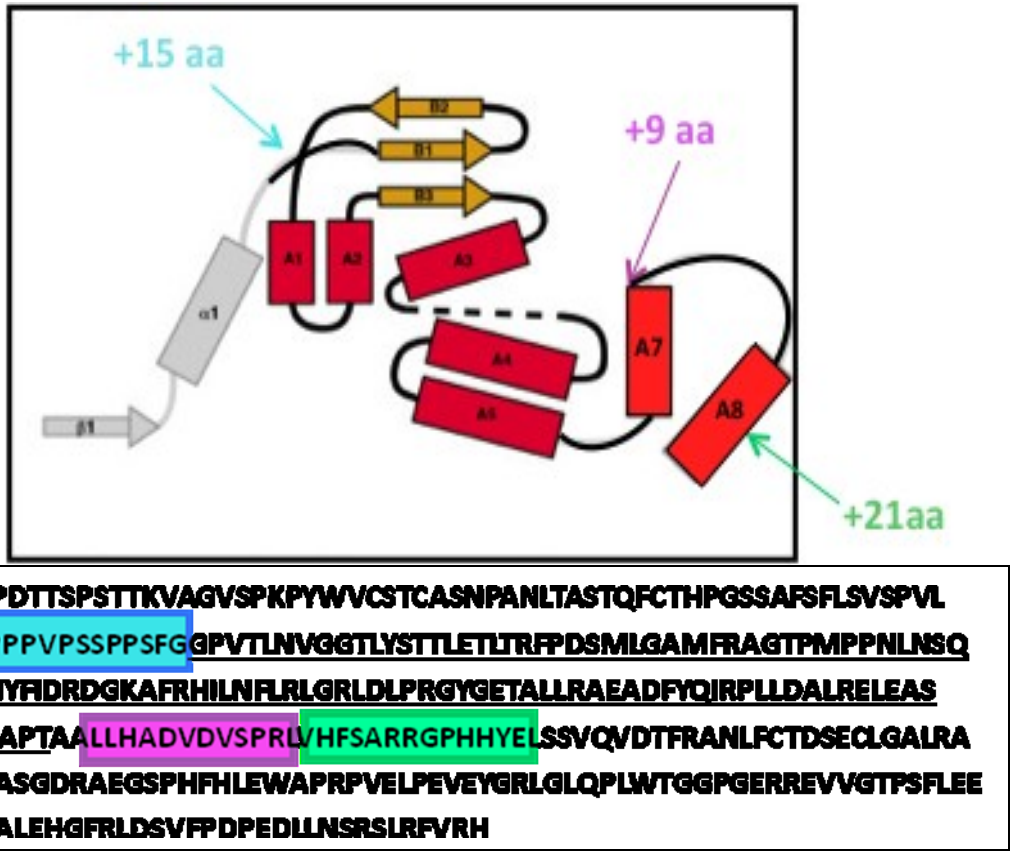

Figure 3.20. Design of three new constructs of POZ/BTB. In cyan the additional aminoacids in the construct +1 - +125, in purple and in green the additional aminoacids in the constructs +15 - +134 and +15 - +146 respectively.

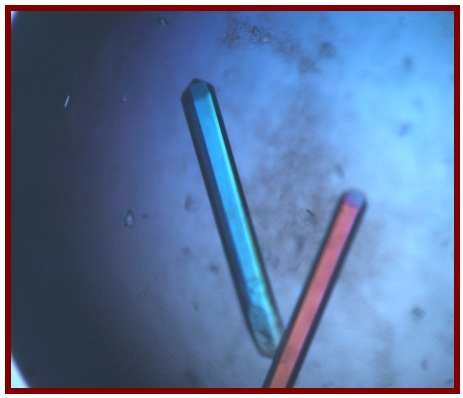

Figure 3.21. Crystals of BTB/POZ +15 - +134 obtained at 20 °C using the hanging-drop vapour-diffusion technique (4.0 Å resolution).

3.11 Design of POZ/BTB mutants by molecular modelling

The BTB/POZ tetramerization domains of the potassium channels Kv4 are the proteins with known 3D structure most closely related to the N-terminal region of REN^{KTCD11}. This observation suggests that using comparative molecular modeling techniques may generate reliable models of BTB/POZ domain of REN^{KTCD11}. The analysis of the 3D model generated POZ/BTB of REN^{KTCD11} suggests analogies and differences with the Kv4 model used as a template. The crystal structure of the Kv4 fragment, which spans from residue 46 to 146, shows that four independent chains of the protein, each characterized by a α/β structure, form a tetramer (figure 3.22). Two different types of interactions stabilize the tetramer interface. The most important ones are mediated by a zinc ion that is coordinated by cysteine and histidine residues belonging to different subunits. In particular, Cys 132, Cys 133, and His 105 of one subunit and Cys 121 of an adjacent chain coordinate the zinc ion. Further stability to the POZ/BTB tetramer of Kv4 is provided by hydrogen bonding and electrostatic interactions among residues located at the inter-subunit interface (Figure 3.23 a and 3.23 b). It is worth noticing that residues that participate in the coordination of the zinc ions in Kv4 POZ/BTB domain are absent in REN^{KTCD11} sequence. On the other hand, most of the residues involved in the other interactions, essentially electrostatic, are present in REN^{KTCD11} sequence. In particular, conserved residues are: Arg93 (Kv4 sequence numbering), Asp 88, Asn 97, and Arg 100. It is also important to mention that, although Glu 110 is replaced by a Tyr residue, a nearby Glu may play the role of Glu 110. A similar situation is observed for the partner of Arg100, i.e. Glu 117, which is replaced by a Lys residue in REN^{KTCD11} sequence (figure 3.24). In conclusion the present analysis clearly indicates that the stability of the REN^{KTCD11} POZ/BTB tetramer essentially relies on electrostatic interactions at the intersubunit interface. So a mutant of POZ/BTB domain has been designed in which four residues, Asp 69, Arg74, Asn78, Arg 81 were mutated into alanine in order to alter the interface of interaction between molecules and to destabilize the tetramer.

The mutant POZ/BTB (construct +15 – +116) was cloned in pETM20 and expressed in the same conditions of wild-type domain. The mutant POZ/BTB aggregates in solution, as demonstrated from the analysis conducted on molecular exclusion chromatography. The results obtained with the mutant POZ/BTB allowed us to identify residues potentially involved in the formation of the tetramer and to confirm the instability in solution of the POZ/BTB as monomer.

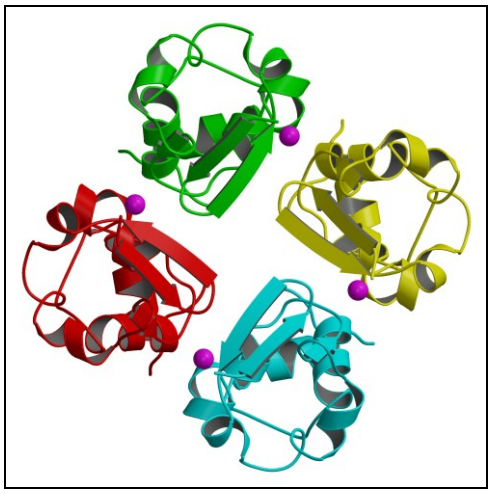

Figure 3.22. Tetrameric structure of the Kv4 POZ/BTB domain. The zinc ions located at the inter-subunit interface are colored in magenta.

a

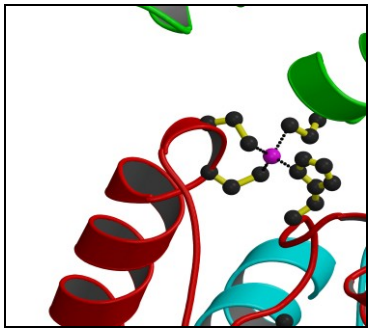

b

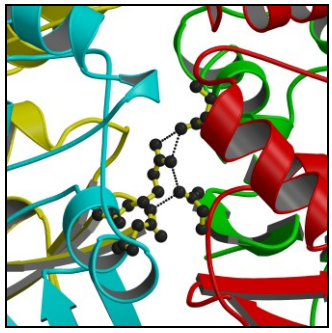

Figure 3.23. Interactions that stabilize the tetramer interface of Kv4 POZ/BTB domain. a: Coordination of the zinc ions located at the inter-subunit interface. b: Electrostatic interactions located at the inter-subunit interface.

```
44.4% identity in 72 aa overlap (3-74:43-108); score:  175 E(10000):
2.5e-11
             10        20        30        40        50        60
BTBPOZ VILEWGGTLYSTTLEILTRFPDSMIGAMFRAGTPMPPELESQGGGHYFIDRDGKMFRHIL
       ..::::.:: ..:  .:: :.::..::.  :    : .       .::.:::   :::::
Kv4    IVLEWSGTRFQTWQDTLERYPDTLIGSSERDFTYHPETQ------QYFTDRDPDIFRHIL
             50        60        70        80              90
             70
BTBPOZ HFLRIGRLDIPR
       :: : :.:  ::
Kv4    HFYRTGKLNYPR
        100
```

Figure 3.24. Sequence alignment of the POZ/BTB domain of REN^{KCTD11} and the potassium channel Kv4. Residues of REN^{KCTD11} sequence that might participate to the inter-subunit interface of the putative protein tetramer are colored in red.

3.12 KCTD21

After a careful analysis of sequence alignments, our attention was focused on a new "open reading frame", kctd21, which presents 42% identity with kctd11 (figure 3.25). The gene *kctd21* is located on chromosome 11, which in some rare cases of medulloblastoma shows events of deletion and encodes a putative protein of 260 amino acids. The full-length form and the domain POZ/BTB were cloned and expressed in *E. coli* in order to obtain structural information that could be extended to REN^{KCTD11}. Despite having tested several fusion constructs and numerous conditions of induction, KCTD21 was unstable in solution and consequently not characterized. With regard to the POZ/BTB of KCTD21, it has been cloned in pETM20 and has been expressed at 22 °C for 16 h in BL21(DE3)STAR as fusion protein with Trx-A. The analysis of the chromatographic profile of molecular exclusion chromatography has provided us data showing that POZ/BTB of KCTD21 is organized in a tetrameric structure, but differently from POZ/BTB of REN^{KCTD11} it is highly unstable in solution, so it was impossible to proceed with the crystallographic investigations (figure 3.26).

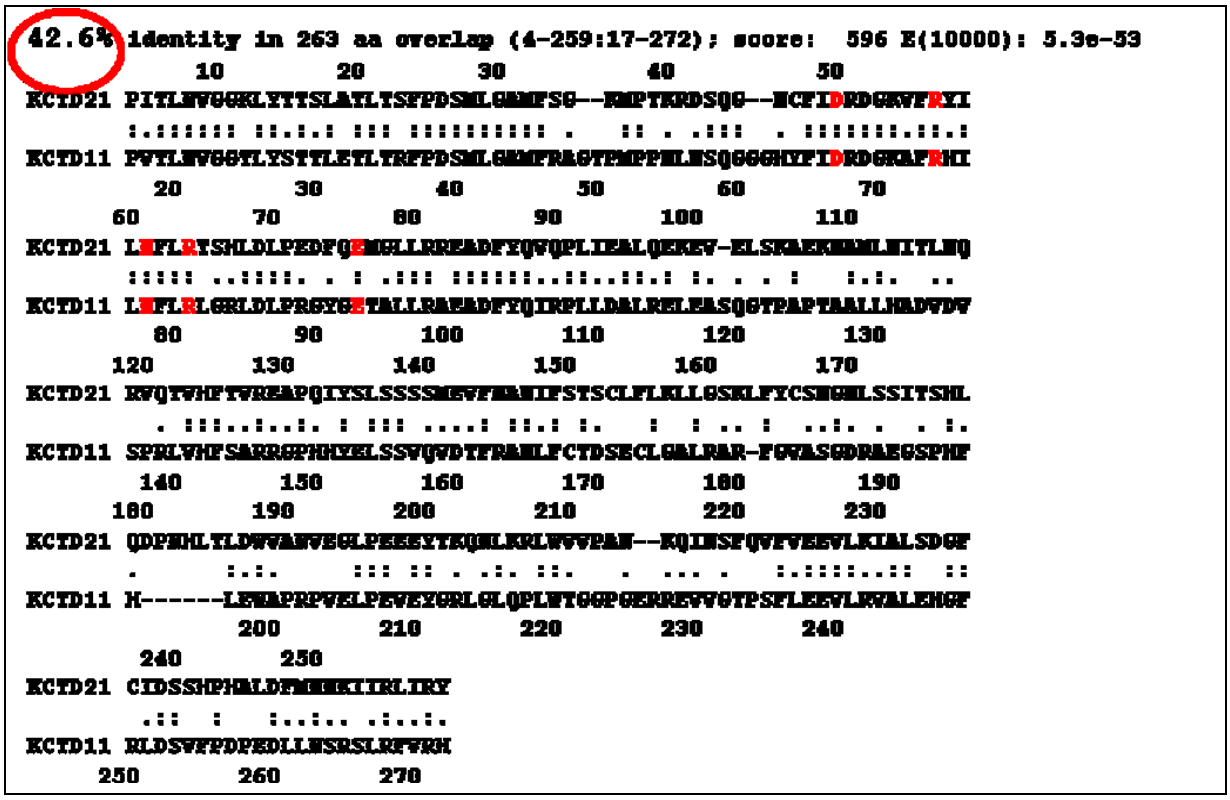

Figure 3.25. Sequence alignment of KCTD21 and REN^{KCTD11}. Residues that participate to the inter-subunit interface of the putative protein tetramer are conserved and are colored in red.

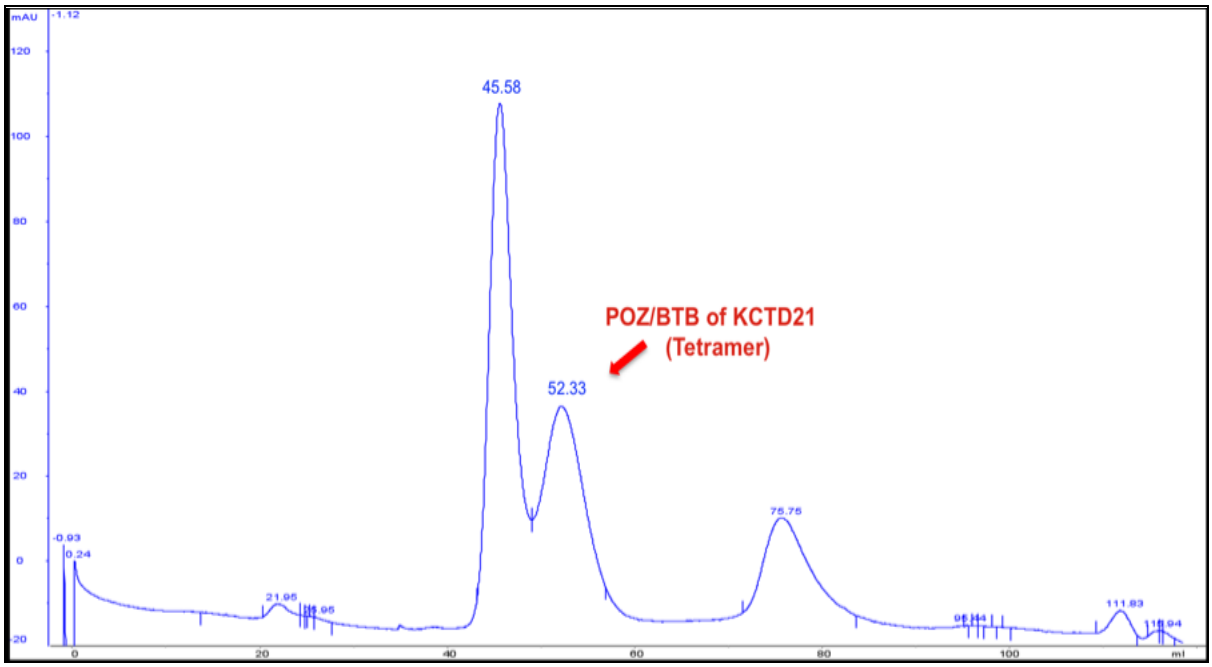

Figure 3.26. Molecular size exclusion chromatographic elution profile of POZ/BTB of KCTD21.

3.13 Model of interaction between POZ/BTB^{KCTD11} and Cul3

It is known in literature that members of the family Cul3 bind proteins containing POZ/BTB domain. Our hypothesis is that REN^{KCTD11} may be involved in large complexes denoted as ubiquitin-protein ligases (E3) and that interacts with Cul3 by its POZ/BTB domains. We investigated the possibility to build 3D models of these complexes. All structures of POZ/BTB-Cul3 complexes hitherto reported contain a single POZ/BTB domain interaction with a single Cul3 molecule. We initially considered the structure of the complex between Cul1 and Skp1 to build a one to one complex of REN^{KTCD11} POZ/BTB–Cul3. The POZ/BTB domain interacts with its partner essentially through the β-strand B3 of the β-sheet and the helix A2. It is worth mentioning that these fragments are present in the sequence of REN^{KTCD11} short form (figure 3.27). This may account for the observed functionality of this form in the regulation of the Hedgehog pathway in cells over expressing the protein. Although the efficient binding of POZ/BTB to Cul3 likely requires the presence of the missing parts, the presence in the short form sequence of these regions allows the anchoring of the protein to the Cul3 when REN^{KTCD11} is over-expressed. The experimental evidence that REN^{KTCD11} POZ/BTB forms stable tetramer in solution prompted us to check the possibility to generate larger POZ/BTB-Cul3 complexes. As shown in figure 3.28, a convincing complex between POZ/BTB of REN^{KTCD11} and Cul3 with a 4:4 stoichiometry could be generated. In this complex the structure of the POZ/BTB must be considered tetrameric and each subunit must interact with one molecule of Cul3. Interestingly, a α-helix of Cul3 docks into a cavity formed at the inter-subunit interface within the tetramer. The analysis of the model also shows that in this complex a larger portion of the POZ/BTB domain is involved at the complex interface if compared to the 1:1 model. Indeed, each POZ/BTB subunit interacts with two distinct Cul3 molecules. The interactions with the first Cul3 molecule are mediated, as described above, by A2 and B3 while with the second A1 is involved. We then considered the possibility to build up a larger aggregate by including other partners

for which structural information are available (Rbx1 and E2). By following the procedure reported in the methods section, a tetrameric REN^{KTCD11} POZ/BTB-Cul3-Rbx1-E2 assembly was performed. This model clearly indicates that the C-terminal of REN^{KTCD11} POZ/BTB, to which the ΔPOZ portion of REN^{KTCD11} and the substrate are likely connected, is on the same side of the complex of E2 (figure 3.29). In other words the organization of this giant complex is compatible with the proposed functional role of REN^{KTCD11}. Intriguingly, the tetrameric nature of REN^{KTCD11} POZ/BTB makes, from the structural point of view, the traditionally complicated ubiquitin-protein ligases even more intricate. This consideration leads to the suggestive hypothesis that the ubiquitination process of specific substrates, which involves REN^{KTCD11} and other related proteins, requires assemblies endowed an even larger molecular complexity compared to 1:1 aggregates.

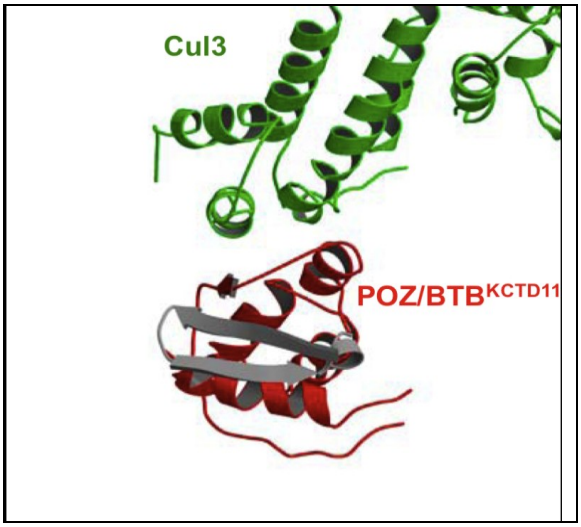

Figure 3.27. Overall view of the interaction of a single subunit of the BTB/POZ ^{KCTD11} domain (in red) with Cul3 (in green). Residues which are missing in the sequence of the “short” form of REN^{KTCD11} are in grey.

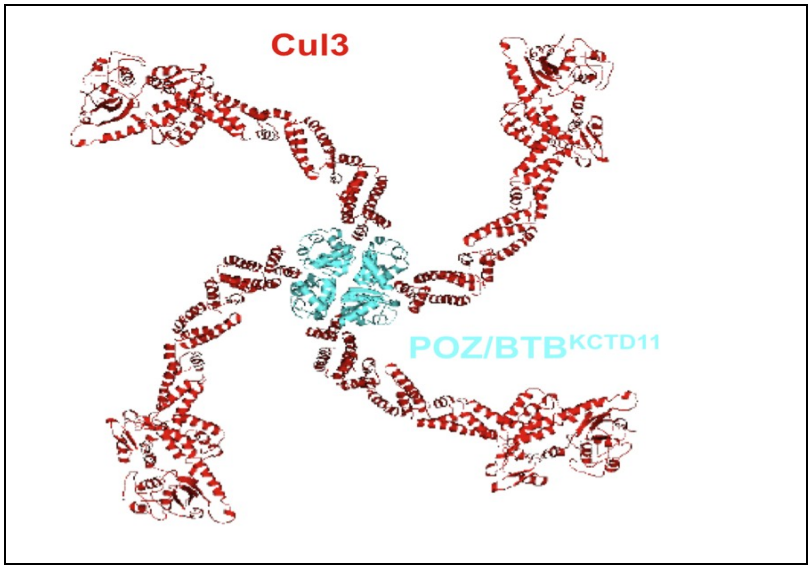

Figure 3.28. POZ/BTB/Cul3 interaction model with a 4:4 stoichiometry, POZ/BTB is reported in cyan, while Cul3 in red.

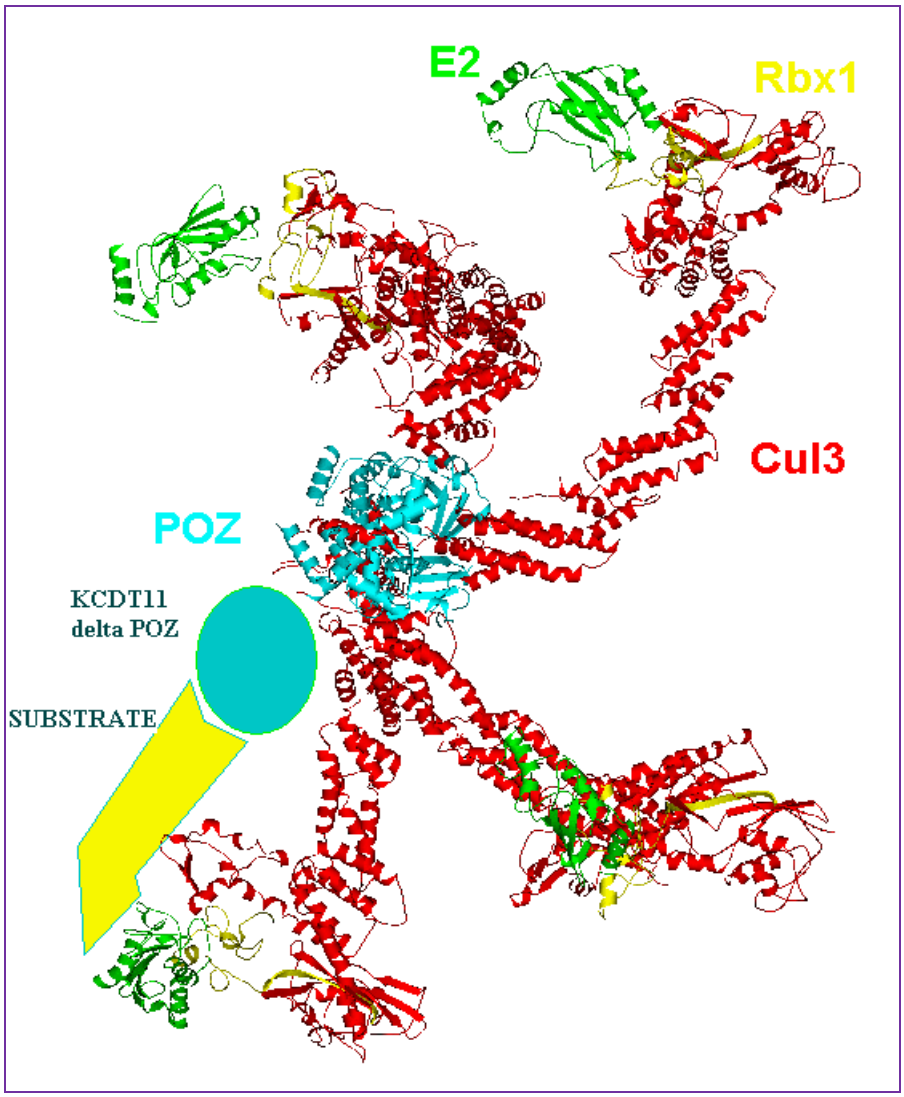

Figure 3.29. Model of complex between REN^{KCTD11} and ubiquitin-ligase E3.

3.14 POZ/BTB^{KCTD11}-Cul3

Our data have been supplemented by Dr. Luigi Vitagliano (IBB, CNR of Naples) molecular modelling studies: the model based on the structure of the known complex Skp1/Cul1 (homologous REN^{KCTD11} and Cul3, respectively), each subunit of the tetramer of POZ/BTB interacts with Cul3 molecule, forming a complex of huge size with which interacting other fusion partners. This model was used to select the region of interaction between Cul3 and POZ/BTB. A peptide corresponding to residues 49-68 (NH_2-NSGLSFEELYRNAYTMVLHK-COOH) of Cul3 has been individuated as responsible of interaction with the domain POZ/BTB of REN^{KCTD11} (figure 3.30). Thus, in collaboration with Dr. Laura Zaccaro (IBB, CNR of Naples), the helix 49-68 of Cul3 was synthesized by solid phase F-moc chemistry. The peptide synthesized was subjected to analysis by CD spectroscopy; the spectrum of peptide highlights a partially organization in alpha-helix (figure 3.31). The peptide 49-68 of Cul3 was used to perform ELISA assay with the Trx-POZ/BTB domain of REN^{KCTD11}. The peptide binds POZ/BTB of REN^{KCTD11} with an affinity constant of 0.8 μM (figure 3.32).

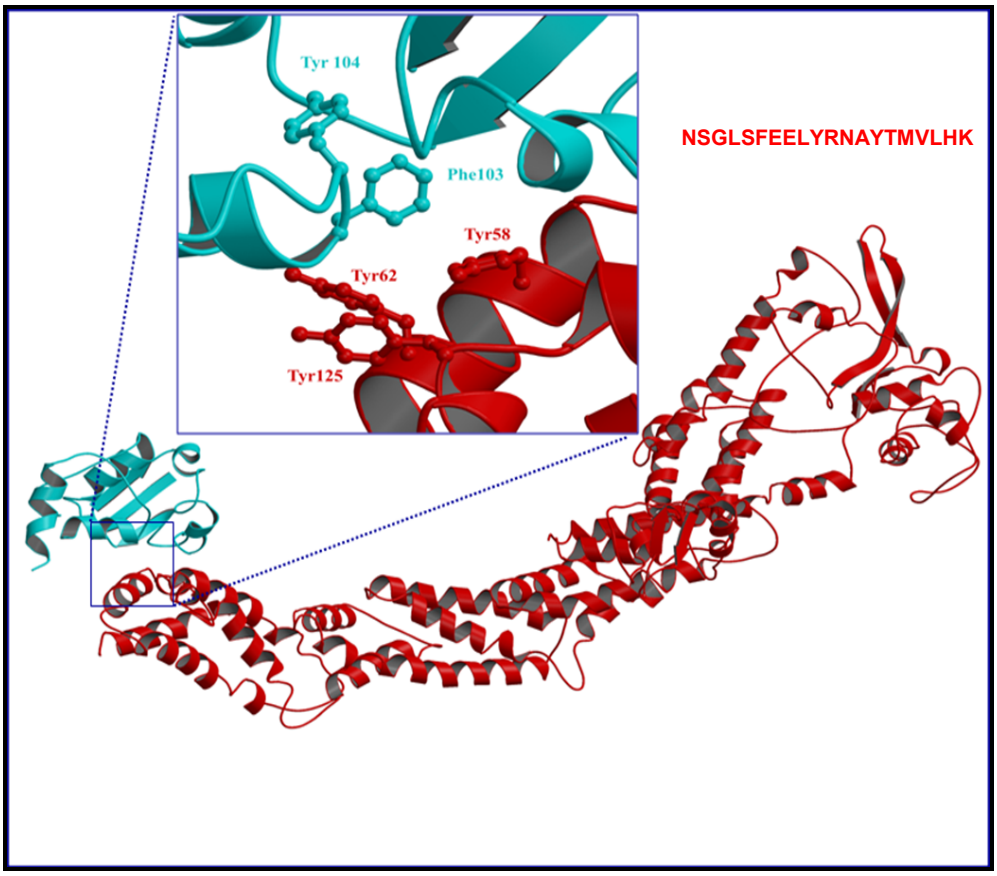

Figure 3.30. Model of interaction of a single subunit of the BTB/POZ^{KCTD11} (cyan) with Cul3 (red).

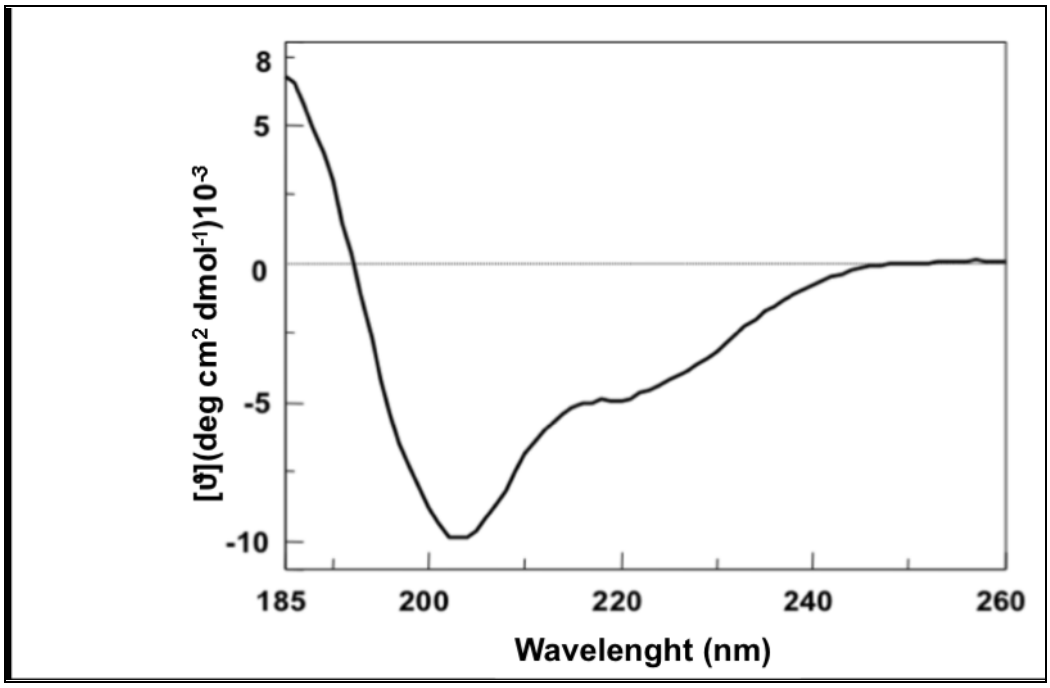

Figure 3.31. Far-UV CD spectrum of peptide 49-68 of Cul3 in 10 mM phosphate pH 7.5 buffer at 25°C.

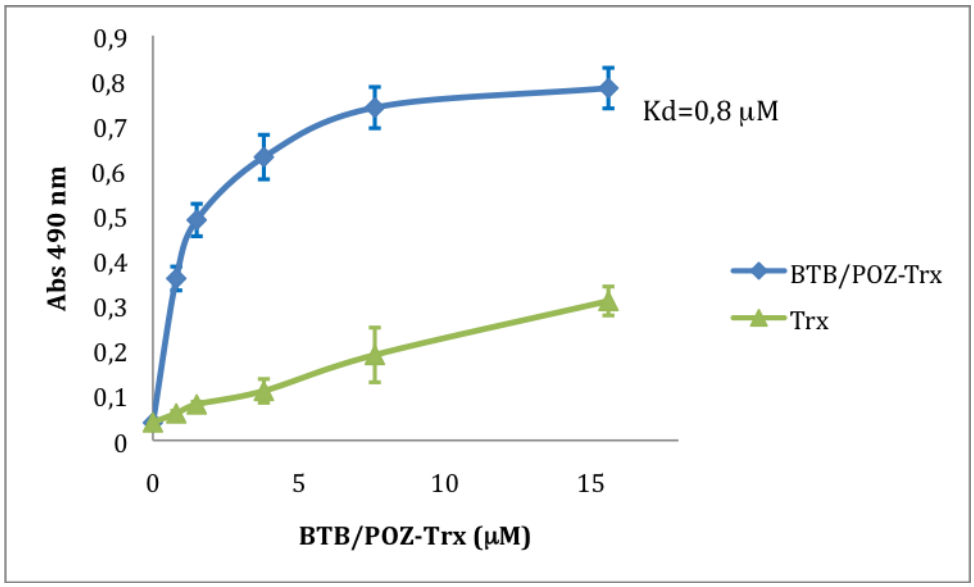

Figure 3.32. Binding curve obtained from ELISA assay with Trx-POZ/BTB^{KCTD11} and 49-68 helix of Cul3.

3.15 Heteronuclear single quantum correlation (HSQC) spectrum of POZ/BTB (+15 - +125)

In order to conferm the interaction and to identify the aminoacid residues of POZ/BTB of REN^{KCTD11} involved in the binding with Cul3 has been conducted in collaboration with the prof. Carla Isernia (Dipartimento di Scienze Ambientali, Seconda Università di Napoli, Caserta,) a nuclear magnetic resonance analysis. POZ/BTB (+15 - +125) domain was expressed in minimal medium in presence of ^{15}N ($^{15}NH_4Cl$) and purified as described in materials and methods. The final yield was been of 18 mg of labelled protein for litre of culture. The HSQC spectrum of POZ/BTB (+15 - +125) acquired at 600 MHz and reported in figure 3.33 exhibits a large part of the expected resonances, which are well dispersed over a chemical shift range of approximately 4.5 ppm in the proton dimension and 35 ppm in the nitrogen dimension. The high degree of dispersion in the spectrum is in accord with the presence of β-strands, as this type of structure is typically associated with extensive dispersion. In contrast, the somewhat more crowded region in the centre of the spectrum is likely to contain resonances from helical regions which are typically associated with a more degenerate local environment leading to a lower degree of NMR resonance dispersion. Overall, the spectrum is consistent with a well-defined native structure with extensive tertiary interactions. When the peptide 49-68 of Cul3 is added to the protein solution all the signals in the ^{1}H-^{15}N HSQC experiments are reduced in intensity. At one-quarter equimolar peptide concentration, the intensity of the signals is sensitively reduced, thus suggesting an interaction between the protein and the peptide. This interaction is further confirmed by the STD experiment reported in figure 3.34. Moreover, for some residues a small chemical shift variation is observed, being probably the result of conformational changes in the fast exchange regime upon peptide binding. The chemical shift variation enhances upon titration of the protein with the peptide. These data clearly prove the interaction between the peptide 49-68 of Cul3 and the domain POZ/BTB and allow to design a future accurate NMR analysis that will clarify the mechanism of interaction between the two molecules.

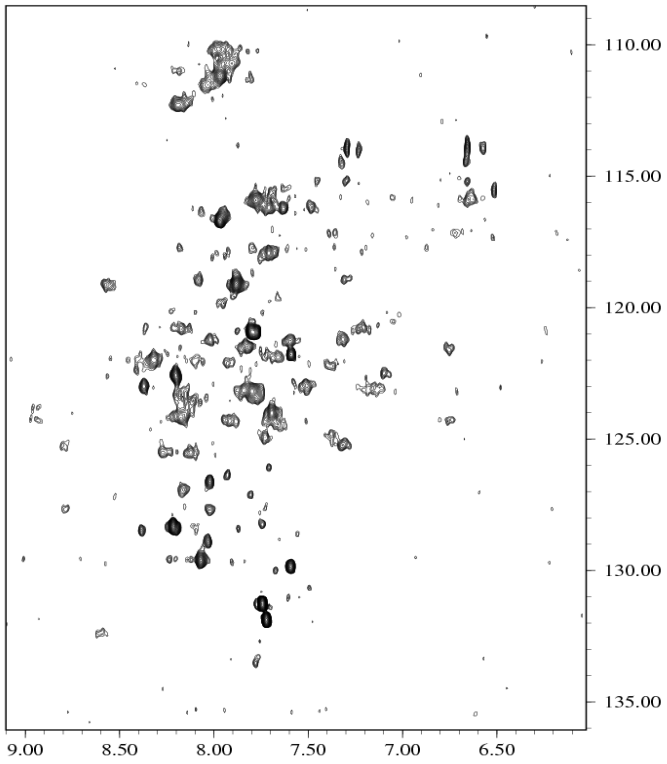

Figure 3.33. HSQC spectrum of POZ/BTB (+15 - 125).

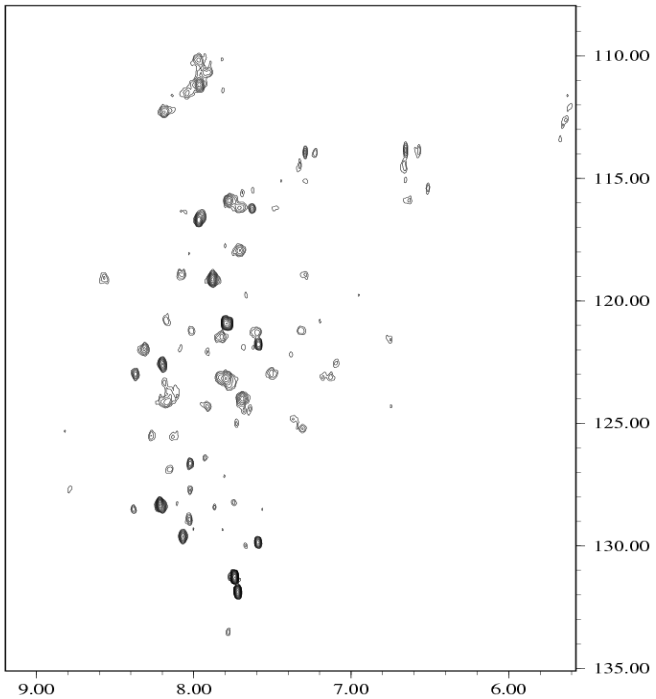

Figure 3.34. HSQC spectrum of POZ/BTB (+15 - +125) with helix 49-68 of Cul3 (ratio 1:8 protein-peptide).

3.16 Interaction between KCTD5 and Cul3 peptide

The helix 49-68 of Cul3 has been identified as region of interaction with the BTB/POZ domain, so we tried to investigate whether the same region of Cul3 was responsible for interaction with POZ/BTB domains of other KCTD proteins. It was chosen as the starting point KCTD5, a cytosolic protein that interacts with GRASP55, and whose crystal structure has been recently deposited (Dementieva I., *et al.* 2009). The POZ/BTB domain of KCTD5 with 5 aminoacids added at N-terminus (region 40-151) (figure 3.35) was cloned in expression vector pETM11 and expressed in *E. coli*. The domain BTB/POZ of KCTD5 was then purified to homogeneity and analyzed by light scattering. Light scattering results revealed a pentameric organization for BTB/POZ of KCTD5 in according with data present in literature. ELISA assay was performed to verify if the POZ/BTB of KCTD5 is able to bind the helix 49-68 of Cul3. The results obtained by ELISA show that POZ/BTB binds the helix 49-68 of Cul3 with an affinity similar to that of the BTB/POZ of REN^{KCTD11} (figure 3.36). Tests of co-crystallization of BTB/POZ of KCTD5 with the helix-Cul3 are in progress in order to identify either the region involved in the interaction of this domain either to obtain information useful for the characterization of the interaction of the BTB/POZ domain of REN^{KCTD11} with Cul3.

Figure 3.35. Aminoacid sequence of the BTB/POZ domain of KCTD5.

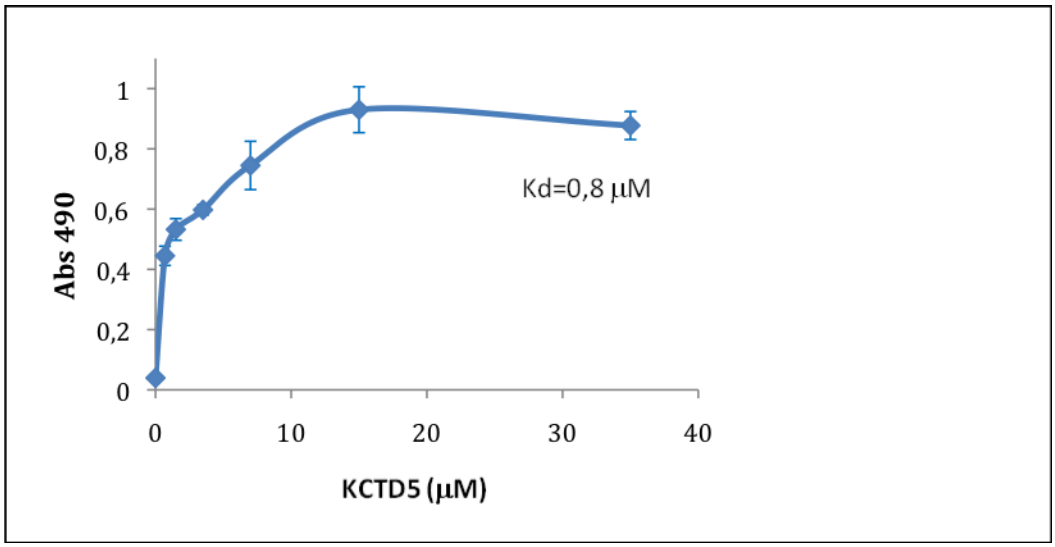

Figure 3.36. Binding curve obtained from ELISA assay with Trx-POZ/BTB of KCTD5 and 49-68 helix of Cul3.

4 DISCUSSION

During the past few years, considerable progress has been made on the characterization of cullin-based ligases and on their possibility to target a very large number of substrates for ubiquitin-dependent degradation. Available evidences strongly suggest that POZ/BTB proteins function as substrate-specific adaptors of Cul3 ligases. The most of the POZ/BTB proteins contain an additional protein–protein interaction domain, however, several Cul3-interacting proteins appear to contain only a BTB domain, and are thus unlikely to possess the ability to interact simultaneously with potential substrates. The discovery that BTB proteins can assemble into a novel class of E3 ligases is of general importance, given the high number of POZ/BTB-containing proteins present in the genome of different organisms. Some POZ/BTB proteins are characterized and are known to be involved in a variety of biological processes, including regulation of microtubules and microfilament dynamics, transcription, and apoptosis. Since POZ/BTB-containing proteins are mutated in some human diseases, re-investigating their function with regard to a possible role in ubiquitin-dependent degradation pathways may be rewarding. For this reason this work has been focused on the protein REN^{KCTD11}. REN^{KCTD11} presents the domain POZ/BTB at N-terminus and its gene is deleted in many cases of medulloblastoma. In particular, REN^{KCTD11} inhibits cell growth by antagonizing Gli1-mediated transactivation of Hedgehog target genes via impairment of Gli1 nuclear transfer. The functional characteritation of REN^{KCTD11} variants with deleted domains has given preliminary data on the role played by the different domains of REN^{KCTD11} on control of medulloblastoma insurgence. These investigations have demonstrated that the mutant of REN^{KCTD11} with the deleted POZ/BTB domain is inactive. Although these data indicate that the POZ/BTB domain is fundamental for REN^{KCTD11} function, the specific biological role of this domain is still unknown. In this PhD thesis we describe, firstly, a novel protein form of REN^{KCTD11}, with a new translational start point placed at 39 aminoacid residues upstream of the +1 methionine previously identified (Gallo R., *et al.* 2002). We have individuated exact extension of POZ/BTB domain located at the N-terminus, containing residues +15 - +116. POZ/BTB of REN^{KTCD11} shows analogies with the T1 domain of Kv4, that mediates homo-tetramerization in numerous crystal structures and so we have verified the oligomeric state of REN^{KCTD11}. Our data demonstrate that REN^{KCTD11} is a tetrameric protein and that its POZ/BTB domain is responsible of tetramerization. *In vitro* experimental analyses have indicated that REN^{KTCD11} interacts with the protein Cul3. This suggests that the protein may be involved in the complex of the ubiquitin-protein ligases. All structures of reported POZ/BTB-Cul3 complexes contain a single POZ/BTB domain interaction with a single Cul3 molecule. A convincing complex between POZ/BTB of REN^{KCTD11} and Cul3 with a 4:4 stoichiometry could be generated considering the structure of the POZ/BTB as tetramer and the interactions of each subunit with Cul3. In particular the helix corresponding to residues 49-68 of Cul3 has been individuated as responsible of interaction with the domain POZ/BTB of REN^{KCTD11}. NMR analyses and immunological assays have confirmed this data. Few informations were obtained on the C-terminal region of REN^{KCTD11}, but it is possible to assume that in this portion not only it is present a motif involved in protein–protein interaction but also post-translational modifications that could explain the difficulties came across during the heterologous expression in *E. coli*. In fact, it is reported in literature that in addition to POZ/BTB domain, the adaptors contain a second protein–protein interaction motif that binds the targeted substrate [Petroski M.D., *et al.* 2005]. Our findings unveil a

possible mechanism of regulation of the Hedgehog signalling, in which REN^{KCTD11} is a critical mediator of Gli1 function. In this mechanism REN^{KCTD11} regulates indirectly Gli1. In fact, REN^{KCTD11} binds, probably with its POZ/BTB, Cul3 and in the same time with its C-terminal the effective regulator of Gli1. The results of these interactions are the ubiquitination and the proteasomal degradation of Gli1 regulator. The consequent impairment of Gli1 function results in the inhibition of cell growth. These data provide a novel mechanism of regulation of Gli1 transcriptional activation, which may have important implication in tumour developmental and biology and further emphasize the design of new class of therapeutic agents to use for treatment of medulloblastoma. KCTD proteins contain a N-terminus POZ/BTB domains and variable C-terminal with biological function unclear yet. KCTD5 has been the first member of the family KCTD to be characterized so far [Bayon Y., *et al.* 2008]. Recent studies demonstrate that KCTD5 interacts specifically with Cul3, and forms oligomers through its POZ/BTB domain [Dementieva I. S., *et al.,* 2009]. Our results show that POZ/BTB of KCTD5 binds the helix 49-68 of Cul3 with an affinity similar to that of the BTB/POZ of REN^{KCTD11}. These findings confirm that KCTD5 is a substrate-specific adaptor for Cul3-based E3 ligases and that other members of KCTD family can be involved in similar mechanism of regulation. The tumour development is often connected with alterations of these mechanisms of regulation that according to dysfunction is necessary to have on or off. So, the characterization of the regions of interaction constitutes the base to design molecules with agonist/antagonist function to use for therapy. Our studies not only represent a crucial step to understand the molecular mechanism of REN^{KCTD11} but also lay the foundations to develop molecules of pharmaceutical interest for the therapy of disease in which proteins belonging to the KCTD family are involved.

5 REFERENCES

Ahmad KF, Engel CK, Privé GG, "*Crystal structure of the BTB domain from PLZF*". Proc Natl Acad Sci U S A. 1998 Oct 13; 95(21): 12123-8.

Aravind L, Koonin EV. "*Fold prediction and evolutionary analysis of the POZ domain: structural and evolutionary relationship with the potassium channel tetramerization domain*". J Mol Biol. 1999 Jan 29; 285(4): 1353-61.

Argenti B, Gallo R, Di Marcotullio L, Ferretti E, Napolitano M, Canterini S, De Smaele E, Greco A, Fiorenza MT, Maroder M, Screpanti I, Alesse E, Gulino A, "*Hedgehog antagonist REN(KCTD11) regulates proliferation and apoptosis of developing granule cell progenitors".* J Neurosci. 2005 Sep 7; 25(36): 8338-46.

Bardwell VJ, Treisman R, "*The POZ domain: a conserved protein-protein interaction motif*". Genes Dev. 1994 Jul 15;8(14): 1664-77.

Bayon Y, Trinidad A. G., De la Puerta M. L., Rodrıguez M., Bogetz J., Rojas A., De J. M.Pereda, Rahmouni S., Williams S., Matsuzawa S., Reed J. C., Crespo M., Mustelin T.and A. Alonso "*KCTD5, a putative substrate adaptor for cullin3 ubiquitin ligases*". FEBS Journal 275 (2008) 3900–3910.

Bradford M, "*A rapid and sensitive method for the quantitation of microgram quantities of protein utilizing the principle of protein dye-binding*". Anal. Biochem. 72, 248-254 (1976).

Cardozo T, Pagano M, " *The SCF ubiquitin ligase: insights into a molecular machine".* Nat Rev Mol Cell Biol. 2004 Sep; 5(9): 739-51. Review.

Carlotti CG Jr, Smith C, Rutka JT. "*The molecular genetics of medulloblastoma: an assessment of new therapeutic targets*". Neurosurg Rev. 2008 Oct; 31(4): 359-68.

Crawford JR, MacDonald TJ, Packer RJ, "*Medulloblastoma in childhood: new biological advances".* Lancet Neurol. 2007 Dec; 6(12): 1073-85. Review.

Dahmane N, Ruiz i Altaba A. "*Sonic hedgehog regulates the growth and patterning of the cerebellum".* Development. 1999 Jun; 126(14): 3089-100.

De Bont JM, Roger J. Packer, Erna M. Michiels, Monique L. den Boer, and Rob Pieters, "*Biological background of pediatric medulloblastoma and ependymoma: A review from a translational research perspective*." Neuro Oncol. 2008 Dec; 10(6): 1040-60.

Dellovade T, Romer JT, Curran T, Rubin LL. "*The hedgehog pathway and neurological disorders*". Annu Rev Neurosci. 2006; 29: 539-63. Review.

Dementieva IS, Tereshko V., McCrossan Z. A., Solomaha E., Araki D., Xu C., Grigorieff N., Goldstein S. A. N. "*Pentameric Assembly of Potassium Channel Tetramerization Domain-Containing Protein 5*" J. Mol. Biol. (2009) 387, 175–191

De Smaele E, Di Marcotullio L, Ferretti E, Screpanti I, Alesse E, Gulino A. "*Chromosome 17p deletion in human medulloblastoma: a missing checkpoint in the Hedgehog pathway*." Cell Cycle. 2004 Oct; 3(10): 1263-6. Review.

De Smaele E, Fragomeli C, Ferretti E, Pelloni M, Po A, Canettieri G, Coni S, Di Marcotullio L, Greco A, Moretti M, Di Rocco C, Pazzaglia S, Maroder M, Screpanti I, Giannini G, Gulino A. "*An integrated approach identifies Nhlh1 and Insm1 as Sonic Hedgehog-regulated genes in developing cerebellum and medulloblastoma.* Neoplasia. 2008 Jan; 10(1): 89-98.

Di Marcotullio L, Ferretti E, De Smaele E, Argenti B, Mincione C, Zazzeroni F, Gallo R, Masuelli L, Napolitano M, Maroder M, Modesti A, Giangaspero F, Screpanti I, Alesse E, Gulino A. "*REN(KCTD11) is a suppressor of Hedgehog signaling and is deleted in human medulloblastoma*." Proc Natl Acad Sci U S A. 2004 Jul 20; 101(29): 10833-8.

Di Marcotullio L, Ferretti E, Greco A, De Smaele E, Po A, Sico MA, Alimandi M, Giannini G, Maroder M, Screpanti I, Gulino A. "*Numb is a suppressor of Hedgehog signalling and targets Gli1 for Itch-dependent ubiquitination*." Nat Cell Biol. 2006 Dec;8(12): 1415-23.

Di Marcotullio L, Ferretti E, De Smaele E, Screpanti I, Gulino A. "*Suppressors of hedgehog signaling: Linking aberrant development of neural progenitors and tumorigenesis*." Mol Neurobiol. 2006 Dec; 34(3): 193-204. Review.

Ellison D, "*Classifying the medulloblastoma: insights from morphology and molecular genetics*". Neuropathol. Appl. Neurobiol. (2002) 28, 257–282

Ferretti E, De Smaele E, Di Marcotullio L, Screpanti I, Gulino A. "*Hedgehog checkpoints in medulloblastoma: the chromosome 17p deletion paradigm*". Trends Mol Med. 2005 Dec; 11(12): 537-45. Review.

Fuccillo M, Joyner AL, Fishell G. "*Morphogen to mitogen: the multiple roles of hedgehog signalling in vertebrate neural development*". Nat Rev Neurosci. 2006 Nov; 7(11): 902.

Furukawa M, He YJ, Borchers C, Xiong Y, "*Targeting of protein ubiquitination by BTB-Cullin 3-Roc1 ubiquitin ligases".* Nat Cell Biol. 2003 Nov; 5(11): 1001-7.

Gallo R, Zazzeroni F, Alesse E, Mincione C, Borello U, Buanne P, D'Eugenio R, Mackay AR, Argenti B, Gradini R, Russo MA, Maroder M, Cossu G, Frati L, Screpanti I, Gulino A. "*REN: a novel, developmentally regulated gene that promotes neural cell differentiation*. "J Cell Biol. 2002 Aug 19; 158(4): 731-40.

Gandhi TK, Zhong J, Mathivanan S, Karthick L, Chandrika KN, Mohan SS, Sharma S, Pinkert S, Nagaraju S, Periaswamy B, Mishra G, Nandakumar K, Shen B, Deshpande N, Nayak R, Sarker M, Boeke JD, Parmigiani G, Schultz J, Bader JS, Pandey A. "*Analysis of the human protein interactome and comparison with yeast, worm and fly interaction datasets*". Nat Genet. 2006 Mar; 38(3): 285-93.

Geyer R, Wee S, Anderson S, Yates J, Wolf DA. "*BTB/POZ domain proteins are putative substrate adaptors for cullin 3 ubiquitin ligases*". Mol Cell. 2003 Sep; 12(3): 783-90.

Gilbertson RJ, *"Medulloblastoma: signalling a change in treatment".* Lancet Oncol. 2004 Apr; 5(4): 209-18. Review.

Grill J, Bhangoo R, "*Recent development in chemotherapy of paediatric brain tumours".* Curr Opin Oncol. 2007 Nov; 19(6): 612-5. Review.

Gulino A, Di Marcotullio L, Ferretti E, De Smaele E, Screpanti I. "*Hedgehog signaling pathway in neural development and disease*". Psychoneuroendocrinology. 2007 Aug;32 Suppl 1:S52-6. Review.

Huangfu D, Anderson KV, "*Signaling from Smo to Ci/Gli: conservation and divergence of Hedgehog pathways from Drosophila to vertebrates".* Development. 2006 Jan; 133(1): 3-14. Review.

Kamura T, Sato S, Haque D, Liu L, Kaelin WG Jr, Conaway RC, Conaway JW, "*The Elongin BC complex interacts with the conserved SOCS-box motif present in members of the SOCS, ras, WD-40 repeat, and ankyrin repeat families".* Genes Dev. 1998 Dec 15; 12(24): 3872-81.

Kreusch A, Pfaffinger PJ, Stevens CF, Choe S, "*Crystal structure of the tetramerization domain of the Shaker potassium channel*". Nature. 1998 Jul 16; 394(6690): 216.

Kwon JE, La M, Oh KH, Oh YM, Kim GR, Seol JH, Baek SH, Chiba T, Tanaka K, Bang OS, Joe CO, Chung CH, "*BTB domain-containing speckle-type POZ protein (SPOP) serves as an adaptor of Daxx for ubiquitination by Cul3-based ubiquitin ligase*". J Biol Chem. 2006 May 5; 281(18): 12664-72.

Laemmli U, "*Cleavage of structural proteins during the assembly of the head of bacteriophage T4*". Nature 227, 680-685 (1970).

Lai K, Kaspar BK, Gage FH, Schaffer DV, "*Sonic hedgehog regulates adult neural progenitor proliferation in vitro and in vivo"*. Nat Neurosci. 2003 Jan; 6(1): 21-7.

Marino S, "*Medulloblastoma: developmental mechanisms out of control*". Trends Mol Med. 2005 Jan; 11(1): 17-22. Review.

Palma V, Ruiz i Altaba A. "*Hedgehog-GLI signaling regulates the behavior of cells with stem cell properties in the developing neocortex*". Development. 2004 Jan; 131(2): 337-45.

Palma V, Lim DA, Dahmane N, Sánchez P, Brionne TC, Herzberg CD, Gitton Y, Carleton A, Alvarez-Buylla A, Ruiz i Altaba A. "*Sonic hedgehog controls stem cell behavior in the postnatal and adult brain".* Development. 2005 Jan; 132(2):335-44.

Petroski MD, Deshaies RJ. "*Function and regulation of cullin-RING ubiquitin ligases".* Nat Rev Mol Cell Biol. 2005 Jan; 6(1): 9-20. Review.

Pintard L, Willems A, Peter M, "*Cullin-based ubiquitin ligases: Cul3-BTB complexes join the family".* EMBO J. 2004 Apr 21; 23(8): 1681-7.

Rossi A, Caracciolo V, Russo G, Reiss K, Giordano A. "*Medulloblastoma: from molecular pathology to therapy*". Clin Cancer Res. 2008 Feb 15; 14(4): 971-6. Review.

Rubin LL, de Sauvage FJ, "*Targeting the Hedgehog pathway in cancer".* Nat Rev Drug Discov. 2006 Dec; 5(12): 1026-33. Review.

Ruiz i Altaba A, Palma V, Dahmane N., "*Hedgehog-Gli signalling and the growth of the brain*". Nat Rev Neurosci. 2002 Jan; 3(1): 24-33. Review.

Schulman BA, Carrano AC, Jeffrey PD, Bowen Z, Kinnucan ER, Finnin MS, Elledge SJ, Harper JW, Pagano M, Pavletich NP, "*Insights into SCF ubiquitin ligases from the structure of the Skp1-Skp2 complex*". Nature. 2000 Nov 16; 408(6810): 381-6.

Shorter J, Watson R, Giannakou ME, Clarke M, Warren G, Barr FA, "*GRASP55, a second mammalian GRASP protein involved in the stacking of Golgi cisternae in a cell-free system".* EMBO J. 1999 Sep 15; 18(18) :4949-60.

Taylor MD, Liu L, Raffel C, Hui CC, Mainprize TG, Zhang X, Agatep R, Chiappa S, Gao L, Lowrance A, Hao A, Goldstein AM, Stavrou T, Scherer SW, Dura WT, Wainwright B, Squire JA, Rutka JT, Hogg D. "*Mutations in SUFU predispose to Medulloblastoma*". (2002) Nat. Genet. 31, 306–310.

Thompson MC, Fuller C, Hogg TL, Dalton J, Finkelstein D, Lau CC, Chintagumpala M, Adesina A, Ashley DM, Kellie SJ, Taylor MD, Curran T, Gajjar A, Gilbertson RJ, "*Genomics identifies medulloblastoma subgroups that are enriched for specific genetic alterations".* J Clin Oncol. 2006 Apr 20; 24(12): 1924-31.

Wechsler-Reya R J, Scott MP., "*Control of neuronal precursor proliferation in the cerebellum by Sonic Hedgehog*". Neuron. 1999 Jan; 22(1): 2-3.

Wechsler-Reya R J, Scott MP., "*The developmental biology of brain tumors*". Annu Rev Neurosci. 2001; 24: 385-428. Review.

Welchman R L, Gordon C, Mayer RJ, "*Ubiquitin and ubiquitin-like proteins as multifunctional signals*". Nat Rev Mol Cell Biol. 2005 Aug; 6(8): 599-609.

Xu L, Wei Y, Reboul J, Vaglio P, Shin TH, Vidal M, Elledge SJ, Harper JW. "*BTB proteins are substrate-specific adaptors in an SCF-like modular ubiquitin ligase containing CUL-3*". Nature. 2003 Sep 18; 425(6955): 316-21.

Zawlik I, Zakrzewska M, Witusik M, Golanska E, Kulczycka-Wojdala D, Szybka M, Piaskowski S, Wozniak K, Zakrzewski K, Papierz W, Liberski PP, Rieske P., "*KCTD11 expression in medulloblastoma is lower than in adult cerebellum and higher than in neural stem cells".* Cancer Genet Cytogenet. 2006 Oct 1; 170(1): 24-8.

Zhang Q, Zhang L, Wang B, Ou CY, Chien CT, Jiang J., "*A hedgehog-induced BTB protein modulates hedgehog signaling by degrading Ci/Gli transcription factor*". Dev Cell. 2006 Jun; 10(6): 719-29.

Zhou P, Howley PM, "*Ubiquitination and degradation of the substrate recognition subunits of SCF ubiquitin-protein ligases".* Mol Cell. 1998 Nov; 2(5): 571-80.

Zhuang M, Calabrese MF, Liu J, Waddell MB, Nourse A, Hammel M, Miller DJ, Walden H, Duda DM, Seyedin SN, Hoggard T, Harper JW, White KP, Schulman BA. "*Structures of SPOP-Substrate Complexes: Insights into Molecular Architectures of BTB-Cul3 Ubiquitin Ligases*". Mol Cell. 2009 Oct 9; 36(1): 39-50.

Zollman S, Godt D, Privé GG, Couderc JL, Laski FA, "*The BTB domain, found primarily in zinc finger proteins, defines an evolutionarily conserved family that includes several developmentally regulated genes in Drosophila*". Proc Natl Acad Sci U S A. 1994 Oct 25; 91(22): 10717-21.

COMUNICATIONS

S. Correale, **L. Pirone**, S. Di Gaetano, L. Vitagliano, G. De Simone, M. Moretti, E. De Smaele, L. Di Marcotullio, A. Gulino, C. Pedone and E. Pedone "*Identification and characterization of a new BTB/POZ domain*". Congresso Nazionale della Divisione di Chimica dei Sistemi Biologici 8-9 Novembre Montagnana (Pd) 2007.

B. Farina, L. Zaccaro, **L Pirone**, E. Pedone, F. Viparelli, M. Ruvo, C. Miele, F. Beguinot, C. Pedone and R. Fattorusso. "*Identification of PED binders through NMR spectroscopy*". Convegno Nazionale della Divisone Chimica dei Sistemi Biologici della Società Chimica italiana, Montagnana (PD) 8-9 Novembre 2007.

L. Pirone, S. Correale, V. Alterio, S. Di Gaetano, L. Vitagliano, G. De Simone, M. Moretti, E. De Smaele, L. Di Marcotullio, A. Gulino, C. Pedone and E. Pedone "*Identification and characterization of a new form of oncosuppressor KCTD11*". Scuola Nazionale Di Chimica Bioinorganica della Società Chimica Italiana Napoli 14-16 Settembre 2008.

L. Pirone, S. Correale, S. Di Gaetano, L. Di Marcotullio, A. Gulino, I. de Paola, L. Zaccaro, G. De Simone, L. Vitagliano, C. Pedone and E. Pedone "*KCTD11 regulates Hedgehog signaling by interaction with Cullin3 ubiquitin ligase*". XXIII Congresso Nazionale della Società Chimica Italiana Sorrento 5-10 Luglio 2009.

S. Correale, **L. Pirone**, A. Ruggiero, E. Pedone, R. Berisio. "*Structural and funziona studies of RpfB, a key protein for M. tuberculosis exit from latency*". XXIII Congresso Nazionale della Società Chimica Italiana Sorrento 5-10 Luglio 2009.

B. Farina, L. Russo, **L. Pirone**, E. Pedone, F. Viparelli, M. Ruvo, C. Pedone, R. Fattorusso. "*Backbone dynamics of Phosphoprotein Enriched in Diabetes studies by ^{15}N NMR relaxion*". XXIII Congresso Nazionale della Società Chimica Italiana Sorrento 5-10 Luglio 2009.